

EFFECTIVE FIELD THEORY BASED ON THE QUANTUM
INVERTED HARMONIC OSCILLATOR AND THE INVERSE
SQUARE POTENTIAL WITH APPLICATIONS TO SCHWINGER
PAIR CREATION

EFFECTIVE FIELD THEORY BASED ON
THE QUANTUM INVERTED HARMONIC
OSCILLATOR AND THE INVERSE
SQUARE POTENTIAL WITH
APPLICATIONS TO SCHWINGER PAIR
CREATION

By

SRIRAM SUNDARAM, BS-MS., MSc.

A Thesis Submitted to the School of Graduate Studies in
Partial Fulfilment of the Requirements for the Degree DOC-
TOR OF PHILOSOPHY

DOCTOR OF PHILOSOPHY (2024)
(Physics)

McMaster University
Hamilton, Ontario, Canada

TITLE: Effective field theory based on the quantum inverted harmonic oscillator and the inverse square potential with applications to Schwinger pair creation

AUTHOR: Sriram Sundaram, BS-MS., MSc.

SUPERVISOR: Professor Duncan H. J. O'Dell

NUMBER OF PAGES: xv, 110

LAY ABSTRACT

In this thesis we focus on two elementary unstable quantum systems, the inverted harmonic oscillator and the inverse square potential, using the methods of effective field theory (EFT) and the renormalization group (RG). We demonstrate that the phenomenon of fall to the centre associated with the inverse square potential is an example of a \mathcal{PT} symmetry breaking transition. We also demonstrate a mapping between the inverted harmonic oscillator and the inverse square potential including a one-to-one mapping between the quantum states and boundary conditions using an EFT framework in a renormalization group invariant way. We apply these methods to the phenomenon of Schwinger pair production and study finite size effects using the RG scheme for the quantum inverted harmonic oscillator.

ABSTRACT

This thesis deals with an EFT study based on the quantum mechanics of the inverted harmonic oscillator (IHO) and inverse square potentials (ISP).

Paper 1 focusses on the quantum mechanics of the ISP and its connection to \mathcal{PT} phase transitions. As we tune the strength of the ISP α to be greater than a critical value $\alpha_c = 1/4$, the spectrum becomes unbounded from below, termed as fall to the centre. The ISP system is known for its ambiguities in choosing the boundary condition at the origin. Following Burgess et al. [1], we implement a linear (Robin) boundary condition that dominates at low energies and can be complex in order to describe absorption and emission. EFT methods allow us to compute the RG evolution of the boundary condition. We show that the renormalized boundary coupling exhibits a \mathcal{PT} phase transition in the complex plane as we tune α , from a \mathcal{PT} symmetric phase, where there are two real fixed points of the RG flow in the sub-critical regime, to a complex conjugated pair in the super-critical regime which breaks \mathcal{PT} symmetry.

Paper 2 discusses the mapping of the quantum mechanics of an IHO to a super critical ISP using a canonical transformation. We use the Berry-Keating Hamiltonian $H = xp$ to connect the IHO system to the super critical ISP system. We also map the linearly independent ISP states to the IHO states using a quantum canonical transformation. Furthermore, with the knowledge of how the states map to each other, we also map the linear boundary condition for the ISP system near the origin to the IHO system far from the origin using the methods of EFT in an RG invariant way. We show that the RG evolution of the boundary condition of the IHO at long distances exhibits limit cycles like the super critical ISP system.

Paper 3 discusses the implications of the RG behaviour of the IHO to the classical field theory of Schwinger pair production. We implement appropriate non-selfadjoint extensions to the IHO boundary condition that describe pair creation. The RG evolution of the boundary coupling involves fixed points and limit cycles. We show that Schwinger's result for the pair production probability in a constant field emerges at one of the scale invariant fixed points. However, away from fixed points we find that

the physical observables exhibit oscillatory behaviour (faster than log periodic) as a function of electric field strength.

ACKNOWLEDGEMENTS

I miss my mother who passed away during the final year of my PhD tenure, all of a sudden. She was everything for our family. She was my first Guru (teacher) who taught me mathematics. She taught me the value of education. Without her sacrifices, love and affection I am sure I would not have reached to the level of pursuing a PhD degree.

I humbly dedicate this thesis to her memory.

First and foremost I would like to thank my supervisor Dr. Duncan O'Dell for being a *Guru* (in Sanskrit Guru refers to a teacher who dispels the darkness of ignorance by the light of knowledge) to the true sense of the word, without whose support and guidance this thesis would not have been possible. I am grateful for his countless hours of time and attention, his patience, trust and for his deep physical insights that led to this thesis. Next I would like to thank my supervisory committee member Dr. C. P. Burgess, for his deep insights and knowledge in the area of EFT, his motivation and constructive criticism that helped shaping up this thesis. I am grateful for his time, patience and guidance. I would also like to thank my supervisory committee member Dr. Erik Sorensen for his valuable insights. I can't thank Dr. Duncan O'Dell enough for his unwavering support and personal attention during the event of two emergencies I had in the course of my tenure as a PhD student. I would also like to thank my committee members Dr. C. P. Burgess and Dr. Erik Sorensen for their support and understanding during those times.

I would like to thank Rajat Bhaduri (late) and Donald Sprung (late) for their valuable insights during the very initial phases of the project. Next, I would like to thank my current and former group members and colleagues at McMaster in no particular order: Dr. Ryan Plestid, Dr. Wyatt Kirkby, Dr. Jesse Mumford, Matt, Liam, Denise, Josh, Dr. Greg, Dr. James Lambert, Dr. Anton, for many fruitful discussions. I also express my gratitude to the former and current administration staff at the department of Physics and Astronomy Rose, Tina, Mara, Jennifer and others for all the help. I would also like to thank the international student services team of McMaster University whose help has been valuable for me as an international

PhD student. I would also like to thank my handful of friends I gathered at Hamilton: Naveen & Monicaa, Ananth & Shwetha, Dr. Aarthi, Dr. Abhijit.

I would like to thank Prof. Sir Michael V. Berry and Prof. M Lakshmanan for their encouragement and valuable insights during the initial stages of this thesis. I would also like to thank Dr. Prasanta K. Panigrahi and Dr. Ritesh Singh for their continued guidance and insights. I would like to express my gratitude to Dr. Mainak Sadhukhan and Dr. Vivek Vyas, who have truly been a source of inspiration since my undergraduate and masters days at IISER Kolkata, India. I would like to thank them for their affection and support and many fruitful discussions. Moreover, I would also like to thank my peers and friends: Mayank, Ananya, Kavya, Mansi, Kaveri, Dr. Zacharias, Dr. Varghese, Dr. Ansari, Anagha, Pavithra & Goutham.

Next, I would like to thank my father Sundaram Raman for being there for me as a pillar of support. Without his moral support affection and sacrifices, this would not have been possible. Also, I would like to thank my sister Rajalakshmi Sundaram, my brother-in-law Hareesh Parthasarathy, my charming niece Hira H Lakshmi, my Uncle and Aunt Rajesh & Sudha, my cousins Varun, Revathi & Girish for their love and support and for being there for me in anything and everything. I also would like to thank my Uncle Balan for always being a source of inspiration and support. I would also like to thank my in-laws Hariharan and Vasanthi for their support and affection. Last but not the least, I would like to thank my wife Hema Hariharan for her love and support.

DEDICATION

To the memory of my beloved mother Chithra Narayanan

&

To the memory of my Grandparents:

S. Raman & G. Rajalakshmi, H. S. Narayanan & Sathyabhama

TABLE OF CONTENTS

List of Tables	xi
List of Figures	xi
1 Introduction	1
1.1 Introduction to inverted harmonic oscillator and inverse square potentials	3
1.1.1 Inverted harmonic oscillator and fall to infinity	3
1.1.2 Inverse square potentials and fall to the centre	5
1.2 Canonical transformations	7
1.2.1 Canonical transformation in classical mechanics	8
1.2.2 Canonical transformation in quantum mechanics	10
1.3 Point particle effective field theory	11
1.3.1 Effective field theory	11
1.3.2 Point particle effective field theory	12
1.3.3 Renormalization group	15
1.4 Non-hermitian \mathcal{PT} symmetric quantum mechanics	17
1.4.1 Isolated/closed and open systems	17
1.4.2 \mathcal{PT} symmetric systems	18
1.4.3 \mathcal{PT} transition	21
1.5 Introduction to Schwinger pair production	21
2 Fall to the centre as a \mathcal{PT} transition	25
3 From fall to infinity to fall to the centre	44
4 Schwinger pair production: a non-hermitian quantum mechanics perspective	67

5 Summary, Conclusions, and Future Work	100
Bibliography	104

LIST OF TABLES

Table	Page
1.1 This table lists the different types of generating functions in the theory of canonical transformations and their respective partial derivatives.	9

LIST OF FIGURES

Figure	Page
1.1 The figure shows the plot of an IHO potential with a representative energy eigenvalue shown as a dashed line.	4
1.2 The figure shows the plot of an inverse square potential with strength $g = 2$. The potential has a singularity at $Q = 0$	5
1.3 The figure shows the plot of the real and imaginary parts of the wavefunction for the super-critical ISP system near the origin which exhibits logarithmic phase singularity at the origin.	6
1.4 The figure shows the illustration of different length scales present in the PPEFT framework for the ISP system. The length r depicts the radius of the source located at the origin (in the context of an atom, it is the size of the nucleus). The regulator scale $\epsilon \gg r$ is where one evaluate necessary boundary conditions and the length $a_{\text{Bohr}} \gg \epsilon$ is the long distance laboratory scale (size of an electron orbital).	12
1.5 The figure shows a cartoon of a source (an emitter) and a sink (an absorber). Under time reversal \mathcal{T} source becomes sink and sink becomes source. And under spatial reflection \mathcal{P} the systems change their position from $x \rightarrow -x$. Thus the system is \mathcal{PT} symmetric	19

1.6	The figure shows a cartoon of production of particle antiparticle pairs from the vacuum in the presence of an electric field.	23
-----	--	----

LIST OF ABBREVIATIONS

IHO – Inverted harmonic oscillator

BK – Berry-Keating

ISP – Inverse square potential

EFT – Effective field theory

PPEFT – Point particle effective field theory

RG – Renormalization group

DECLARATION OF ACADEMIC ACHIEVEMENT

Chapter 2

S. Sundaram, C. P. Burgess, and D. H. J. O'Dell

Fall-to-the-centre as a \mathcal{PT} symmetry breaking transition

Journal of Physics: Conference Series **2038**, 012024 (2021).

The idea of this project was conceived by Duncan O'Dell. All calculations present in the article were performed by Sriram Sundaram. The main sections in the article were written by Sriram Sundaram, with edits by Duncan O'Dell. The abstract, introduction and conclusion were written by Duncan O'Dell and C. P. Burgess.

Chapter 3

S. Sundaram, C. P. Burgess, and D. H. J. O'Dell

Duality between the quantum inverted harmonic oscillator and inverse square potentials

New Journal of Physics **26** 053023 (2024).

This project was originally conceived by Duncan O'Dell. All the results and calculations were done by Sriram Sundaram. The first draft of the paper was written by Sriram Sundaram and it was further edited and streamlined by C. P. Burgess in the way the article appears, with the exception of the introduction and conclusions which were mostly written by Duncan O'Dell with inputs from Sriram Sundaram.

Chapter 4

S. Sundaram, C. P. Burgess, and D. H. J. O'Dell

Scale anomaly and \mathcal{PT} symmetry breaking : EFT of finite size effects in Schwinger pair production

Manuscript in preparation (2024).

The basic idea of the project was conceived by Duncan O'Dell with inputs from Sriram

Sundaram. All the results were produced by Sriram Sundaram. The major sections of the paper was written by Duncan O'Dell and C. P. Burgess with edits done by Sriram Sundaram. The introduction and conclusion were written by Duncan O'Dell with inputs from Sriram Sundaram.

INTRODUCTION

"The career of a young theoretical physicist consists of treating the harmonic oscillator in ever-increasing levels of abstraction." - Sidney Coleman

In this thesis our goal is to study two elementary unstable quantum systems, the inverted harmonic oscillator (IHO) and inverse square potential (ISP) using the framework of effective field theory (EFT). The close relative to the ubiquitous simple harmonic oscillator is its unstable version, the inverted harmonic oscillator which is also a multi-faceted simple prototype of unstable equilibrium [2, 3]. However to the best of our knowledge, it was only in 1986, that a detailed investigation of the quantum mechanics of the IHO was presented by Gabriel Barton [4]. The IHO potential $V(x) \propto -x^2$ is an upside down parabola. It is a model that exhibits fall to infinity, in the sense that it is a simple example of unstable equilibrium, where classically the particle rolls off to $\pm\infty$. The span of the applications of the IHO system ranges from quantum mechanics [2, 7], statistical mechanics [11], cosmology [8], quantum field theory [5, 6, 13] etc. One of the main subtleties in implementing singular potentials is the delicate question of boundary conditions. This is perhaps best known in the case of the ISP, $V(x) \propto -\frac{1}{x^2}$ [34]. However, for the ISP, the singularity of the potential is located at the origin and exhibits fall-to-the-centre.

Taming instabilities in quantum mechanics and ways of properly regulating divergences has been a long standing puzzle and is still an active areas of research. Such investigations gave birth to versatile tools of regularization and the renormalization group (RG) approach [42, 48]. These methods, even though originally developed to handle divergences/infinities in quantum field theory, have also been proven to be use-

ful in understanding singular potentials in non-relativistic quantum mechanics [36,49]. Another modern development that is connected to singular potentials is non-hermitian \mathcal{PT} symmetric quantum mechanics [51], more about which will be discussed in the later sections of this chapter.

One of the main results of this thesis is the mapping of the IHO system to the ISP system using a canonical transformation, including one-on-one mapping of the ISP states to the IHO states and also the mapping of the boundary conditions using the methods of EFT. Moreover, we also point out how one can incorporate non-hermitian effects using the boundary condition in both the systems which leads to consequences such as \mathcal{PT} symmetry breaking. Another important part of this thesis is the application of EFT methods to the IHO system to study the classical field theory of Schwinger pair production, that describes vacuum instability in the presence of a static electric fields, and its associated finite size effects.

Overview of this Thesis

In this chapter we will provide an introduction to the relevant topics that form the central part of this thesis as covered in Chapters 2 - 4. In section 1.1.1 we describe the subtleties involved in the quantum mechanics of the IHO, the need for implementing appropriate boundary condition at long distances, various applications etc. In section 1.1.2 we will describe the properties and applications of the dual model to the IHO, the inverse square potential which has a singularity at the origin. In section 1.2 we give a brief overview of the method of canonical transformations in classical and quantum mechanics in an attempt to build the necessary background tools used in chapter 3. The dual mapping of the IHO system to the ISP system using a canonical transformation, including mapping of its states using a quantum canonical transform and mapping its boundary conditions, is one of the main results of this thesis and is the subject of chapter 3. In section 1.3 we provide an introduction to the basic idea of point particle effective field theory (PPEFT) and renormalization group (RG). We provide an overview of how PPEFT helps in dealing with implementing appropriate boundary conditions in a systematic way. We use this EFT framework to implement appropriate boundary conditions in an RG invariant way in all the three papers presented here (chapters 2-4). One of the important aspects of PPEFT is the concept of the classical renormalization group, which ensures physical predictions will only be functions of the invariants of the RG flow. One of the advantages of the PPEFT framework is that it allows one to address non-hermitian effects such as absorption and emission in both the IHO and ISP system, which leads to consequences such

as \mathcal{PT} symmetry breaking. In section 1.4 we present an overview to the subject of non-hermitian \mathcal{PT} symmetric quantum mechanics that describes systems with gain or loss. Finally in the last section of this chapter we provide a brief introduction to the physical model of Schwinger pair production, the phenomenon of vacuum instability in the presence of an external electric field, which is the subject of chapter 4.

Chapters 2-4 consist of three papers each with a mini summary of the paper and a statement by the author. Chapter 2 (Paper 1) deals with the quantum mechanics of inverse square potential, the method of systematically regulating the system using PPEFT and its connection to \mathcal{PT} phase transitions as we tune the strength of the inverse square potential. Chapter 3 (Paper 2) addresses the mapping of the IHO system to the ISP system using a canonical transformation. Apart from mapping the Hamiltonians, the paper also discusses mapping of the quantum states and the boundary conditions of the ISP (at short distances) to the IHO (at long distances) using the methods of PPEFT. In both cases the boundary conditions are implemented in an RG invariant way. Chapter 4 (Paper 3) provides an investigation of the classical field theory of Schwinger pair production using non-hermitian quantum mechanics. We apply classical renormalization methods of the IHO developed in chapter 3 to describe pair production in the presence of an external electric field. We implement appropriate non-hermitian boundary conditions for the IHO using the methods of EFT and RG to understand the finite size effects of pair creation.

1.1 Introduction to inverted harmonic oscillator and inverse square potentials

1.1.1 Inverted harmonic oscillator and fall to infinity

The IHO system provides a good approximation for decay from an unstable equilibrium. It appears in many branches of physics as it is the simplest toy model describing an unstable equilibrium. It appears in the classical field theory of Schwinger pair production where the Klein-Gordon mode function in the presence of a static electric field satisfies a time independent IHO Schrödinger equation [5, 6]. This physical model is the subject of chapter 4 of this thesis. Apart from the Schwinger effect, the IHO also arises in the field theory of Hawking radiation [14], in inflationary cosmology, in quantum Hall lowest Landau levels [2], as the generator of squeezing [9] and the Glauber oscillator in quantum optics [10], in quantum phase transitions in the Dicke

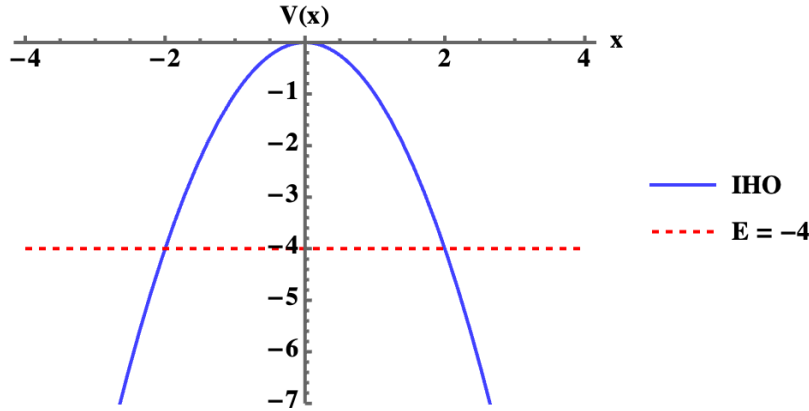


Figure 1.1: The figure shows the plot of an IHO potential with a representative energy eigenvalue shown as a dashed line.

model in statistical mechanics [11], tachyon physics [15] and string theory [16, 17].

The inverted harmonic oscillator Hamiltonian has the form:

$$H(x, p) = \frac{p^2}{2m} - \frac{1}{2}m\omega^2 x^2. \quad (1.1)$$

In the dimensionless coordinate $\xi = \sqrt{m\omega/\hbar}x$, the time independent Schrödinger equation can be written as:

$$\frac{\pi^2 - \xi^2}{2}\phi = E\phi \quad (1.2)$$

where $\pi = -i\hbar\frac{\partial}{\partial\xi}$ in the position representation obeys $[\xi, \pi] = i\hbar$, and E is the energy eigenvalue. The potential energy is an upside down parabola, as shown in Fig. (1.1).

The Schrödinger equation in the position representation can be written as :

$$-\frac{1}{2}\frac{\partial^2\phi}{\partial\xi^2} - \frac{1}{2}\xi^2\phi = E\phi \quad (1.3)$$

when $E > 0$, we have an over the barrier reflection problem and when $E < 0$ we have a tunneling problem. The Schrödinger equation in the momentum representation can be written as :

$$\frac{\partial^2\Phi}{\partial p^2} + p^2\Phi = E\Phi. \quad (1.4)$$

Thus an above the barrier reflection problem is a tunneling problem in momentum space for an IHO.

The solutions to the classical equations of motion are hyperbolic in nature and the phase space trajectories become exponentially separated over time. The quantum mechanics of the IHO is exactly solvable [2, 4], and for energy E can be expressed in terms of two linearly independent parabolic cylinder functions:

$$\phi(\xi) = C_1 D_{iE-1/2} \left(\sqrt{2}e^{-i3\pi/4}\xi \right) + C_2 D_{-iE-1/2} \left(\sqrt{2}e^{-i\pi/4}\xi \right) \quad (1.5)$$

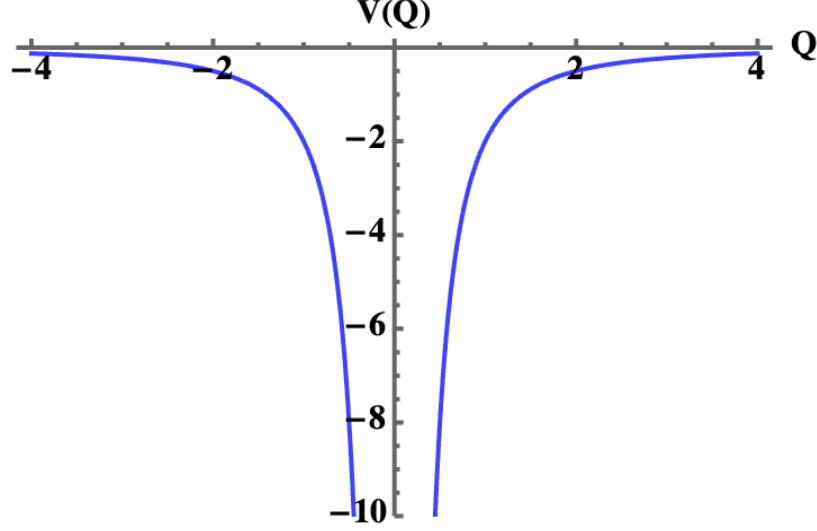


Figure 1.2: The figure shows the plot of an inverse square potential with strength $g = 2$. The potential has a singularity at $Q = 0$.

Note that parabolic cylinder functions are not square integrable. The wavefunction for large values of $|\xi|$ is oscillatory and hence is not normalizable, and so normalization cannot determine the combination of C_1 and C_2 and therefore one needs to implement appropriate boundary conditions at large ξ to choose the state. Furthermore, the IHO Hamiltonian $K_1 = \frac{1}{2}(\pi^2 - \xi^2)$, the SHO Hamiltonian $K_2 = \frac{1}{2}(\pi^2 + \xi^2)$ and the Berry-Keating Hamiltonian $K_3 = \frac{1}{2}(\xi\pi + \pi\xi)$ forms a closed $\mathfrak{su}(1, 1)$ Lie algebra:

$$[K_1, K_2] = -iK_3, \quad [K_2, K_3] = iK_1, \quad [K_3, K_1] = iK_2 \quad (1.6)$$

This suggests there is a mapping between the IHO Hamiltonian and the Berry-Keating Hamiltonian using a canonical transformation. This is a key step in mapping the IHO to the super-critical ISP system and this forms the subject of chapter 3 (Paper 2). The generator $K_3 = \frac{1}{2}(\xi\pi + \pi\xi)$ is known as Berry-Keating Hamiltonian in the literature owing to its applications in attempts to prove the Riemann hypothesis [18]. It is a generator of scale transformations in the following sense:

$$e^{i\zeta K_3} \xi e^{-i\zeta K_3} = e^\zeta \xi, \quad \text{and} \quad e^{i\zeta K_3} \pi e^{-i\zeta K_3} = e^{-\zeta} \pi \quad (1.7)$$

More about the Berry-Keating Hamiltonian will be discussed in chapter 3.

1.1.2 Inverse square potentials and fall to the centre

The attractive ISP system has a potential of the form $V(Q) \propto -1/Q^2$. This potential is singular at the origin. The ISP system is in a sense dual to the IHO system, because

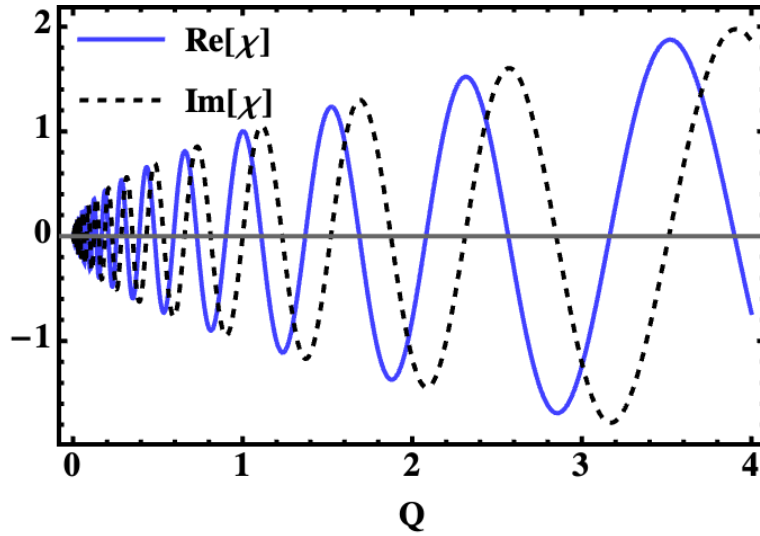


Figure 1.3: The figure shows the plot of the real and imaginary parts of the wavefunction for the super-critical ISP system near the origin which exhibits logarithmic phase singularity at the origin.

the IHO potential is singular at ∞ , where the particle rolls down to $\pm\infty$ whereas the ISP system is singular at the origin and causes fall to the centre [see Fig. (1.2)] [19]. In 3D, the classical trajectory of an ISP system is an unstable spiral to the centre [19]. This happens when the strength of the inverse square potential is strong enough to beat the centrifugal barrier which precisely has the same form. The attractive ISP is the lowest order singular potential that exhibits such an instability.

Like the IHO system, the ISP also arises in various branches of physics such as: in near horizon black hole physics [13, 20, 21, 26], as an effective description of the Efimov physics [30], an atom interacting with a charged wire [25], the optics of Maxwell's fisheye lens [31], the coherence theory of sunlight [32], the Calogero-Sutherland systems [33], anti-de Sitter/conformal field theory (AdS/CFT) correspondence [29] etc. The Hamiltonian for an attractive ISP in 1D can be written as ¹

$$H = \frac{P^2}{2m} - \frac{g}{Q^2} \quad (1.8)$$

where $g > 0$, $[Q, P] = i\hbar$. This Hamiltonian admits continuous scaling symmetry under $Q \rightarrow \zeta Q$. The classical generator for scale transformation is given by $D = QP$ and the conservation law reads

$$\frac{dD}{dt} = 2H \quad (1.9)$$

and so it is conserved only if we restrict the system to zero energy and is termed an *almost* conservation law. Since the exact solutions to the ISP system can be written

¹Throughout this thesis we restrict ourselves to the 1D ISP

in terms of the confluent hypergeometric function, the problem lies not in finding the solutions to the second order Schrödinger equation, rather in choosing appropriate boundary conditions at the origin to choose the quantum state. The general form of the wavefunction for the ISP system near the origin is given by:

$$\chi(Q) = C_+ Q^{1/2+\sigma} + C_- Q^{1/2-\sigma} \quad (1.10)$$

where $\sigma = \sqrt{1/4 - \alpha}$, $\alpha \equiv 2mg/\hbar^2$. To obtain the above expression one should take $Q \rightarrow 0$ limit of the exact solution. There exists a critical value $\alpha_c = 1/4$ for which fall to the centre takes place, or more precisely the Hamiltonian becomes unbounded from below for $\alpha > \alpha_c$. The $\alpha < 1/4$ regime is termed as the sub-critical case and $\alpha > 1/4$ is termed as the super-critical case. In the sub-critical case the exponent of the wavefunction σ is real and thus one can distinguish between the two solutions depending upon their behaviour at the origin. On the other hand in the super-critical regime when $\alpha > 1/4$ the exponent σ is purely imaginary and thus both of the solutions admits a logarithmic phase singularity at the origin [see Fig. (1.3)]. The usual boundary condition requirement in quantum mechanics that the wavefunction does not diverge as $Q \rightarrow 0$ is not adequate in the case of ISP. So, boundedness cannot be a good criteria to choose one state over the other. To fix the ratio C_+/C_- one needs to implement appropriate boundary conditions. The literature has a plethora of proposals for boundary conditions [35–38]. The presence of the phase singularity in the wavefunction is the quantum effect of fall to the centre. Therefore it seems that there is some microscopic (high energy) physics near the origin that needs to be added to make the ISP system well posed. If the microscopic length scale that describes the size of the source located at the origin (for example the size of the nucleus r) is very much less than the physical low energy (long distance) scale (for example the Bohr radius a_{Bohr}) i.e. when $r/a_{\text{Bohr}} \ll 1$, one can use the power of EFT to model the source to the lowest order, which in effect amounts to implementing a Robin (linear) boundary condition at a short distance arbitrary cut-off, more about which will be discussed in section 1.3.2.

1.2 Canonical transformations

In this section we provide an introduction to the theory of canonical transformations in classical and quantum mechanics. It involves describing changes from one set of canonically conjugate variables x, p to another set Q, P , which classically satisfies Poisson brackets $\{x, p\} = \{Q, P\} = 1$, and in quantum mechanics they satisfy

the canonical commutation relations $[x, p] = [Q, P] = i\hbar$. This section provides an overview of the concepts required for chapter 3, that deals with the mapping of the IHO system to ISP system. We use the technique of quantum canonical transforms to map one-to-one the ISP states to the IHO states.

1.2.1 Canonical transformation in classical mechanics

The transformation of variables such as going from cartesian to polar/cylindrical coordinates has the general form:

$$Q = Q(x, t) \quad (1.11)$$

Such transformations in the literature are known as *point transformations* [40]. However, in Hamiltonian mechanics both the generalized coordinates and momenta are independent variables, and hence one must also account for transformation of both coordinates and momenta, $x, p \rightarrow Q, P$

$$Q = Q(x, p, t), \quad P = P(x, p, t) \quad (1.12)$$

The above equations define a *point transformation of phase space* [40]. More precisely, in the theory of Hamiltonian mechanics, we are interested in the transformations for which the new variables are also canonically conjugate. The transformations $x, p \rightarrow Q, P$ that preserve Hamilton's equations of motion are called *canonical transformations*. There then exists a new transformed Hamiltonian $K(Q, P, t)$ (sometimes referred to as the *Kamiltonian*) such that Hamilton's equations in the new set of variables take the standard form

$$\dot{Q} = \frac{\partial K}{\partial P}, \quad \dot{P} = -\frac{\partial K}{\partial Q} \quad (1.13)$$

In both sets of variables the Hamiltonians, $H(x, p, t)$ and $K(Q, P, t)$ should satisfy Hamilton's principle in the form:

$$\delta \int dt \, p\dot{x} - H(x, p, t) = 0 \quad (1.14)$$

and in the new variables

$$\delta \int dt \, P\dot{Q} - K(Q, P, t) = 0. \quad (1.15)$$

For the simultaneous validity of the action principle in old and new variables, one needs to satisfy the condition below [40]:

$$p\dot{x} - H = P\dot{Q} - K + \frac{dF}{dt} \quad (1.16)$$

Generating function	Derivatives
$F = F_1(x, Q, t)$	$p = \frac{\partial F_1}{\partial x}, P = -\frac{\partial F_1}{\partial Q}$
$F = F_2(x, P, t) - QP$	$p = \frac{\partial F_2}{\partial x}, Q = \frac{\partial F_2}{\partial P}$
$F = F_3(p, Q, t) - xp$	$x = -\frac{\partial F_3}{\partial p}, P = -\frac{\partial F_3}{\partial Q}$
$F = F_4(p, P, t) + xp - QP$	$x = -\frac{\partial F_4}{\partial p}, Q = \frac{\partial F_4}{\partial P}$

Table 1.1: This table lists the different types of generating functions in the theory of canonical transformations and their respective partial derivatives.

where F is a function of phase space coordinates and is called the generating function of the canonical transformation. If F is a function of old and new coordinates

$$F = F_1(x, Q, t) \quad (1.17)$$

then, Eq. (1.16) can be rewritten as

$$p\dot{x} - H = P\dot{Q} - K + \frac{\partial F_1}{\partial t} + \frac{\partial F_1}{\partial x}\dot{x} + \frac{\partial F_1}{\partial Q}\dot{Q} \quad (1.18)$$

which then yields

$$p = \frac{\partial F_1}{\partial x}, P = -\frac{\partial F_1}{\partial Q} \quad (1.19)$$

and

$$K = H + \frac{\partial F_1}{\partial t} \quad (1.20)$$

Using the above equations, given a generating function F_1 one can obtain the transformation equations. And on the other hand knowing the canonical transformation, one can integrate the partial differential equation to solve for F_1 , provided it is canonical. Depending upon the transformation, the generating function F can also be function of x, P, t and so on. So, if say p cannot be written as function of x, Q, t and instead can be written as function of x, P, t , one can use the generating function $F = F_2(x, P, t)$. The table 1.1 lists the different types of generating functions and their respective partial derivatives. Each generating function is related to the other by a Legendre transformation.

Example 1 : Consider the following generating function $F_1(x, Q) = xQ$, which yields the following transformation [40]:

$$p = \frac{\partial F_1}{\partial x} = Q, P = -\frac{\partial F_1}{\partial Q} = -x \quad (1.21)$$

which is a canonical transformation, because it preserves the Poisson brackets: $\{Q, P\} = \{p, -x\} = 1$ and hence it preserves the form of Hamilton's equations of motion.

Example 2 : Consider the following transformation to the IHO Hamiltonian

$$Q = \frac{p+x}{\sqrt{2}}, \quad P = \frac{p-x}{\sqrt{2}}. \quad (1.22)$$

The IHO Hamiltonian

$$H(x, p) = \frac{p^2 - x^2}{2} \quad (1.23)$$

is transformed to

$$H(Q, P) = QP \quad (1.24)$$

and is called the Berry-Keating (BK) Hamiltonian in the literature. The generating function $F_1(x, Q)$ for the above canonical transformation can be derived by solving the following partial differential equation:

$$p = \frac{\partial F_1}{\partial x}, \quad P = -\frac{\partial F_1}{\partial Q} \quad (1.25)$$

$$F_1(x, Q) = -\frac{x^2}{2} + \sqrt{2}xQ - \frac{Q^2}{2} \quad (1.26)$$

The generating function of second type $F_2(x, P)$ can be derived by solving the following equations:

$$p = \frac{\partial F_2}{\partial x}, \quad Q = \frac{\partial F_2}{\partial P}, \quad (1.27)$$

which yields

$$F_2(x, P) = \frac{x^2}{2} + \sqrt{2}xP + \frac{P^2}{2} \quad (1.28)$$

In chapter 3, we use this canonical transformation and the Berry-Keating Hamiltonian to relate the IHO to the ISP Hamiltonian.

1.2.2 Canonical transformation in quantum mechanics

One can use the methods of canonical transformations in quantum mechanics to map the Hamiltonian and moreover one can use the technique of quantum canonical transform integrals to map between the quantum states from the old variables to the new ones, due to Dirac [41].

The wavefunction in the x representation can be obtained from the wavefunction in the Q variables using the identity

$$\phi(x) = \int dQ \langle x|Q \rangle \langle Q|\phi \rangle \quad (1.29)$$

where $I = \int dQ |Q\rangle\langle Q|$ and let's the kernel $\langle x|Q \rangle = e^{\frac{i}{\hbar}F_1(x,Q)}$ which can be constructed using the classical generating function. One can obtain the function $F_1(x, Q)$ following Dirac [41]:

$$\langle x|p|Q \rangle = -i\hbar \frac{\partial}{\partial x} \langle x|Q \rangle = \left(\frac{\partial F_1}{\partial x} \right) \langle x|Q \rangle = \langle x| \frac{\partial F_1}{\partial x} |Q \rangle \quad (1.30)$$

Similarly,

$$\langle x|P|Q\rangle = i\hbar \frac{\partial}{\partial Q} \langle x|Q\rangle = -\frac{\partial F_1}{\partial Q} \langle x|Q\rangle = \langle x| -\frac{\partial F_1}{\partial Q} |Q\rangle \quad (1.31)$$

which implies

$$p = \frac{\partial F_1}{\partial x}, \quad P = -\frac{\partial F_1}{\partial Q} \quad (1.32)$$

One can use the above tool of quantum canonical transforms to map the BK state in the Q variables to the IHO state in the x variables. This is discussed in detail in chapter 3. We also use this method to construct a one-to-one map between the ISP quantum states and the IHO states. In classical mechanics, as discussed in the section above, the four types of generating functions are related by Legendre transformation, whereas in quantum mechanics the various kernels that maps the quantum states from one variable to the other are related by a Fourier transform

$$e^{iF_1(x,Q)} = \int dP \langle x|P\rangle \langle P|Q\rangle = \int dP e^{iF_2(x,P)} e^{iQP} \quad (1.33)$$

1.3 Point particle effective field theory

1.3.1 Effective field theory

Natural phenomena present themselves with different length and energy scales ranging from quarks, nuclei, atoms, molecules, proteins, cells, planets, galaxies etc. The intriguing aspect is that we do not need to understand the physics happening at all scales to understand the physics going on at a particular scale that is relevant to us. Effective field theory (EFT) gives the advantage of simplifying the calculations by focusing on the relevant degrees of freedom and neglecting those that are not important in the very initial stages of building the physical model. For example such an effective theory might shed light on hidden symmetries or existence of anomalous symmetries of the model. Effective field theory is now widely used in all branches of physics including particle physics [23], gravity [22], condensed matter physics etc., for a comprehensive review on the subject of EFT, see [23, 24]. In this thesis we apply the methods of point particle effective field theory to model and implement boundary conditions for singular potentials like the inverted harmonic oscillator and inverse square potentials in quantum mechanics. We also apply it to the phenomenon of particle creation in the presence of external electric fields.

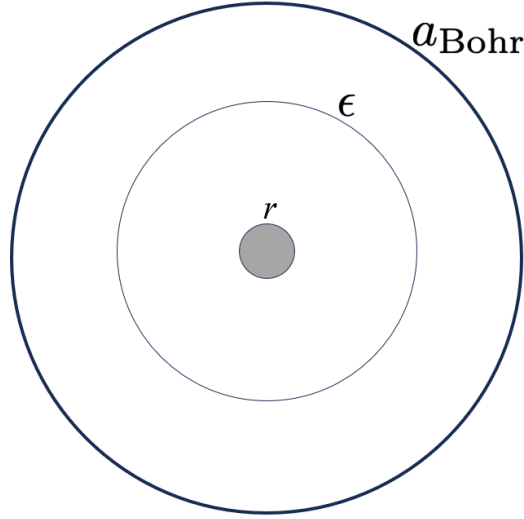


Figure 1.4: The figure shows the illustration of different length scales present in the PPEFT framework for the ISP system. The length r depicts the radius of the source located at the origin (in the context of an atom, it is the size of the nucleus). The regulator scale $\epsilon \gg r$ is where one evaluate necessary boundary conditions and the length $a_{\text{Bohr}} \gg \epsilon$ is the long distance laboratory scale (size of an electron orbital).

1.3.2 Point particle effective field theory

The philosophy of point particle effective field theory involves building a systematic quantitative framework to study the effects of small objects (such as a proton in a nucleus) on large objects (such as an electron orbital in an atom) by means of what can be thought of as generalized multipole expansion. For example, if we consider the physics of the electron orbital in an atom with a length scale typical of the size of an atom i.e. Bohr radius a_{Bohr} , and r being the size of the nuclei which is usually regarded as a point source, in the limit $r \ll a_{\text{Bohr}}$ (see Fig. (1.4)), one can largely ignore the detailed sub structure of the nuclei, and one can therefore use the tools of effective field theory to describe the physics at long distances (low energies). This technique can also be applied to many different models such as inverse square potentials and its applications to near horizon physics of black holes [26], absorption of atoms by a charged wire [25], the nuclear effects on atomic energy levels [27] etc.

PPEFT and boundary conditions for inverse square potentials and inverted harmonic oscillators

ISP case :

For inverse square potentials the action consists of two parts. One is the bulk action

that describes the long distance part (inverse square potentials). In 1D it takes the form

$$S_{\text{Bulk}} = \int dt dQ \left[\frac{i}{2} (\chi^* \partial_t \chi - \chi \partial_t \chi^*) - \frac{1}{2m} |\nabla \chi|^2 + \frac{g}{Q^2} |\chi|^2 \right] \quad (1.34)$$

Using the action principle, one can derive the field equations that take the form of the time-dependent Schrödinger equation with an attractive inverse square potential

$$i \frac{\partial \chi}{\partial t} = -\frac{1}{2m} \frac{\partial^2 \chi}{\partial Q^2} - \frac{g}{Q^2} \chi. \quad (1.35)$$

The above Schrödinger equation exhibits continuous scale invariance, i.e. the equation remains form invariant under space-time scaling $Q \rightarrow \zeta Q$, $t \rightarrow \zeta^2 t$, where ζ is a constant. Second part to the total action is the point particle effective action that describes the physics of the source at short distances

$$S_{\text{PPEFT}} = \int dt dQ \delta(Q) [h |\chi|^2 + \dots] \quad (1.36)$$

where h is an effective source-bulk coupling that parametrizes the localized interactions at the origin. One can in principle add higher order correction terms that depends on higher powers of χ such as $h_4 |\chi|^4$ etc [28]. Here, in this thesis we choose the lowest order quadratic term in χ , which is a good effective description in the limit $r/a_{\text{Bohr}} \rightarrow 0$. The contribution from the higher order terms are much smaller in the limit of source size $r \rightarrow 0$. It is the coupling parameters like h in the effective Lagrangian density that are analogous to multipole moments. Thus to the lowest order, physics at the origin is described by a Dirac delta function.

The total action then modifies the inverse square potential with an added Dirac delta potential with coupling h .

$$V_{\text{eff}} = -\frac{g}{Q^2} + h \delta(Q - \epsilon) \quad (1.37)$$

As we saw in section 1.1.2, the wavefunction near the origin exhibits a logarithmic phase singularity which leads to ambiguity in choosing boundary conditions at the origin. Adopting the method of PPEFT has the advantage of identifying the right parameter that renormalizes the divergences. For the ISP, it is the boundary coupling h , within the PPEFT action, that renormalizes any divergences.

Near origin boundary condition

By integrating the above Schrödinger equation over a small range either side of $Q = \epsilon$, one can see how the boundary condition reduces to a linear Robin type boundary condition for the field χ :

$$\lambda_{\text{ISP}} = \left[\frac{1}{\chi} \frac{\partial \chi}{\partial Q} \right]_{Q=\epsilon} \quad (1.38)$$

where $\lambda_{\text{ISP}} := 2mh/\hbar^2$. We evaluate the boundary condition at a finite cut-off $Q = \epsilon$ because the wavefunctions themselves diverge at $Q = 0$, as shown in section 1.1.2. For historical reasons the above boundary condition is also called the Bethe-Peierls boundary condition owing to its early applications in the study of the quantum theory of the *dipion*, a two body problem involving a proton and a neutron [39]. It is important to note that $\epsilon \gg r$ for PPEFT to work, because the PPEFT action doesn't converge when ϵ becomes close to the order of the size of the source r . Imposing a boundary condition at short distances breaks continuous scale invariance in an elementary example of a quantum anomaly, more about which is discussed in chapters 2 and 3. The short distance regulator cut-off ϵ is arbitrary and should not appear in physical predictions. Hence the coupling λ should be renormalized in the spirit of RG and the physical quantities such as scattering cross section etc. should only be a function of RG invariant scales. A brief introduction to the subject of RG will be given in the next subsection.

PPEFT also provides a way to describe non-selfadjoint extensions to the problem, say when the source does not conserve probability, the boundary coupling λ need not be real, since one can have complex λ in general. Some applications of non-hermitian boundary conditions within the PPEFT framework include absorption of atoms by a charged wire [25] and the near horizon physics of black holes [26] etc.

IHO case : boundary condition at long distances

A similar story holds for the IHO, wherein a linear boundary condition is evaluated, but now at long distances for the IHO system. The ratio of the wavefunction coefficients for the IHO (Eq. (1.5)) at asymptotically large distances can be inferred from such a boundary condition. The fact that the boundary condition is evaluated at a finite but arbitrary long distance cut-off L calls for renormalization like the ISP system. This is precisely the topic of study in the duality mapping of the IHO to ISP system in chapter 3 that explains how the states and the boundary conditions map. The linear boundary condition for the IHO is given by

$$\lambda_{\text{IHO}} = \left[\frac{1}{\phi} \frac{\partial \phi}{\partial x} \right]_{x=L} \quad (1.39)$$

where ϕ is the asymptotic IHO wavefunction and the boundary condition is evaluated at long distance cut-off $x = L$. In chapter 4 of this thesis we discuss the physics of particle production due to external electric fields using the framework of EFT for the inverted harmonic oscillator using a non-hermitian linear boundary condition of the form given in Eq. (1.39).

1.3.3 Renormalization group

Renormalization group (RG) is a versatile tool that helps tame infinities/divergences of the theory. Its initial applications were mostly focused on regulating divergences in QED [42, 43] and to the area of critical phenomenon [46]. In QFTs, the idea of renormalization usually starts with introducing a cut-off regulator in the limit of an integration which is merely a calculation tool, that should drop out of the physical predictions extracted in the end. It is the coupling parameters within the Lagrangian of the theory that determine how it must drop out, or more precisely the couplings would *flow/run* with the cut-off so as to make physical predictions be independent of the cut-off. The physical basis of RG and its connections to scaling was uncovered by Kenneth Wilson, for a critical history of RG see [48]. It was soon realized that the applications of RG are not restricted to the subject of quantum field theory [42, 43, 47] or near a phase transition in statistical mechanics, where its presence is mostly encountered due to emergent scale invariance [44–46], it also occurs in the study of non-relativistic quantum mechanics [34, 36, 49].

The presence of singularities in elementary unstable quantum mechanical systems like inverse square potentials led to regularization/renormalization approaches in non relativistic quantum mechanics [34]. An early study of the RG approach to singular potentials involving Dirac delta potentials is due to Thorn [50] and Jackiw [49]. The regularization/renormalization approaches to the ISP system, and implementing appropriate boundary conditions at the origin has a long history [34, 36]. It led to many physical insights that were otherwise obscure, for example the appearance of the scale anomaly in the ISP system, appearance of a single bound state in the weak coupling regime etc.

For the ISP/IHO system, the general solution to the second order differential equation can be written as a linear combination of two linearly independent wavefunctions:

$$\Psi = C_+ \Psi_+ + C_- \Psi_- \quad (1.40)$$

where the ratio C_+/C_- is fixed by an appropriate linear boundary condition, as discussed in the previous section. We saw that the linear boundary condition is evaluated at a short distance cut-off ϵ for the ISP system (it is a long distance cut-off for the IHO system as we will show in chapter 3) because the wavefunction itself diverges at $Q = 0$. The fact that such a cut-off regulator is arbitrary calls for renormalizing the couplings in the spirit of RG. The RG framework helps determines how the coupling of the theory should flow (or run) as a function of the regulator scale that ensures the physical quantities are fixed. The study of RG involves writing down a Callan-Symanzik type RG evolution equation (or the beta function), which describes how

the coupling in the underlying theory should flow with the scales of the theory. The beta function is defined as

$$\beta(\lambda) = \mu \frac{d\lambda}{d\mu} \quad (1.41)$$

where λ is the coupling of the theory that is renormalized and μ is a flowing parameter. In the context of our interest the flowing parameter is a short distance length scale ϵ in the case of ISP system, and a long distance length scale L for the IHO system, and the coupling λ that gets renormalized turns out to be the boundary coupling, and not the couplings contained in the bulk of the ISP/IHO system. The zeroes of the beta function $\beta(\lambda) = 0$ are the scale invariant fixed points of the theory. The RG evolution equation in the cases of the ISP and IHO turns out to be a nonlinear first order differential equation, as we will demonstrate in chapters 2-4 of this thesis. The RG evolution equation in differential form is exactly solvable given an initial condition, and the solution of the RG evolution equation gives the running of the coupling as a function of the cut-off parameter. When one is away from the fixed point, the RG flow can be parametrized using RG invariant labels that characterize an RG trajectory and physical scales emerges as functions of RG invariants of the flow.

In the upcoming chapter we show that the RG flow of the boundary coupling for the ISP system exhibits interesting physical consequences, including that of a \mathcal{PT} transition as we tune the strength of the inverse square potential, where two real fixed points obeying \mathcal{PT} symmetry in the sub-critical (weak coupling) regime merges and become complex in the super-critical (strong coupling) case which breaks \mathcal{PT} symmetry. The RG evolution of the ISP system is known to exhibit limit cycle behaviour in the super-critical regime. Due to the limit cycles, physical quantities like scattering cross sections are known to exhibit log periodic behaviour as a function of incident energy [25]. The log periodic behaviour is a consequence of scale anomaly, where the continuous scale invariance of the ISP system is broken to a discrete scaling symmetry. To the best of our knowledge such an RG study has not been carried out for the IHO system, and is one of the main goals of this thesis. The RG study for the IHO system is carried out in detail in chapter 3 of this thesis, where we do the mapping of the IHO system to the ISP system and also its boundary conditions, and we renormalize the boundary coupling for the IHO system like we do for the ISP system. Furthermore, we show that like the super-critical ISP system, the IHO boundary coupling also exhibits limit cycle behaviour in the complex plane. As an application of the physics of the IHO, we also discuss the implications of such an RG running in finite size effects on Schwinger pair production in chapter 4 of this thesis.

1.4 Non-hermitian \mathcal{PT} symmetric quantum mechanics

1.4.1 Isolated/closed and open systems

A system is said to be isolated or closed if it is not in direct contact with the surrounding/environment, such that there is no exchange of energy and/or matter. The time evolution of such a closed quantum system is described by a Hermitian Hamiltonian. A hermitian Hamiltonian is an operator that satisfies $H^\dagger = H$ where the action of \dagger is the combined operation of transpose and conjugate. In quantum mechanics, a hermitian Hamiltonian has important physical consequences [53]:

1. The energy eigenvalues of a hermitian operator are real [53].

Proof : Let us consider a Hermitian operator A that satisfies the eigenvalue equation

$$A|a\rangle = a|a\rangle \quad (1.42)$$

and since the operator is hermitian $A = A^\dagger$

$$\langle a'|A = a'^*\langle a'| \quad (1.43)$$

where a, a' are the eigenvalues of the operator. If we apply $\langle a'|$ to both sides of equation Eq. (1.42) and apply $|a\rangle$ to both sides of Eq. (1.43) and then subtract the two equations we obtain

$$(a - a'^*)\langle a|a'\rangle = 0 \quad (1.44)$$

If a, a' are the same, we get

$$a = a^* \quad (1.45)$$

which implies the eigenvalues are real. On the other hand, if a, a' are different, the difference $a - a'$ (due to the reality condition just proved) cannot vanish, so the inner product

$$\langle a|a'\rangle = 0 \quad (1.46)$$

which implies the states are orthogonal.

2. A hermitian Hamiltonian that generates unitary time evolution preserves the norm of the quantum state, or probability is conserved.

The time evolution operator $U = e^{-iHt}$ for such a system is unitary ($U^\dagger U = I$). Consider the time dependent Schrödinger equation with a real potential $V(x)$ of the form

$$i\hbar\partial_t\psi = -\frac{\hbar^2}{2m}\partial_x^2\psi + V(x)\psi \quad (1.47)$$

By multiplying the above equation with ψ^* and subtracting that with the complex conjugate of the above equation multiplied with ψ , we obtain the continuity equation

$$\partial_t\rho + \nabla\cdot J = 0 \quad (1.48)$$

where $\rho(x, t) = \psi^*\psi$ is the probability density and $J = \frac{i\hbar}{2m}(\psi\partial_x\psi^* - \psi^*\partial_x\psi)$ is the probability current. Integrating the above continuity equation over a region and applying the divergence theorem we get

$$\frac{dP}{dt} = \mathcal{F}(t) \quad (1.49)$$

where $P = \int dx \rho$ and \mathcal{F} is the net probability flux passing through the surface. For an isolated/closed system there is no net flow of probability through the surface, $\mathcal{F} = 0$ and hence probability is conserved, and is constant in time.

On the other hand if the system is open, there is a net flow of probability/energy, $\mathcal{F} \neq 0$ and thus the probability is not conserved. The concept of an isolated/closed system is somewhat an idealized scenario because physically any measurement done in a lab involves interactions with the environment.

1.4.2 \mathcal{PT} symmetric systems

The class of \mathcal{PT} symmetric non-hermitian quantum systems are an intermediate between closed and open quantum systems. In such systems the gain/loss is exactly balanced by the combined operation of \mathcal{PT} transformation to the Hamiltonian, where \mathcal{P} is the parity operator and \mathcal{T} is the time reversal operator. The parity transformation involves spatial reflection $x \rightarrow -x$. The time reversal operator in quantum mechanics is usually defined as an anti-unitary operator $t \rightarrow -t$, $i \rightarrow -i$. The time reversal operator in quantum mechanics is usually chosen to be anti-unitary due to the fact that a unitary time reversal transformation involves $H \rightarrow -H$ [53]. In systems such as an IHO or inverse square potentials, which are unbounded from below, then following Wigner [54], for such cases one can define time reversal as a unitary operator where $t \rightarrow -t$, alone so energy also changes sign [2, 7].

The philosophy of \mathcal{PT} symmetric systems involves a non-isolated system with a balanced gain-loss. An example to demonstrate the notion of balanced loss-gain

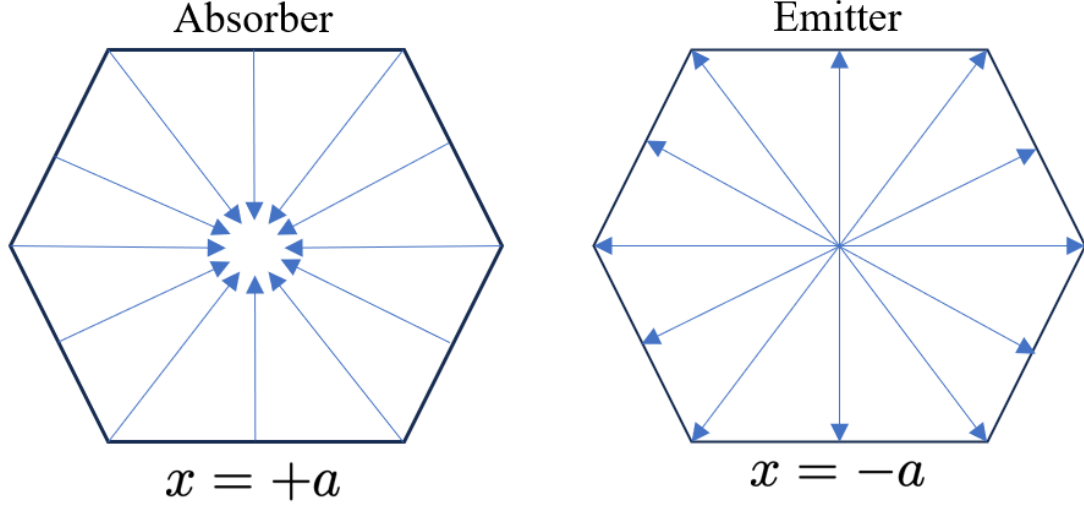


Figure 1.5: The figure shows a cartoon of a source (an emitter) and a sink (an absorber). Under time reversal \mathcal{T} source becomes sink and sink becomes source. And under spatial reflection \mathcal{P} the systems change their position from $x \rightarrow -x$. Thus the system is \mathcal{PT} symmetric

and its connection to \mathcal{PT} symmetry, following Bender [52, 56], is to consider a total composite system where one subsystem involves the non-isolated system with gain (or loss) and another subsystem which is a time reverse of the first system. The net flux of probability is equal but exactly opposite to the original system, i.e. if one system has a gain (or loss), the other system involves equal but opposite loss (or gain). The full system thus has no net probability flux due to the balanced loss-gain. Under time reversal \mathcal{T} , loss becomes gain and gain becomes loss and under parity \mathcal{P} , the two subsystems are exchanged, see Fig. (1.5) for a cartoon representation of a \mathcal{PT} symmetric physical system.

Example 1:

To demonstrate the example of a \mathcal{PT} symmetric system, consider a 1×1 matrix Hamiltonian given by [52]

$$H = [c + id] \quad (1.50)$$

where $c, d \in \mathbb{R}$, are constants. The Hamiltonian is complex and non-hermitian if $d \neq 0$. The solution to the time dependent Schrödinger equation is given by

$$\psi = C e^{(-ci+dt)t} \quad (1.51)$$

where C is an integration constant. The probability is given by

$$\rho = |C|^2 e^{2dt}. \quad (1.52)$$

The probability grows exponentially in time if $d > 0$ and decays if $d < 0$. This Hamiltonian is not \mathcal{PT} symmetric. Now considering the time reversed counterpart of H

$$H_{\text{Treverse}} = [c - id] \quad (1.53)$$

The probability of the time reversed state is then

$$\rho = |D|^2 e^{-2dt} \quad (1.54)$$

The probability of the time reversed Hamiltonian decays in time when $d > 0$ and grows exponentially for $d < 0$. The composite system can be written as 2×2 matrix

$$H_{\text{composite}} = \begin{bmatrix} c + id & 0 \\ 0 & c - id \end{bmatrix} \quad (1.55)$$

Note that the above matrix is non-hermitian because $H_{\text{composite}}^\dagger \neq H_{\text{composite}}$, but it is \mathcal{PT} symmetric, where the \mathcal{P} operation that exchanges two subsystems is given by

$$\mathcal{P} = \begin{bmatrix} 0 & 1 \\ 1 & 0 \end{bmatrix}. \quad (1.56)$$

Thus,

$$\mathcal{PT}H_{\text{composite}}(\mathcal{PT})^{-1} = H_{\text{composite}} \quad (1.57)$$

Hence, even though the composite Hamiltonian is non-hermitian, it is \mathcal{PT} symmetric. For this system, even though the gain and loss of probability are balanced, the composite system is not in dynamic equilibrium because probability grows in one subsystem and decays in the other subsystem with time. One has to couple the two subsystems for the probability to readily flow from one to the other so that the system may be in dynamic equilibrium. If the composite system is in dynamic equilibrium, it is said to be in an unbroken \mathcal{PT} symmetric phase, and if the system is not in equilibrium it is said to be in a broken \mathcal{PT} symmetric phase.

The composite Hamiltonian with a coupling parameter γ in the off-diagonal elements can be written as

$$H_{\text{coupled}} = \begin{bmatrix} c + id & \gamma \\ \gamma & c - id \end{bmatrix} \quad (1.58)$$

The coupled Hamiltonian is non-hermitian ($H^\dagger \neq H$) but \mathcal{PT} symmetric

$$\mathcal{PT}H_{\text{coupled}}(\mathcal{PT})^{-1} = H_{\text{coupled}} \quad (1.59)$$

The energy eigenvalues of the coupled Hamiltonian can be evaluated using the characteristic polynomial

$$\det(H - \lambda I) = \lambda^2 - 2c\lambda + c^2 + d^2 - \gamma^2 = 0 \quad (1.60)$$

Thus the eigenvalues are the roots of this equation, and are given by

$$\lambda_{\pm} = c \pm \sqrt{\gamma^2 - d^2}. \quad (1.61)$$

1.4.3 \mathcal{PT} transition

In the above example, if the coupling $\gamma^2 > d^2$, the spectrum is real and the system is in the \mathcal{PT} symmetric phase and if $\gamma^2 < d^2$, the energy eigenvalues are complex conjugates of each other and the system is said to be in a *broken* \mathcal{PT} symmetric phase. The $\gamma^2 > d^2$ case is termed as the strongly coupled regime and the $\gamma^2 < d^2$ case is called the weakly coupled regime. This is an elementary example of a \mathcal{PT} phase transition. When $\gamma = \pm d$, at the critical point of the \mathcal{PT} transition, two real eigenvalues merge and become complex.

The critical points at which the eigenvalues cross are termed as the exceptional points. Exceptional points set the boundary between unbroken \mathcal{PT} phases and \mathcal{PT} broken phases. Such \mathcal{PT} phase transitions appear in higher dimensional quantum systems [57, 58, 61–63], optics [59, 60], simple mechanical systems, in polymers such as unzipping of DNA [66], analogue Hawking radiation [68], deconfinement to confinement transitions in QCD [64], superconductivity [67], systems with complex magnetic fields [63, 67] etc. Apart from theoretical studies, \mathcal{PT} phase transitions have also been realized experimentally in simple mechanical systems [56], optics [55, 69], electrical circuits [70] etc.

In chapter 2 of this thesis, we show that as we tune the strength of the inverse square potential, the boundary coupling exhibits an analogous \mathcal{PT} transition in the complex plane. The RG fixed point merger of the boundary coupling is analogous to a \mathcal{PT} transition in the complex plane, where the sub-critical case has two real fixed points that merge at the critical strength of the inverse square potential $\alpha_c = 1/4$, and become complex as the system becomes super-critical, breaking \mathcal{PT} symmetry. It is the boundary condition that can be non-hermitian in this case. In chapter 4 we show that Schwinger pair production is described by a similar non-hermitian boundary condition for the IHO that breaks \mathcal{PT} symmetry.

1.5 Introduction to Schwinger pair production

The instability of the vacuum due to external electric fields is termed as Schwinger pair production. The Klein-Gordon equation in the presence of an external static constant

electric field, for a given mode, can be described by an effective IHO Schrödinger equation that exhibits instability of the vacuum. This elementary process of particle creation in quantum field theory has a long history dating at least back to 1931, when F. Sauter computed the pair production probability [71]:

$$P_{\text{pair}} = e^{-\pi m^2 c^3 / q \mathcal{E} \hbar} \quad (1.62)$$

using the Dirac equation in the presence of an electric field \mathcal{E} , where q is the charge and m is the mass of the particles. The above pair production formula is nonperturbative in strength of electric field \mathcal{E} . The exponent in the pair production formula involves the ratio of rest mass energy to the work done by the electric field over a Compton wavelength :

$$q \mathcal{E} \frac{\hbar}{mc} = 2mc^2 \quad (1.63)$$

The critical value of the electric field $\mathcal{E}_c = 2m^2 c^3 / q \hbar \sim 10^{18} \text{V/m}$, is now called the Schwinger limit. After writing the above formula for pair production, Sauter in his 1931 paper states as follows:

This agrees with the conjecture made by N. Bohr that was given in the introduction, that one first obtains the finite probability for the transition of an electron into the region of negative impulse when the potential ramp $\mathcal{E} \hbar / mc$ over a distance of Compton wavelength \hbar / mc has the order of magnitude of the rest mass energy...this case would correspond to around 10^{16}V/cm . - Sauter [71]

The constant electric field result for pair production was further put into an effective field theory setting by Euler and Heisenberg, the translated version of the paper in English is given in [72]. Further, in 1951 Schwinger formulated the theory of vacuum polarization in the language of renormalized QED in his seminal paper [74]. For a comprehensive history of Schwinger pair production see the review by Gerald Dunne [73]. Owing to the astronomically huge value of the Schwinger limit, this phenomenon has not yet been experimentally realized. However, there has been progress in the field of strong laser fields and extreme light infrastructure [75, 76, 82]. Schwinger pair production has been studied in various forms such as with inhomogeneous fields, time dependent pulses and the dynamical Schwinger effect. Moreover, enormous interest has also emerged in studying Schwinger pair production in analogue systems such as Landau-Zener transitions in atomic systems [80], cold atom systems, trapped ions, graphene [77–79] and other condensed matter systems [81].

In this thesis, chapter 4 discusses the study of Schwinger pair production using non-hermitian quantum mechanics. In non-relativistic quantum mechanics, usually one

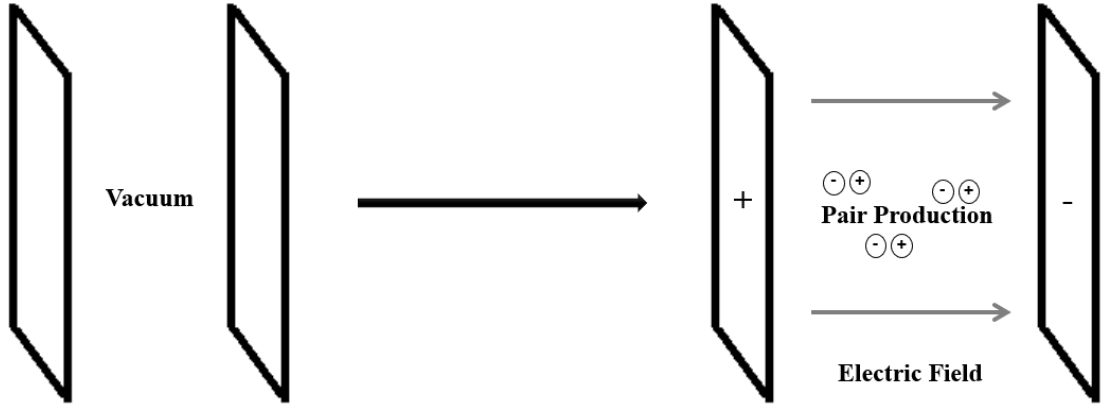


Figure 1.6: The figure shows a cartoon of production of particle antiparticle pairs from the vacuum in the presence of an electric field.

does not encounter pair creation. However, using non-hermitian quantum mechanics one can address the issues of non-unitary physics and probability loss/gain as we discussed in the previous section. Each mode of the Klein-Gordon theory in the presence of a static electric field can be mapped to an IHO Schrödinger equation. The question we answer in this thesis is what boundary condition is necessary for the IHO to describe pair production.

The constant field pair production involves an electric field extending over infinite distances, which is in some sense an unrealistic scenario. Thinking of a realistic experiment, physically, one has to turn on and off the electric field over a finite distance D . We implement a non-hermitian boundary condition using the PPEFT framework, which is a linear (Robin) boundary condition (as given in Eq. (1.39) in section 1.3.2) evaluated at long distance cut-off L which satisfies $a \ll L \ll D$, where a is the length scale set by the pair production process: $a = 2mc^2/q\mathcal{E}$. We renormalize the boundary coupling so that the arbitrary cut-off L drops out of the physical predictions and we show that Schwinger's constant field result emerges at the scale invariant RG fixed point. When away from the fixed point the RG flow of the IHO boundary coupling exhibits a limit cycle behaviour in the complex plane, suggesting that certain observables like current correlation function can exhibit periodic (faster than log periodic) behaviour as a function of system size or electric field.

FALL TO THE CENTRE AS A \mathcal{PT} TRANSITION

Sriram Sundaram, C. P. Burgess, and D. H. J. O'Dell

Fall-to-the-centre as a \mathcal{PT} symmetry breaking transition

J Phys.: Conf. Ser **2038**, 012024 (2021).

DOI: 10.1088/1742-6596/2038/1/012024

Published under licence by IOP Publishing Ltd.

In this paper we discuss the quantum mechanics of an attractive inverse square potential in 1D using the methods of PPEFT. As discussed in section 1.1.2 of the introduction, tuning the strength of the inverse square potential $\alpha > \alpha_c = 1/4$, the system becomes unstable wherein the Hamiltonian becomes unbounded from below and admits infinite negative energy states. We show that this transition is an example of a \mathcal{PT} symmetry breaking transition. The $\alpha < 1/4$ case is termed as the sub-critical case and $\alpha > 1/4$ is termed as the super-critical case.

In this paper we use methods of PPEFT as developed by Burgess et.al [1] to implement appropriate boundary conditions, which turn out to be Robin type (linear) boundary conditions at the origin that dominate at low energies. The boundary condition is unitary if the coupling is real and is non-unitary if the coupling is complex. The specification of the boundary condition near the origin in general breaks the continuous scaling symmetry of the inverse square potential, in an elementary example of a scale anomaly. The boundary coupling evaluated at a short distance cut-off needs to be renormalized in the spirit of RG so that physical predictions are independent of the arbitrary cut-off. In this paper we compute the beta function for the boundary

coupling and show that the character of the RG flow changes as one goes from the sub-critical case with two real fixed points (\mathcal{PT} symmetric phase) to a limit cycle type RG flow in the super-critical case, with imaginary fixed points (\mathcal{PT} broken phase).

PAPER • OPEN ACCESS

Fall-to-the-centre as a PT symmetry breaking transition

To cite this article: Sriram Sundaram *et al* 2021 *J. Phys.: Conf. Ser.* **2038** 012024

View the [article online](#) for updates and enhancements.

You may also like

- [Protection of entanglement in two independently decohering qubits via local prior and post parity-time symmetry operations](#)

Wen-Juan Li and Yang Leng

- [Generation and enhancement of sum sideband in a parity-time-symmetric optomechanical system](#)

Shi Rao and Yanxia Huang



The Electrochemical Society

Advancing solid state & electrochemical science & technology

DISCOVER
how sustainability
intersects with
electrochemistry & solid
state science research



Fall-to-the-centre as a \mathcal{PT} symmetry breaking transition

Sriram Sundaram¹, C P Burgess^{1,2} and Duncan H J O'Dell¹

¹ Department of Physics and Astronomy, McMaster University, 1280 Main St. W., Hamilton, Ontario, Canada, L8S 4M1

² Perimeter Institute for Theoretical Physics, 31 Caroline St. N., Waterloo, Ontario, Canada, N2L 2Y5

E-mail: dodell@mcmaster.ca

Abstract. The attractive inverse square potential arises in a number of physical problems such as a dipole interacting with a charged wire, the Efimov effect, the Calgero-Sutherland model, near-horizon black hole physics and the optics of Maxwell fisheye lenses. Proper formulation of the inverse-square problem requires specification of a boundary condition (regulator) at the origin representing short-range physics not included in the inverse square potential and this generically breaks the Hamiltonian's continuous scale invariance in an elementary example of a quantum anomaly. The system's spectrum qualitatively changes at a critical value of the inverse-square coupling, and we here point out that the transition at this critical potential strength can be regarded as an example of a \mathcal{PT} symmetry breaking transition. In particular, we use point particle effective field theory (PPEFT), as developed by Burgess *et al* [1], to characterize the renormalization group (RG) evolution of the boundary coupling under rescalings. While many studies choose boundary conditions to ensure the system is unitary, these RG methods allow us to systematically handle the richer case of nonunitary physics describing a source or sink at the origin (such as is appropriate for the charged wire or black hole applications). From this point of view the RG flow changes character at the critical inverse-square coupling, transitioning from a sub-critical regime with evolution between two real, unitary fixed points (\mathcal{PT} symmetric phase) to a super-critical regime with imaginary, dissipative fixed points (\mathcal{PT} symmetry broken phase) that represent perfect-sink and perfect-source boundary conditions, around which the flow executes limit-cycle evolution.

1. Introduction

In the presence of an attractive $1/r$ potential a classical particle will follow either an elliptic, hyperbolic or parabolic trajectory. However, in more singular potentials the particle can exhibit a new type of behaviour where it spirals down onto the origin, a phenomenon called “fall to the centre” [2, 3, 4]. The least singular potential where this occurs is the attractive inverse square potential $-g/r^2$ which has precisely the same radial dependence as the centrifugal barrier and hence can overcome it for large enough g .

The behaviour of quantum particles in an attractive inverse square potential has been studied in an experiment by Denschlag, Umshauss and Schmiedmayer [5] who scattered cold lithium atoms from a thin (radius $\sim 1\mu\text{m}$) charged wire and observed fall to the centre. The existence of the inverse square potential in this case is easily understood: consider a neutral but polarizable atom interacting with a charged wire; the radial electric field \mathcal{E} emanating from the wire falls



Content from this work may be used under the terms of the [Creative Commons Attribution 3.0 licence](https://creativecommons.org/licenses/by/3.0/). Any further distribution of this work must maintain attribution to the author(s) and the title of the work, journal citation and DOI.

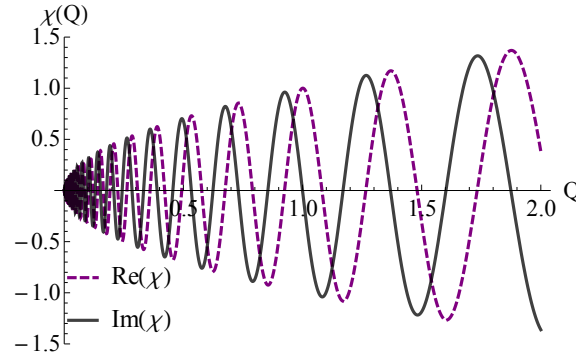


Figure 1. The wavefunction $Q^{-i|\sigma|+1/2} = Q^{1/2}e^{-i|\sigma|\log Q}$ in the supercritical regime with $|\sigma| = 20$. Note the logarithmic phase singularity at $Q = 0$ where the phase is undefined because it oscillates so fast it takes all values at once. The purple dashed line shows the real part and the black solid line shows the imaginary part.

off as $1/r$ and induces a dipole moment d in the particle that in the linear response regime is proportional to the strength of the field. The interaction energy $-(1/2)d\mathcal{E}$ between the atom and the wire must then go as the inverse square $-1/r^2$ of the distance between the atom and the wire. The Schrödinger equation describing this situation takes the form

$$-\frac{\hbar^2}{2m} \frac{\partial^2 \psi}{\partial Q^2} - \frac{g}{Q^2} \psi = i\hbar \frac{\partial \psi}{\partial t} \quad (1)$$

(since in this paper we will only consider one-dimensional problems we have replaced the radial coordinate r with the coordinate Q which lies in the range $-\infty \leq Q \leq \infty$). Other physical situations where the inverse square potential appears include the Efimov effect (a counter-intuitive family of bound states of three particles with an infinite bound state spectrum given by a geometric series) [6, 7, 8, 9, 10, 11, 12, 13, 14, 15, 16, 17], Calogero-Sutherland models [18], and near the event horizon of black holes [19, 20, 21]. Analogue inverse square potentials also appear in various ways in optics, such as in the optical coherence of sunlight [22], and in Maxwell fisheye lenses where the refractive index takes an inverse square form [23, 24, 25].

The peculiar properties of inverse square potentials in quantum mechanics have been widely discussed in the literature, and good introductions can be found in Refs. [26, 27]. The key feature of Eq. (1) is that it is scale invariant under joint continuous scaling of space and time, $Q \rightarrow sQ$ and $t \rightarrow s^2t$. This means that, unlike the Coulomb potential where the Bohr radius provides a length scale, there is no natural length scale in the inverse square problem. Indeed, even if we consider the one dimensional case (as we do here) such that there is no centrifugal barrier, the system is still saved from collapse in the Coulomb case by the zero-point kinetic energy $\sim \frac{\hbar^2}{2ma^2}$ associated with a state of size a beating the potential energy $-\frac{q_1q_2}{4\pi\epsilon_0 a}$ at small enough a . The same is *not* true in the inverse square case where both the zero-point energy and the potential scale in the same way. In fact, if we can find one solution of Eq. (1) then we have found an infinite family of them related by s . Thus, if we can find one bound state with (negative) energy E then there is a continuum of bound states s^2E with every possible negative energy and the spectrum is therefore unbounded from below.

Despite this pathology, Eq. (1) has exact stationary solutions $\psi(Q, t) = \chi(Q) \exp(-iEt/\hbar)$, where $\chi(Q)$ are Hankel functions in the case of scattering states ($E > 0$) and modified Bessel functions in the case of bound states ($E < 0$). The problem lies, however, in finding appropriate

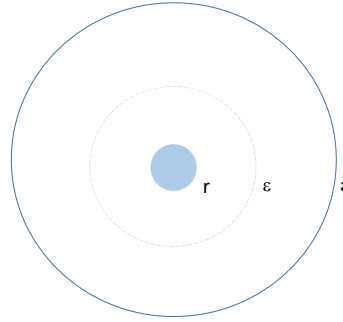


Figure 2. A figurative illustration of the hierarchy of length scales in the regularization of the fall-to-the-centre problem. The length a is the scale we have access to in experiments which is very large compared to the regulator scale ϵ which is in turn very large compared to r , the size of the source located at the origin, i.e. $r \ll \epsilon \ll a$. The boundary condition is derived using the PPEFT action that describes the properties of the source at the regulator scale ϵ (which is arbitrary). Renormalizing the source-bulk coupling ensures that physical predictions at scale a are independent of the regulator ϵ .

boundary conditions, i.e. the linear combination of these solutions that describes a particular physical situation. In the Coulomb problem we are able to choose one of the two linearly independent solutions to the radial equation simply by its asymptotic behaviour: at small distances where the centrifugal barrier dominates, the solution to the hydrogenic radial equation with angular momentum quantum number l (an integer) takes the form

$$u(r) = A r^{l+1} + B r^{-l} \quad (2)$$

and since r^{-l} blows up as $r \rightarrow 0$ (assuming $l \neq 0$) we can set $B = 0$ without further thought. The same logic cannot in general be applied to the inverse square potential. At small distances where we can ignore the eigenvalue E in comparison to the other terms in the eigenvalue equation, the solutions are of the form

$$\chi(Q) = C_+ Q^{1/2+\sigma} + C_- Q^{1/2-\sigma} \quad (3)$$

where $\sigma = \sqrt{1/4 - \alpha}$ and $\alpha \equiv 2mg/\hbar^2$. Defining $\alpha_c \equiv 1/4$, which is the critical value at which fall to the centre first takes place, we see that when $\alpha < \alpha_c$ (subcritical regime) the two solutions are distinguishable in terms of their behaviour as $Q \rightarrow 0$, but when $\alpha > \alpha_c$ (supercritical regime) the modulus of both solutions is identical and they only differ by a phase (see Figure 1), and there is no simple criterion like boundedness at the origin for choosing one solution over the other. Clearly we need to supply a boundary condition to fix the ratio C_+/C_- ; the fact we did not need to do this in the Coulomb case is a reflection of the latter's rather special properties (superintegrability). Furthermore, the logarithmic phase divergence present in both solutions in Eq. (3) indicates that our problem is missing some physics near the origin.

A resolution to these issues is suggested by the atom-wire problem. The inverse square potential is merely the long range behaviour of the atom-wire interaction and when they approach closely the fact that the wire has a finite width becomes important. This introduces the microscopic length scale r (the radius of the wire), see Figure 2, that provides a short-distance cut-off that regulates the singularity in the inverse square potential and breaks the continuous scaling symmetry. The breaking of classical continuous scale invariance in a quantum theory is termed a *scale anomaly* [26]. Although anomalies were originally conceived in the context of particle physics, they have recently been realized in ultracold atomic systems through the Efimov

effect [9, 10, 11, 12, 13, 14, 15, 16, 17], and frequency shifts of breathing modes in trapped 2D Fermi gases [28, 29, 30, 31, 32, 33]. A scale anomaly has also been observed in graphene where the relativistic nature of the dispersion relation means that it is the Coulomb potential that leads to a scale invariant system in that case [34].

The ‘high-energy’ physics at the microscopic length scale r might be complicated, and we might even be ignorant of its detailed form, but if all we can observe is the low-energy behaviour at large distances then we can treat the problem using the techniques of effective field theory which provide systematic methods for regulating the theory. The version that we apply in this paper is known as point particle effective field theory (PPEFT) and allows us to specify the boundary condition in an intuitive and physical way through the presence of an imagined point ‘particle’ that sits the origin [1, 35]. The theory is conveniently formulated in terms of the action $S_{\text{total}} = S_B + S_p$, where S_B is the action for the ‘bulk’ field χ that has Eq. (1) as its equation of motion, and S_p is the point particle effective action that describes the microscopic physics localized at the origin and how it couples to the bulk field. In this paper we will review the application of PPEFT to the inverse square problem and confirm that at lowest order the effect of the microscopic physics on the inverse square problem is simply to add a *compulsory* Dirac δ -function to Eq. (1) so that the time-independent Schrödinger equation reads

$$-\frac{d^2\chi}{dQ^2} - \frac{\alpha}{Q^2}\chi + \lambda\delta(Q)\chi = k^2\chi \quad (4)$$

where $k^2 = 2mE/\hbar^2$. By integrating this equation over an infinitesimal range $-\epsilon < Q < \epsilon$ we can see that the value of the coupling constant λ determines the jump in gradient of χ at the origin and provides the necessary boundary condition at the origin. This boundary condition is unitary (with hermitian Hamiltonian) when λ is real, but is generically not unitary if λ is complex.

The boundary condition fixes the ratio of integration constants, C_+/C_- , and this ratio determines the problem’s intrinsic length scale: the ratio of the solutions in Eq. (3) gives the length scale $L = (C_+/C_-)^{-\frac{1}{2\sigma}}$ which breaks the scale invariance as long as both C_+ and C_- are finite. In this picture the coupling λ is to be regarded as depending on the position ϵ at which the boundary condition is imposed in such a way as to ensure that the physical scale C_+/C_- remains fixed. This defines a renormalization-group (RG) flow for λ under scale transformations. The interpretation of this flow is clearest when σ is real, i.e. $\alpha < \alpha_c$. Through the boundary condition λ controls the relative weight of the two solutions $Q^{1/2\pm\sigma}$ at $Q = \pm\epsilon$. This relative weight changes as Q changes, with the $Q^{1/2+\sigma}$ solution eventually dominating at large length scales, corresponding to an infrared (IR) fixed point for which the wavefunction will become scale invariant. In other words, we flow towards a scale invariant IR fixed point associated with $C_- = 0$. Conversely, in the opposite ultraviolet (UV) limit we have a scale invariant fixed point for which $Q^{1/2-\sigma}$ dominates, associated with $C_+ = 0$. These simple arguments will be made more concrete in the rest of this paper, but the upshot is that λ depends on the energy/length scale of our observations, i.e. undergoes renormalization [36, 26, 21, 37, 38, 39, 1].

The full renormalization group (RG) flow of λ with scale is nonlinear. In the subcritical regime there are two fixed points where the solution is scale invariant, as argued above. The UV fixed point is unstable, the IR one is stable, and the flow between them can in general pass through complex values of λ (see Figures 3 and 4) so that the Hamiltonian in Eq. (4) is generically non-hermitian, although in the special case where the flow starts on the real axis λ will always remain real. Either way, all trajectories in the subcritical regime eventually tend to the real value of λ at the IR fixed point. However, as α increases the two fixed points approach one another and merge exactly at $\alpha = \alpha_c$; thereafter they proceed to evolve as complex conjugates in the complex plane [38]. This heralds a topological change in the RG flow such that the trajectories become limit cycles that can never reach the fixed points, see Figure 4. The evolution of λ along

a limit cycle is periodic on a logarithmic scale and this implies that in the supercritical regime continuous scale invariance is broken in favour of a discrete version (quantum anomaly). This is the explanation for the geometric series bound state spectrum found in the Efimov problem [8], although the Efimov case is exceptional because λ is real and this corresponds to a self-adjoint extension of the original inverse square problem. The general case again corresponds to complex values of λ that give a complex extension of the supercritical inverse square problem and have been used to describe inelastic scattering [39] and the absorption of particles on a charged wire [35]. Close examination of the trajectories in Figure 4 shows that the flow near the real λ axis in the supercritical regime is unstable because it forms a separatrix between trajectories in the upper and lower half planes such that a small deviation can lead to very different flow (around one fixed point or the other). In fact, the closer the trajectory approaches the real axis during that part of its motion, the further it gets swept away during the rest. Of the two complex stationary points, one corresponds to a perfect absorber of probability, and the other a perfect emitter of probability.

One of the articles of faith of quantum mechanics used to be that the Hamiltonian should be hermitian: this leads to a real energy spectrum and guarantees unitary time evolution where probability is preserved. However, starting in 1998 it was pointed out by Bender and coworkers [40, 41, 42] that non-hermitian Hamiltonians possessing \mathcal{PT} symmetry can have exclusively real eigenvalues. \mathcal{P} is the parity operator that effects the transformation $Q \rightarrow -Q$, and \mathcal{T} is the time-reversal operator that effects the transformations $t \rightarrow -t$ and $i \rightarrow -i$. Furthermore, there exists a phase transition as a function of a parameter where some of the eigenstates spontaneously break \mathcal{PT} symmetry and the corresponding eigenvalues become complex. This observation has led to an explosion of interest in non-hermitian Hamiltonians in quantum mechanics [43, 44, 45, 46, 47, 48, 49, 50, 51], and optics [52, 53, 54, 55, 56], including experimental confirmation [57, 58, 59, 60].

In a far-sighted paper on RG fixed point mergers, Kaplan *et al.* [38] point out that the Berezinskii-Kosterlitz-Thouless (BKT) phase transition (vortex-antivortex pair unbinding transition) is also an example of a phase transition where conformal scaling is lost when two real fixed points merge and enter the complex plane, exactly as happens in the inverse square potential problem. In this paper we also focus on the behaviour of the fixed points of the RG flow and suggest that it is analogous to Bender's \mathcal{PT} symmetry breaking transition. Indeed, the Hamiltonian in Eq. (4) is typically non-hermitian and undergoes a transition as a function of the parameter α from the subcritical regime, where the flow is organized by real fixed points, to the supercritical regime where it is organized by complex ones. Whereas the real fixed points display \mathcal{T} symmetry, this is broken when they become complex (one representing a source, the other a sink of probability). The eigenfunctions $Q^{1/2 \pm \sigma}$ also change their nature when $\alpha > \alpha_c$, going from being real to complex and developing a phase singularity at the origin. While not all aspects of the connection are clear to us at the time of writing (such as the role of \mathcal{P}) the basic scenarios are similar enough to warrant investigation.

The rest of this paper is organized as follows : in Section 2 we recapitulate the inverse square Hamiltonian and mention a few points not already covered in the Introduction. In Section 3 we introduce PPEFT and use it to derive a boundary condition due to a microscopic 'source' at the origin, and apply this boundary condition in Section 4 to analyze the continuity equation governing probability conservation, and in Section 5 to the 'bulk' wavefunction in both the sub- and supercritical regimes. Since the wavefunction is singular at the source, we implement renormalization of the effective source-bulk coupling in Section 6 that leads to the emergence of a scale anomaly. We also calculate the reflection and transmission probabilities; as these are observable physical quantities they should remain invariant under the RG flow. Our expressions for the reflection and transmission probabilities are therefore expressed in terms of RG invariant parameters. We finish with some perspectives and conclusions in Section 7. Note that in the

rest of this paper we specialize to the wavefunction in the scattering regime ($E > 0$). However, this leads to the same basic critical behaviour and RG flow as the bound state case ($E < 0$).

2. Hamiltonian for the inverse square problem

The Hamiltonian we will work with is given by

$$H = \frac{P^2}{2m} - \frac{g}{Q^2}. \quad (5)$$

As noted above, both the potential and the kinetic energy scale in the same way, and this holds true in any dimension, unlike, say, δ -function interactions which only scale in this way in two dimensions (in this paper we consider the 1D case). Classically, the conserved quantity corresponding to the continuous scale invariance of the inverse square Hamiltonian is the generator of the scale transformations $D = QP$,

$$\frac{dD}{dt} = 2H \quad (6)$$

which is conserved if energy is zero, and is sometimes termed an *almost* conservation law [61]. In terms of the dimensionless parameter $\alpha = 2mg/\hbar^2$, fall to the centre occurs when $\alpha > \alpha_c = 1/4$ (supercritical regime). In this regime neither the boundedness of the Hamiltonian nor normalizability turn out to be good criteria for selecting either one of the two eigenfunctions over the other, as demonstrated by Burgess *et al.* in [1]. Furthermore, the energy in the supercritical regime is unbounded from below. This is demonstrated explicitly in Ref. [36] by using a cleverly chosen trial wavefunction to show that

$$\alpha \int \frac{|\chi(Q)|^2}{Q^2} dQ > \int |\chi'(Q)|^2 dQ \quad (7)$$

when $\alpha > \alpha_c$. In 3D, the classical dynamics in the supercritical case gives rise to an unstable trajectory which spirals to the centre.

According to von Neumann's theorem, when a Hamiltonian is essentially self-adjoint the eigenvalue problem is mathematically well-posed. When the Hamiltonian is not self-adjoint one can attempt to prune the unsavoury parts by applying a self-adjoint extension. It turns out that the inverse square problem is only self-adjoint for the strongly repulsive case and is not self-adjoint for any attractive potential, i.e. when $\alpha > 0$. While self-adjoint extensions can be applied in both the sub- and supercritical cases (like in the Efimov problem which is in the supercritical regime), they are not unique and so there is some arbitrariness involved [62]. Furthermore, they do not necessarily remove the problem of unboundedness from below [36, 63, 64]. In the next section we introduce the PPEFT method which uses a source particle at the origin as a transparent way of choosing an appropriate boundary condition [1]. The source could be unitary (self-adjoint extension) or nonunitary (complex extension), either of which could be physically acceptable, depending on the situation. When combined with renormalization the results are independent of the regulator. PPEFT gives the same results as other methods (in particular, it also does not remove unboundedness from below), but has the advantage of being intuitive and systematic.

3. Point particle effective field theory and boundary condition

PPEFT starts from an action and this allows us to specify the physics and symmetries of the problem rather than imposing an arbitrary cut-off. The total action is written as $S_{\text{total}} = S_B + S_p$,

where S_B is the action for the Schrödinger bulk field $\chi(Q)$ describing the long distance, low energy physics, and is given by

$$S_B = \int dt dQ \left[\frac{i\hbar}{2} (\chi^* \partial_t \chi - \chi \partial_t \chi^*) - \left(\frac{\hbar^2}{2m} |\nabla \chi|^2 + V(Q) |\chi|^2 \right) \right] \quad (8)$$

with $V(Q) = -\frac{g}{Q^2}$, and S_p is the action describing the coupling between the bulk field and the microscopic (short distance, high energy) source localized around $Q = 0$

$$S_p = \int dt dQ \mathcal{L}_p(\chi^*, \chi) \delta(Q). \quad (9)$$

The key to PPEFT is a series expansion of the lagrangian density $\mathcal{L}_p(\chi^*, \chi) = -h\chi^*\chi + \dots$ where higher terms contain higher powers of χ and χ^* and/or their derivatives. This can be viewed as analogous to a multipole expansion where successive terms build in more information about the source but are less important at large distances. Thus, the coupling h can be considered to be the ‘monopole’ moment, and since each term must have the same total dimension, the multipole moments of higher terms will have correspondingly higher dimensions. Referring to Figure 2, the relevant scale for the source particle is r and therefore the higher order moments will generically be proportional to r/a raised to some power and hence smaller, allowing us to build in finer details about source-bulk coupling in a controlled fashion. In this paper we will not use the full power of PPEFT and will only retain the leading term meaning that we have just one coupling parameter h .

The field equations can be obtained by extremizing the action $\delta S = 0$, to obtain the time dependent Schrödinger equation

$$\left(-\frac{\partial^2}{\partial Q^2} + U(Q) \right) \chi = i \frac{2m}{\hbar} \frac{\partial \chi}{\partial t} \quad (10)$$

with

$$U(Q) = -\frac{\alpha}{Q^2} + \lambda \delta(Q), \quad (11)$$

where $\lambda = 2mh/\hbar^2$ is the redefined source-bulk coupling constant. We see that the point particle effective action has modified the potential $V(Q)$ by adding a Dirac δ -function, as previously claimed in Eq. (4).

The boundary condition is obtained by integrating the Schrödinger equation over the infinitesimal region $-\epsilon \leq Q \leq \epsilon$, which gives

$$\lambda = \left[\frac{\partial \ln(\chi)}{\partial Q} \right]_{Q=-\epsilon}^{Q=\epsilon}. \quad (12)$$

The length scale ϵ is a cut-off or regulator which should be much shorter than the observable length scale a , but much larger than the size of the source r located at the origin because the PPEFT action does not converge at distances where $\epsilon \approx r$. In other words, we need the hierarchy $a \gg \epsilon \gg r$ to be obeyed [see Fig. 2]. Furthermore, physical observables like reflection and transmission probabilities should both be finite and independent of the regularization scale ϵ , and this is where renormalization of the source-bulk coupling λ comes in. However, before coming to the renormalization there are two other tasks we can accomplish using the boundary condition given in (12). The first is to use it in combination with the continuity equation to analyze probability conservation and the second is to apply it to the wavefunction.

4. Continuity equation

The continuity equation is a basic tool for analyzing probability conservation. In a hermitian system we expect probability to be conserved, but in a nonhermitian system such basic properties can be violated. In this section we show how probability conservation is determined by the source-bulk coupling constant λ by evaluating the probability current at the boundaries $Q = \pm\epsilon$.

Proceeding from the Schrödinger equation and its complex conjugate in the usual way we find the continuity equation

$$\partial_t \rho + \nabla \cdot J = \frac{2}{\hbar} \rho \Im \left[-\frac{g}{Q^2} + \frac{\hbar^2 \lambda}{2m} \delta(Q) \right] \quad (13)$$

where ρ is the probability density, and J is the standard probability current

$$J = \frac{i\hbar}{2m} (\chi \partial_Q \chi^* - \chi^* \partial_Q \chi). \quad (14)$$

The term in the square brackets in Eq. (13) is the total potential term in the Schrödinger equation. Since g is assumed to be real, the first term will make no contribution, but the second term will if λ is complex.

The boundary condition Eq. (12) can be used to calculate the net probability current out of the origin

$$J(\epsilon) - J(-\epsilon) = \frac{i\hbar}{2m} (\lambda^* - \lambda) \chi^*(\epsilon) \chi(\epsilon). \quad (15)$$

We can therefore refine our condition for probability conservation violation to saying that λ must be complex (nonhermitian Hamiltonian) and the probability for finding the particle at the source must be nonzero. The origin will be a sink if $\Im(\lambda) < 0$ or a source if $\Im(\lambda) > 0$, as pointed out in [35].

5. Wavefunction of the inverse square Hamiltonian in 1D and the boundary condition

The time-independent Schrödinger equation with energy eigenvalue $E = \hbar^2 k^2 / 2m > 0$ and purely inverse square potential is given by

$$\left(-\frac{d^2}{dQ^2} - \frac{\alpha}{Q^2} \right) \chi(Q) = k^2 \chi(Q). \quad (16)$$

Putting $z = kQ$ and $\chi(Q) = \sqrt{z} u(z)$, this is transformed to the Hankel differential equation

$$z^2 u'' + zu' + (z^2 - \sigma^2) u = 0 \quad (17)$$

where $\sigma^2 = 1/4 - \alpha$. The parameter σ is real in the subcritical regime, but in the supercritical regime it is an imaginary number which we write as $\sigma = \pm i\zeta$, where $\zeta \in \mathbb{R}$. It is notable that, unlike σ^2 , the eigenvalue k^2 does not appear as an explicit parameter in Eq. (17) but instead occurs only as a scaling factor in the argument of the solutions. We also note in passing that the Hankel differential equation is invariant under $z \rightarrow -z$, i.e. under parity \mathcal{P} , and also under $\sigma \rightarrow -\sigma$.

The independent solutions to the Hankel equation are the two Hankel functions $H_\sigma^{(1)}(z)$ and $H_\sigma^{(2)}(z)$ whose properties, including asymptotics, are summarized in the Appendix. From these it can be inferred that $H_\sigma^{(1)}(z)$ asymptotes at large z to a right moving wave and $H_\sigma^{(2)}(z)$ asymptotes to a left moving wave. Translating back to the original wavefunction $\chi(Q)$, and assuming an

initial wave coming in from the right, the general solution to the scattering problem can be written as

$$\chi_{\text{in+ref}}(Q) = \sqrt{kQ} \left(H_{\sigma}^{(2)}(kQ) + R H_{\sigma}^{(1)}(kQ) \right), Q \geq \epsilon \quad (18)$$

$$\chi_{\text{trans}}(Q) = T \sqrt{kQ} H_{\sigma}^{(2)}(kQ), Q \leq -\epsilon \quad (19)$$

where, R and T are the reflection and transmission amplitudes to be determined by the boundary condition at $Q = \pm\epsilon$.

5.1. Boundary condition for the subcritical case

In the subcritical case $\sigma \in \mathbb{R}$. We can find a relation between R and T by demanding continuity of the wavefunction near the origin $\chi_{\text{in+ref}}(\epsilon) = \chi_{\text{trans}}(-\epsilon)$, yielding

$$R + iT \exp(i\pi\sigma) = -\frac{H_{\sigma}^{(2)}(k\epsilon)}{H_{\sigma}^{(1)}(k\epsilon)} \quad (20)$$

where we have used the reflection identities of the Hankel functions given in the Appendix. For $k\epsilon \ll 1$, this relation becomes

$$R + iT \exp(i\pi\sigma) \approx \frac{1 - X \exp(i\pi\sigma)}{1 - X \exp(-i\pi\sigma)} \quad (21)$$

where

$$X = \frac{\Gamma(1-\sigma)}{\Gamma(1+\sigma)} \left(\frac{k\epsilon}{2} \right)^{2\sigma}. \quad (22)$$

We now consider the boundary condition given in Eq. (12). When expressed in terms of the scattering solution it reads

$$\lambda = \frac{\partial \ln[\chi_{\text{in+ref}}(\epsilon)]}{\partial Q} - \frac{\partial \ln[\chi_{\text{trans}}(-\epsilon)]}{\partial Q} \quad (23)$$

and we find the following expression for the coupling constant

$$\lambda = \frac{1}{\epsilon} \left(1 - \sigma \left[\frac{1 + X \exp(i\pi\sigma) - R(1 + X \exp(-i\pi\sigma))}{1 - X \exp(i\pi\sigma) - R(1 - X \exp(-i\pi\sigma))} + \frac{1 + X \exp(-i\pi\sigma)}{1 - X \exp(-i\pi\sigma)} \right] \right). \quad (24)$$

In general λ is complex and hence breaks \mathcal{PT} symmetry. However, in this paper we focus on the fixed points of the RG flow and we will show in Section 6 that in the subcritical case the UV and IR fixed points are real and hence preserve \mathcal{PT} symmetry. Expanding Eq. (24) in powers of X in the small $k\epsilon$ regime we obtain

$$\Lambda \approx -2\sigma \left[1 + X \exp(i\pi\sigma) \left(\frac{1 - R \exp(-2i\pi\sigma)}{1 - R} \right) + X \exp(-i\pi\sigma) + \mathcal{O}(X^2) \right] \quad (25)$$

where in order to simplify the expression we have defined

$$\Lambda \equiv 2(\lambda\epsilon - 1). \quad (26)$$

5.2. Boundary condition for the supercritical case

A very similar calculation to that given above can be performed to find the coupling constant λ in the supercritical case, the only difference being that σ is purely imaginary. Of the two possible choices for the square root, we choose $\sigma = -i\zeta$. We find

$$\chi_{\text{in+ref}}(Q) = \frac{\sqrt{kQ} \left(\frac{-(\frac{kQ}{2})^{i\zeta}}{\Gamma(1+i\zeta)} + \frac{\exp(\pi\zeta) (\frac{kQ}{2})^{-i\zeta}}{\Gamma(1-i\zeta)} \right) + R \left(\frac{(\frac{kQ}{2})^{i\zeta}}{\Gamma(1+i\zeta)} - \frac{\exp(-\pi\zeta) (\frac{kQ}{2})^{-i\zeta}}{\Gamma(1-i\zeta)} \right)}{\sinh(\pi\zeta)}, \quad Q \geq \epsilon \quad (27)$$

$$\chi_{\text{trans}}(Q) = \frac{T\sqrt{kQ}}{\sinh(\pi\zeta)} \left(\frac{-1}{\Gamma(1+i\zeta)} \left(\frac{kQ}{2} \right)^{i\zeta} + \frac{\exp(\pi\zeta)}{\Gamma(1-i\zeta)} \left(\frac{kQ}{2} \right)^{-i\zeta} \right), \quad Q \leq -\epsilon. \quad (28)$$

Demanding continuity near the origin yields the relation

$$R + iT \exp(\pi\zeta) = -\frac{H_{-i\zeta}^{(2)}(k\epsilon)}{H_{-i\zeta}^{(1)}(k\epsilon)}. \quad (29)$$

For small $k\epsilon \ll 1$, this relation can be written

$$R + iT \exp(\pi\zeta) \approx \frac{1 - X \exp(\pi\zeta)}{1 - X \exp(-\pi\zeta)}. \quad (30)$$

The coupling constant in the super critical case is then given by :

$$\lambda = \frac{1}{\epsilon} \left(1 + i\zeta \left[\frac{1 + X \exp(\pi\zeta) - R(1 + X \exp(-\pi\zeta))}{1 - X \exp(\pi\zeta) - R(1 - X \exp(-\pi\zeta))} + \frac{1 + X \exp(-\pi\zeta)}{1 - X \exp(-\pi\zeta)} \right] \right) \quad (31)$$

where

$$X = \frac{\Gamma(1-\sigma)}{\Gamma(1+\sigma)} \left(\frac{k\epsilon}{2} \right)^{2\sigma}. \quad (32)$$

Expanding Eq. (31) in powers of X in the small $k\epsilon$ regime we obtain

$$\Lambda \approx 2i\zeta \left[1 + X \exp(\pi\zeta) \left(\frac{1 - R \exp(-2\pi\zeta)}{1 - R} \right) + X \exp(-\pi\zeta) + \mathcal{O}(X^2) \right]. \quad (33)$$

We now proceed to renormalize the source-bulk coupling constant so that the reflection and transmission probabilities do not depend upon the regulator scale ϵ and are finite. We also discuss the fixed point merger of the renormalization group as a \mathcal{PT} symmetry breaking transition as the strength of the inverse square potential α is tuned from the subcritical to supercritical regime.

6. Renormalization group

6.1. Renormalization group and fixed point merger exhibiting a \mathcal{PT} transition

If we blindly let $\epsilon \rightarrow 0$ we run into trouble because the wavefunction develops singularities at small Q [see Eq. (3)]. PPEFT then breaks down because the bulk wavefunction is singular at the source located at $Q = 0$. To deal with this we must renormalize the source-bulk coupling constant λ . Following Ref. [1], we start by writing down the RG flow equation for the coupling constant λ , or more conveniently its close relative $\Lambda = 2(\lambda\epsilon - 1)$. This can be obtained by taking the derivative with respect to ϵ of the above equation for Λ , keeping all observables (such as k) fixed. After some algebra this gives

$$\epsilon \frac{d}{d\epsilon} \left(\frac{\Lambda}{2\sigma} \right) = \sigma \left(1 - \left(\frac{\Lambda}{2\sigma} \right)^2 \right). \quad (34)$$

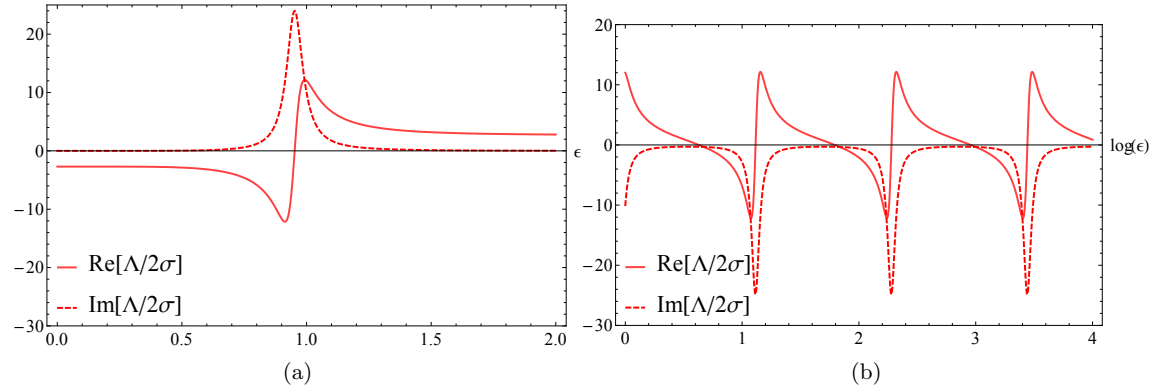


Figure 3. Panel (a) shows the real and imaginary parts of the RG flow as a function of ϵ for the subcritical case which means that σ is real. Panel (b) shows the real and imaginary parts of the RG flow in the supercritical case which means that σ is imaginary. In the supercritical case the flow exhibits a log periodic behaviour.

This equation determines how the coupling constant λ must depend on the regulator ϵ to renormalize any divergences such that physical quantities are independent of ϵ . The non-trivial zeroes of the right hand side at $\Lambda = \pm 2\sigma$ correspond to the fixed points of the flow. At fixed points the theory is scale invariant. An important consequence of the RG running of the coupling of the Dirac δ -function is as follows: the vanishing of the coefficient of the δ -function ($\lambda = 0$) only happens at $\Lambda = -2$, which is not a fixed point unless $\sigma = \pm 1$, but this value of σ is impossible to realize with an attractive inverse square potential because $\sigma = \sqrt{1/4 - \alpha}$. Thus, a δ -function term is inevitable: the flow will always produce one.

The above RG evolution equation, considered as a first order differential equation, has a relatively simply quadratic right hand side and can be integrated analytically. In terms of the initial condition $\lambda(\epsilon_0) \equiv \lambda_0$, one finds

$$\frac{\Lambda}{2\sigma} = \frac{\frac{\lambda_0}{2\sigma} + \tanh(\sigma \ln(\epsilon/\epsilon_0))}{1 + \frac{\lambda_0}{2\sigma} \tanh(\sigma \ln(\epsilon/\epsilon_0))}. \quad (35)$$

6.1.1. Supercritical case In the supercritical case when $\alpha > 1/4$, the fixed points for Eq. (34) are given by $\Lambda = \pm 2\sigma = \pm 2i\zeta$, $\zeta \in \mathbb{R}$. Thus, there are two fixed points and they are purely imaginary complex conjugates of each other. The RG evolution when σ is imaginary is dealt with in detail in [35], but the resulting flow of the coupling Λ as ϵ is increased is shown in Fig. 3(b). The limit cycle behaviour of the trajectories is illustrated in Fig. 4(b), and combined with the logarithmic derivative in Eq. (34) means that the flow exhibits a log periodic behaviour as a function of ϵ . Note that each trajectory can be uniquely labelled by, for example, its value where it crosses the imaginary axis ($\Re[\Lambda] = 0$) and this label is then an RG invariant. In fact, the flow picks a scale ϵ_* at this point and hence breaks continuous scale invariance, exhibiting discrete scale invariance instead. The limit cycle behaviour means that trajectories that start away from the fixed points can never reach them. Physically, these fixed points correspond to the (scale invariant) scenarios of a perfect sink when $\Im(\lambda) < 0$ and a perfect source when $\Im(\lambda) > 0$ and because they are complex they break \mathcal{PT} symmetry.

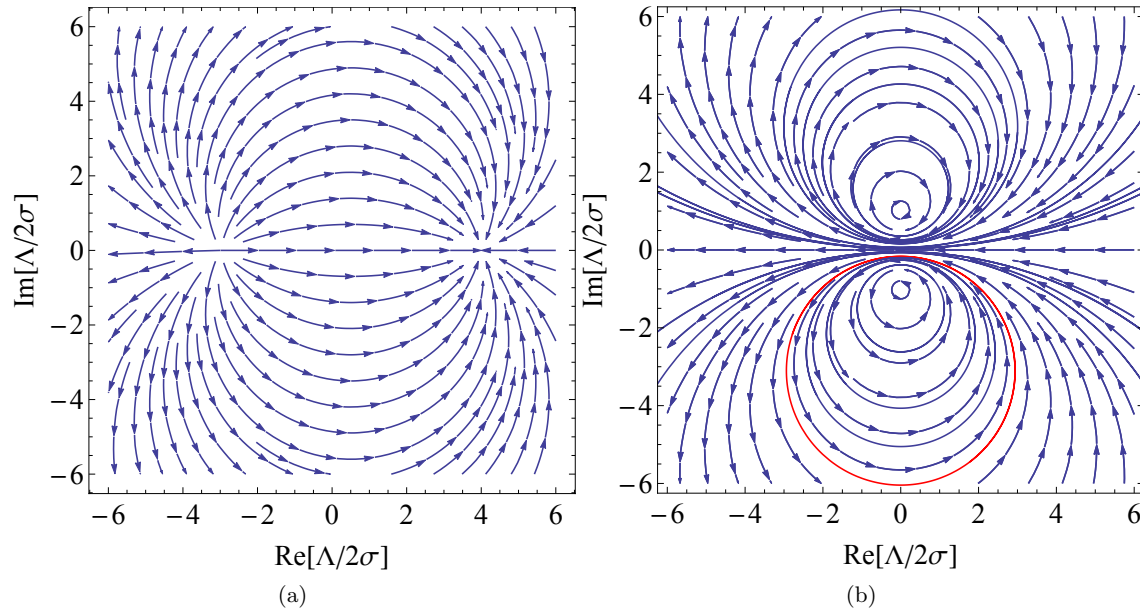


Figure 4. Panel (a) shows the phase portrait of the RG flow in the subcritical case (real σ) which has two real fixed points, one stable and the other unstable. Panel (b) shows a limit cycle behaviour in the supercritical case (imaginary σ). Each RG trajectory picks a length scale ϵ_* when $\Re[\hat{\lambda}] = 0$. Arrows indicate the direction of flow. Each trajectory is characterized by the values of ϵ_* and y_* , where $y_* = \Im[\lambda(\epsilon_*)]$.

To calculate the reflection coefficient we can use the small ϵ expansion of Eq. (35)

$$\frac{\Lambda}{2\sigma} \approx -1 - 2 \left(\frac{\epsilon}{\epsilon_*} \right)^{2\sigma}, \quad (\epsilon \ll \epsilon_*) \quad (36)$$

and substitute it into Eq. (33) to obtain

$$R = \frac{X_* \cosh(\pi\zeta) - 1}{X_* \exp(-\pi\zeta) - 1} \quad (37)$$

where,

$$X_* = \frac{\Gamma(1-\sigma)}{\Gamma(1+\sigma)} \left(\frac{k\epsilon_*}{2} \right)^{2\sigma} \quad (38)$$

and using the small $k\epsilon$ limit in Eq. (30) finally yields

$$T = -i \exp(-\pi\zeta)(1-R) = \frac{iX_* \exp(-\pi\zeta) \sinh(\pi\zeta)}{X_* \exp(-\pi\zeta) - 1}. \quad (39)$$

Note that all observables are expressed entirely in terms of RG invariant quantities.

6.1.2. Subcritical case In the subcritical case $\sigma \in \mathbb{R}$. The solution of the RG flow equation as a function of ϵ for this case is shown in Fig. 3(a). If we chose to start with real Λ as an

initial condition, the coupling will stay real as the flow evolves: hermiticity is itself an RG invariant. The RG phase portraits in sub- and supercritical cases are strikingly different: every RG trajectory in the phase portrait for the subcritical case flows from the UV fixed point $\Lambda = -2\sigma$ to the IR fixed point $\Lambda = +2\sigma$ as shown in Fig. 4(a). The two real fixed points correspond to scale invariant phases and are also \mathcal{PT} symmetric. If we tune the strength of the inverse square potential α the critical points merge at $\alpha_c = 1/4$. Hence, we view the fixed point merger as a form of \mathcal{PT} symmetry breaking transition.

To calculate the reflection coefficient, we follow a similar procedure to the supercritical case. We use the small ϵ expansion of Eq. (35)

$$\frac{\Lambda}{2\sigma} \approx -1 - 2 \left(\frac{\epsilon}{\epsilon_*} \right)^{2\sigma}, \quad (\epsilon \ll \epsilon_*) \quad (40)$$

to obtain [1]

$$R = \frac{X_* \cos(\pi\sigma) - 1}{X_* \exp(-i\pi\sigma) - 1} \quad (41)$$

where,

$$X_* = \frac{\Gamma(1-\sigma)}{\Gamma(1+\sigma)} \left(\frac{k\epsilon_*}{2} \right)^{2\sigma}. \quad (42)$$

Finally, the transmission coefficient can be expressed as

$$T = -i \exp(-i\pi\sigma)(1 - R) = \frac{iX_* \exp(-i\pi\sigma) \sin(\pi\sigma)}{X_* \exp(-i\pi\sigma) - 1}. \quad (43)$$

7. Conclusion

In this work we have argued that fall to the centre is a form of \mathcal{PT} symmetry breaking transition if one focuses on the fixed point structure of the RG flow. The seemingly simple inverse square Hamiltonian presents some subtle difficulties and by itself is not a fully defined problem: one must impose a boundary condition representing additional microscopic ‘source’ physics at the origin to make the eigenvalue problem well posed. We use the PPEFT tools of ref. [1] to derive the boundary condition for the 1D case in both the sub- and supercritical regimes. This amounts to adding an inevitable Dirac δ -function at the origin. Depending upon the nature of the physics at the origin, one can choose a unitary or a non-unitary boundary condition and the Hamiltonian becomes non-hermitian when a non-unitary boundary condition is implemented. The source-bulk coupling λ is evaluated by a boundary condition on the wavefunction at the length scale ϵ (which is a regulator scale that is arbitrary). The RG flow of the source-bulk coupling shows several interesting properties, and in this paper we show that the fixed point merger that occurs as the strength of the inverse square potential α is tuned from subcritical to supercritical [39] is also a \mathcal{PT} symmetry breaking transition. In particular, the two real RG fixed points of the source-bulk coupling λ in the subcritical case ($\alpha < 1/4$), which are attractive/repulsive and preserve \mathcal{PT} symmetry, merge as we tune α to the critical value $\alpha_c = 1/4$. As the strength of the potential is further increased above the critical value, i.e. when $\alpha > 1/4$, we enter the supercritical regime and the fixed points disappear into the complex plane, breaking \mathcal{PT} symmetry. Thus, while the system can be both scale invariant (at a fixed point) *and* unitary for $\alpha < 1/4$, one must choose *either* scale invariance *or* unitarity for $\alpha > 1/4$. We do not claim that fall to the centre is an exact realization of the standard \mathcal{PT} breaking transition [40, 41, 42], but it has many similar elements. One of the differences is that, although the Hamiltonian is generically nonhermitian in both phases, it can also be chosen to be hermitian (λ real) in both phases, rare though these trajectories are. It is, however, nonselfadjoint in both phases if one does not regulate it. The precise role of \mathcal{P} is also elusive (although the Hamiltonian and the

boundary condition both always appear to be \mathcal{P} symmetric), and this remains a topic for further investigation.

Acknowledgments

We acknowledge the support of the Natural Sciences and Engineering Research Council of Canada (NSERC) [Ref. No. RGPIN-2017-06605 and SAPIN-2020-00045]. Research at the Perimeter Institute is supported in part by the Government of Canada through NSERC and by the Province of Ontario through MRI.

Appendix A. Properties and asymptotics of Hankel functions

In this appendix we state some of the properties of the Hankel function that are used in the paper. The Hankel differential equation is given by:

$$z^2 u'' + zu' + (z^2 - \sigma^2)u = 0. \quad (\text{A.1})$$

Hankel functions of first and second kind are defined by:

$$H_\sigma^{(1)}(z) = J_\sigma(z) + iN_\sigma(z) \quad (\text{A.2})$$

and

$$H_\sigma^{(2)}(z) = J_\sigma(z) - iN_\sigma(z) \quad (\text{A.3})$$

where J_σ is the Bessel function and N_σ is the Neumann function.

The asymptotic large z behaviour of Hankel functions is given by:

$$H_\sigma^{(1)}(z) \sim \sqrt{\frac{2}{\pi z}} \exp \left[i \left(z - \frac{\pi \sigma}{2} - \frac{\pi}{4} \right) \right] \quad (\text{A.4})$$

$$H_\sigma^{(2)}(z) \sim \sqrt{\frac{2}{\pi z}} \exp \left[-i \left(z - \frac{\pi \sigma}{2} - \frac{\pi}{4} \right) \right]. \quad (\text{A.5})$$

and they have the following reflection properties:

$$H_\sigma^{(1)}(\exp(i\pi)z) = -\exp(-i\pi\sigma)H_\sigma^{(2)}(z) \quad (\text{A.6})$$

$$H_\sigma^{(2)}(\exp(-i\pi)z) = -\exp(i\pi\sigma)H_\sigma^{(1)}(z). \quad (\text{A.7})$$

For small z , Hankel functions reduce to monomials:

$$H_\sigma^{(1)}(z) \approx \frac{1}{i \sin(\pi\sigma)} \left(\frac{1}{\Gamma(1-\sigma)} \left(\frac{z}{2} \right)^{-\sigma} - \frac{\exp(-i\pi\sigma)}{\Gamma(1+\sigma)} \left(\frac{z}{2} \right)^\sigma \right) \quad (\text{A.8})$$

$$H_\sigma^{(2)}(z) \approx \frac{1}{i \sin(\pi\sigma)} \left(-\frac{1}{\Gamma(1-\sigma)} \left(\frac{z}{2} \right)^{-\sigma} + \frac{\exp(i\pi\sigma)}{\Gamma(1+\sigma)} \left(\frac{z}{2} \right)^\sigma \right) \quad (\text{A.9})$$

References

- [1] Burgess C P, Hayman P, Williams M and Zalavári L 2017 *Journal of High Energy Physics* **2017** 106
- [2] Lifshitz E M and Landau L D 1981 *Quantum Mechanics: Non-Relativistic Theory* 3rd ed (Butterworth-Heinemann)
- [3] Case K M 1950 *Phys. Rev.* **80** 797
- [4] Perelomov A M and Popov V S 1970 *Theoretical and Mathematical Physics* **4** 664–677
- [5] Denschlag J, Umshaus G and Schmiedmayer J 1998 *Phys. Rev. Lett.* **81** 737
- [6] Efimov V 1970 *Phys. Lett.* **33B** 563

- [7] Efimov V 1973 *Nucl. Phys.* **A210** 157
- [8] Braaten E and Hammer H W 2007 *Ann. Phys.* **322** 120
- [9] Kraemer T, Mark M, Waldburger P, Danzl J G, Chin C, Engeser B, Lange A D, Pilch K, Jaakkola A, Nägerl H C and Grimm R 2006 *Nature (London)* **440** 315
- [10] Pollack S E, Dries D and Hulet R G 2009 *Science* **326** 1683
- [11] Ferlaino F and Grimm R 2010 *Physics* **3** 9
- [12] Bhaduri R K, Chatterjee A and van Zyl B P 2011 *Am. J. Phys.* **79** 274–281
- [13] Huang B, Sidorenkov L A, Grimm R and Hutson J M 2014 *Phys. Rev. Lett.* **112** 190401
- [14] Pires R, Ulmanis J, Häfner S, Repp M, Arias A, Kuhnle E D and Weidemüller M 2014 *Phys. Rev. Lett.* **112** 250404
- [15] Tung S K, Jiménez-García K, Johansen J, Parker C V and Chin C 2014 *Phys. Rev. Lett.* **113** 240402
- [16] Moroz S, D’Incao J P and Petrov D S 2015 *Phys. Rev. Lett.* **115** 180406
- [17] Kunitski M, Zeller S, Voigtsberger J, Kalinin A, Schmidt L P H, Schöffler M, Czasch A, Schöllkopf W, Grisenti R E, Jahnke T, Blume D and Dörner R 2015 *Science* **348** 551
- [18] Gurappa N and Panigrahi P K 1999 *Phys. Rev. B* **59** R2490
- [19] Srinivasan K and Padmanabhan T 1999 *Phys. Rev. D* **60** 024007
- [20] Birmingham D, Gupta K S and Sen S 2001 *Physics Letters B* **505** 191–196
- [21] Camblong H and Ordóñez C 2003 *Phys. Rev. D* **68** 125013
- [22] Sundaram S and Panigrahi P K 2016 *Optics letters* **41** 4222–4224
- [23] Alonso M 2015 *New J. Phys.* **17** 073013
- [24] Frank A, Leyvraz F and Wolf K B 1990 *Journal of Mathematical Physics* **31** 2757–2768
- [25] Leonhardt U 2009 *New Journal of Physics* **11** 093040
- [26] Coon S A and Holstein B R 2002 *Am. J. Phys.* **70** 513–519
- [27] Essin A M and Griffiths D J 2006 *Am. J. Phys.* **74** 109–117
- [28] Pitaevskii L P and Rosch A 1997 *Phys. Rev. A* **55** R853
- [29] Olshanii M, Perrin H and Lorent V 2010 *Phys. Rev. Lett.* **105** 095302
- [30] Taylor E and Randeria M 2012 *Phys. Rev. Lett.* **109** 135301
- [31] Holten M, Bayha L, Klein A C, Murthy P A, Preiss P M and Jochim S 2018 *Phys. Rev. Lett.* **121** 120401
- [32] Peppler T, Dyke P, Zamorano M, Herrera I, Hoinka S and Vale C J 2018 *Phys. Rev. Lett.* **121** 120402
- [33] Murthy P A, Defenu N, Bayha L, Holten M, Preiss P M, Enss T and Jochim S 2019 *Science* **365** 268
- [34] Ovdut O, Mao J, Jiang Y, Andrei E and Akkermans E 2017 *Nature communications* **8** 1–6
- [35] Plestid R, Burgess C P and O’Dell D H J 2018 *Journal of High Energy Physics* **2018** 59
- [36] Gupta K S and Rajeev S G 1993 *Phys. Rev. D* **48** 5940
- [37] Mueller E J and Ho T L 2004 *arXiv preprint cond-mat/0403283*
- [38] Kaplan D B, Lee J W, Son D T and Stephanov M A 2009 *Phys. Rev. D* **80** 125005
- [39] Moroz S and Schmidt R 2010 *Annals of Physics* **325** 491–513
- [40] Bender C M and Boettcher S 1998 *Phys. Rev. Lett.* **80** 5243
- [41] Bender C M, Boettcher S and Meisinger P N 1999 *Journal of Mathematical Physics* **40** 2201–2229
- [42] Bender C M, Brody D C and Jones H F 2002 *Phys. Rev. Lett.* **89** 270401
- [43] Bender C M, Brody D C and Jones H F 2003 *Am. J. Phys.* **71** 1095–1102
- [44] Bender C M and Mannheim P D 2010 *Phys. Lett. A* **374** 1616–1620
- [45] Das A and Greenwood L 2009 *Phys. Lett. B* **678** 504–507
- [46] Bazeia D, Das A, Greenwood L and Losano L 2009 *Phys. Lett. B* **673** 283–287
- [47] Dorey P, Dunning C and Tateo R 2001 *J. Phys. A: Math. Gen.* **34** L391
- [48] Abhinav K and Panigrahi P K 2010 *Annals of Physics* **325** 1198–1206
- [49] Abhinav K, Jayannavar A and Panigrahi P K 2013 *Annals of Physics* **331** 110–119
- [50] Mandal B P, Mourya B K and Yadav R K 2013 *Phys. Lett. A* **377** 1043–1046
- [51] Mandal B P, Mourya B K, Ali K and Ghatak A 2015 *Annals of Physics* **363** 185–193
- [52] Lumer Y, Plotnik Y, Rechtsman M C and Segev M 2013 *Phys. Rev. Lett.* **111** 263901
- [53] Zyablovsky A A, Vinogradov A P, Pukhov A A, Dorofeenko A V and Lisyansky A A 2014 *Physics-Uspekhi* **57** 1063
- [54] Raja S V, Govindarajan A, Mahalingam A and Lakshmanan M 2019 *Phys. Rev. A* **100** 033838
- [55] Raja S V, Govindarajan A, Mahalingam A and Lakshmanan M 2020 *Phys. Rev. A* **101** 033814
- [56] Longhi S 2018 *EPL (Europhys. Lett.)* **120** 64001
- [57] Bender C M, Berntson B K, Parker D and Samuel E 2013 *Am. J. Phys.* **81** 173–179
- [58] Schindler J, Li A, Zheng M C, Ellis F M and Kottos T 2011 *Phys. Rev. A* **84** 040101
- [59] Guo A, Salamo G J, Duchesne D, Morandotti R, Volatier-Ravat M, Aimez V, Siviloglou G A and Christodoulides D N 2009 *Phys. Rev. Lett.* **103** 093902
- [60] Rüter C E, Makris K G, El-Ganainy R, Christodoulides D N, Segev M and Kip D 2010 *Nat. Phys.* **6** 192–195

- [61] Rajeev S G 2013 *Advanced mechanics: from Euler's determinism to Arnold's chaos* (OUP Oxford)
- [62] Capri A Z 1977 *Am. J. Phys.* **45** 823–825
- [63] Basu-Mallick B and Gupta K S 2001 *Phys. Lett. A* **292** 36
- [64] Gopalakrishnan S 2006 *Self-Adjointness and the Renormalization of Singular Potentials* Ph.D. thesis
Department of Physics of Amherst College

FROM FALL TO INFINITY TO FALL TO THE CENTRE

Sriram Sundaram, C. P. Burgess, and D. H. J. O'Dell

Duality between the inverted harmonic oscillator and inverse square potentials

New J. Phys. **26**, 053023 (2024).

DOI: 10.1088/1367-2630/ad3a91

Copyright 2024 The Author(s). Published by IOP Publishing Ltd on behalf of the Institute of Physics and Deutsche Physikalische Gesellschaft

In this paper we discuss the dual mapping of the inverted harmonic oscillator (IHO) to inverse square potentials (ISP) in quantum mechanics. We do so by connecting the IHO to the Berry-Keating Hamiltonian $H = (xp + px)/2$ using a canonical transformation. We show in the paper that the squared Berry-Keating Schrödinger equation, using an integrating factor, then reduces to a zero energy super-critical inverse square Schrödinger equation. We do a one-to-one mapping of the inverse square quantum states to the IHO states using a quantum canonical transformation. As discussed in chapter 2, inverse square potential involves ambiguities in choosing appropriate boundary conditions at the origin and in this paper we show how this ambiguity is mapped to the IHO system. One of the main ideas of the paper also involves using PPEFT methods to implement a Robin (linear) boundary condition near the origin for the ISP system and its mapping to a linear boundary condition for the IHO system, but now at long distances. We also renormalize the boundary coupling for both the IHO and ISP systems and show that similar to the super-critical ISP system the IHO also admits limit cycle type RG flow. For the ISP system the

limit cycles arise as a consequence of a discrete scaling symmetry. However, for the IHO system such a scaling symmetry is not explicit. But the IHO and the generator of scale transformations $(xp + px)/2$ form an $\text{su}(1, 1)$ spectrum generating algebra.

PAPER • OPEN ACCESS

Duality between the quantum inverted harmonic oscillator and inverse square potentials

To cite this article: Sriram Sundaram *et al* 2024 *New J. Phys.* **26** 053023

View the [article online](#) for updates and enhancements.

You may also like

- [Nitrogen-seeded divertor detachment in TCV L-mode plasmas](#)

O Février, C Theiler, J R Harrison et al.

- [MULTIEPOCH OPTICAL SPECTROPOLARIMETRY OF THREE MICROQUASARS. Cyg X-1, LS 5039, AND LS I +61° 303](#)

Osamu Nagae, Koji S. Kawabata, Yasushi Fukazawa et al.

- [DISK-LOSS AND DISK-RENEWAL PHASES IN CLASSICAL Be STARS. II. CONTRASTING WITH STABLE AND VARIABLE DISKS](#)

Zachary H. Draper, John P. Wisniewski, Karen S. Bjorkman et al.



OPEN ACCESS

RECEIVED

21 February 2024

REVISED

24 March 2024

ACCEPTED FOR PUBLICATION

4 April 2024

PUBLISHED

17 May 2024


Original Content from
this work may be used
under the terms of the
[Creative Commons
Attribution 4.0 licence](#).

Any further distribution
of this work must
maintain attribution to
the author(s) and the title
of the work, journal
citation and DOI.



PAPER

Duality between the quantum inverted harmonic oscillator and inverse square potentials

Sriram Sundaram¹, C P Burgess^{1,2,3} and D H J O'Dell^{1,*} ¹ Department of Physics and Astronomy, McMaster University, 1280 Main Street W., Hamilton, Ontario L8S 4M1, Canada² Perimeter Institute for Theoretical Physics, Waterloo, Ontario N2L 2Y5, Canada³ School of Theoretical Physics, Dublin Institute for Advanced Studies, 10 Burlington Rd., Dublin, Co. Dublin, Ireland

* Author to whom any correspondence should be addressed.

E-mail: dodell@mcmaster.ca**Keywords:** inverted harmonic oscillator, inverse square potential, duality, renormalisation group

Abstract

In this paper we show how the quantum mechanics of the inverted harmonic oscillator (IHO) can be mapped to the quantum mechanics of a particle in a super-critical inverse square potential (ISP). We demonstrate this by relating both of these systems to the Berry–Keating system with Hamiltonian $H = (xp + px)/2$. It has long been appreciated that the quantum mechanics of the ISP has an ambiguity in choosing a boundary condition near the origin and we show how this ambiguity is mapped to the IHO system. Imposing a boundary condition requires specifying a distance scale where it is applied and changes to this scale come with a renormalisation group (RG) evolution of the boundary condition that ensures observables do not directly depend on the scale (which is arbitrary). Physical scales instead emerge as RG invariants of this evolution. The RG flow for the ISP is known to follow limit cycles describing the discrete breaking of classical scale invariance in a simple example of a quantum anomaly, and we find that limit cycles also occur for the IHO. However, unlike the ISP where the continuous scaling symmetry is explicit, in the case of the IHO it is hidden and occurs because the Hamiltonian is part of a larger $su(1,1)$ spectrum generating algebra. Our map does not require the boundary condition to be self-adjoint, as can be appropriate for systems that involve the absorption or emission of particles.

1. Introduction

The inverted harmonic oscillator (IHO) describes a particle moving in a potential $V_{\text{IHO}}(x) \propto -x^2$ which is singular at infinity, whereas the attractive inverse-square potential (ISP) varies as $V_{\text{ISP}}(x) \propto -1/x^2$ and is singular at the origin. These two well-studied systems are generic models for unstable and scale-invariant systems, respectively, and at first sight seem to give rise to opposite behaviour because the IHO potential drives particles to large x , whereas the ISP causes ‘fall to the centre’ [1, 2]. In this paper we demonstrate how in fact the Hamiltonians and quantum states of these systems can be explicitly mapped into one another, showing them to be in some sense alternative descriptions of equivalent physics. In so doing we also relate both of these models to the Berry–Keating (BK) system which has the classical Hamiltonian xp which in quantum mechanics we symmetrise to $H = (xp + px)/2$ to make it formally hermitian (but not necessarily self-adjoint). Although the canonical transformation that relates the IHO and BK models has been extensively studied before [3–8], we believe that the connection to the ISP is new.

The quantum mechanics of the IHO is exactly solvable [9] and appears in many branches of physics where it provides a simple prototype for instability or tunnelling through a smooth barrier [7, 10, 11]. Particular examples include the Landau–Zener model in atomic and molecular physics [12, 13], squeezed states, amplifiers, and the Glauber oscillator in quantum optics [14–17], the quantum Hall effect in condensed matter physics [7], non-equilibrium phase transitions in statistical physics [18], studies of chaos and complexity [19, 20], and Riemann zeroes [21]. In quantum field theory the IHO arises in Schwinger pair

production [4, 22], Hawking radiation from black holes [23], squeezing of states in inflationary cosmology [24], tachyon physics [25], is widely used in string theory [26–29], and so on.

The ISP likewise arises in multiple scenarios. It occurs as the interaction potential between an electron and a neutral polar molecule [30, 31] (or similarly between a charged wire and an atom [32, 33]), as an effective description for three-body bound states in the Efimov effect [34–39] that was originally predicted in nuclear physics and has been studied experimentally in detail using ultracold atoms [40–44], in statistical mechanics through the exactly solvable Calogero–Sutherland quantum many-body problem with pairwise ISPs [45–48], as a model for winding transitions relevant to polymers such as DNA [49], in the study of coherence in optics [50], in supersymmetric quantum mechanics [51, 52], in the anti-de Sitter/conformal field theory (AdS/CFT) correspondence [53], in the near-horizon physics of black holes [22, 54–56], and in gravitational waves [57].

A key feature of the ISP is that the non-relativistic Schrödinger equation with this potential is scale invariant as both the kinetic energy and potential terms scale as length^{-2} and thus there is no natural length scale present (such as the Bohr radius in the Coulomb problem, say). However, if the singular nature of the ISP at the origin is tamed by introducing a cut-off or boundary condition at short distance (in the physical examples given above the ISP only models the long wavelength behaviour), this regulator necessarily breaks the scale invariance in a simple example of a quantum anomaly [58–64]. Furthermore, in order to ensure that the long wavelength physics is independent of the regulator the theory's couplings should be renormalised [65]. In the case of the super-critical ISP (where the strength of the potential overcomes the zero-point energy) this leads to a characteristic renormalisation group (RG) flow that includes limit cycles [66–69]. In a previous paper on these limit cycles, we emphasised that the change from sub- to super-criticality is a type of \mathcal{PT} symmetry breaking transition where the fixed points of the RG flow change from real valued, describing unitary physics, to a complex conjugate pair, one describing pure emission and the other pure absorption [70] (see also [71]).

The third system in our trio is the BK Hamiltonian. It has been extensively studied in the context of quantum chaos and attempts to prove the Riemann hypothesis [5, 72–77]. The dynamics generated by the classical BK Hamiltonian is exponentially unstable, unbounded, and breaks time reversal symmetry [5]. Although it does not have distinct kinetic and potential energies, the BK Hamiltonian is manifestly scale invariant, like the ISP. A particular way of modifying the BK Hamiltonian exhibits a cyclic RG flow similar to the ISP and has been used to map to ‘Russian-doll’ models of superconductivity [78]. It has also been argued to capture aspects of black hole physics [79, 80]. A Dirac-type variant of the BK model in two dimensions in which the operator p is replaced by $\sigma \cdot p = \sigma_x p_x + \sigma_y p_y$, where $\sigma = \{\sigma_x, \sigma_y\}$ are Pauli spin operators, has been proposed by Gupta *et al* [81] and shown to be equivalent to a Schrödinger equation with an ISP plus an additional Coulomb potential. This model finds physical applications in describing gaped graphene with a super-critical Coulomb charge. In fact, the Dirac equation for a massless fermion in the presence of an attractive Coulomb potential is also scale invariant because both terms scale as $1/r$ and the quantum anomaly that breaks this continuous scaling symmetry has been observed in an experiment on graphene [82].

In the duality scheme we lay out in this paper, the BK model provides a stepping stone between the IHO and the ISP. In the first step the BK Hamiltonian is obtained from the IHO via a canonical transformation, and in the second step the Schrödinger equation with an ISP is reached by squaring the BK Hamiltonian and then applying an integrating factor to remove a first order derivative. Since the exact solutions of the Schrödinger equations defining the IHO, BK, and ISP models are all already known (parabolic cylinder functions, monomials, and confluent hypergeometric functions, respectively) the difficulty in treating these models does not lie in finding solutions to differential equations. Rather, it lies in choosing the correct boundary conditions that these solutions must obey especially in view of the fact that their energies form a continuum and are unbounded from below. One of the novelties of the present paper therefore lies in mapping the boundary conditions between the models and exhibiting how they behave under renormalisation.

The rest of this paper is organised as follows: after putting the current work in a larger historical context in section 2, section 3 describes the three dual systems, their eigenfunctions and symmetries. The need for appropriate far field physics (boundary condition at long distances) for the quantum mechanics of an IHO is discussed. Using a canonical transformation we map the Schrödinger equation with an IHO potential in one set of variables ξ , to a Schrödinger equation with a super-critical ISP in another set of variables Q , which, however, now has ambiguities in fixing a boundary condition for the wavefunction near the origin. This problem can be tackled systematically using point particle effective field theory (PPEFT) which suggests a general linear (Robin) form for the boundary condition. In section 4 we apply this boundary condition for the wavefunction near the origin of the ISP in an RG invariant way. Furthermore, we do a one-to-one mapping of the inverse square states to the IHO states using a quantum canonical transform. For the IHO problem, the boundary condition for the asymptotic parabolic cylinder functions is also fixed by a linear

boundary condition, but now at large distances, and also in an RG invariant way. Conclusions are given in section 5. We also include three appendices that discuss the properties of parabolic cylinder functions, quantum canonical transformations, and other details needed for the mappings.

2. A brief history of power law dualities

To put the current paper in context it is worth mentioning the history of dualities between power law potentials (for fascinating reviews of this topic, that goes to the very foundations of modern physics, see [83, 84]). The most famous duality is the relation between classical motion in a gravitational potential $V_{\text{grav}} \propto -1/r$ and a (stable) planar harmonic oscillator potential $V_{\text{HO}} \propto r^2$, which are associated with the names of Newton and Hooke, respectively. Both give rise to closed orbits which are ellipses: in the harmonic oscillator case the force centre is located at the centre of the ellipse whereas in the gravitational case the force centre is at a focus. The two cases can be mapped onto each other by *squaring* the harmonic oscillator ellipse to obtain the gravitational ellipse, as described by Bohlin in [85, 86] (we note that the mapping between the IHO and the ISP to be discussed in this paper also involves a step where the Hamiltonian is squared). In fact, there is a continuous family of dual potentials $V \propto r^\alpha \leftrightarrow V \propto r^{\bar{\alpha}}$ determined by the relation [87–89]

$$(\alpha + 2)(\bar{\alpha} + 2) = 4 \quad (1)$$

of which the harmonic oscillator-gravity duality $(\alpha, \bar{\alpha}) = (-1, 2)$ is only one example. The other integer-valued cases are $(-3, -6)$, $(-4, -4)$, and $(0, 0)$ (the last case can be interpreted as corresponding to a logarithmic potential). This duality relation was derived by Kasner in 1913 [87], but seems to have also been included in the 1720 treatise by C MacLaurin (see Albouy and Zhao [90]), and Newton discussed the self-dual cases $(-4, -4)$ and $(0, 0)$ in the Principia [83, 91–93]. Extensions to quantum mechanics and other generalisations have also been widely studied, see for example [94–96]. A case which is particularly relevant in current ultracold atom physics is the equivalence between free quantum particles and those in harmonic potentials [97, 98] since in experiments the atoms are often confined in harmonic traps but calculations of interacting many-particle systems are of course easier for plane wave states.

Does the duality considered in this paper fit into the above scheme? On the one hand, putting $\alpha = -2$ for the ISP into equation (1) makes the left hand side vanish so that $\bar{\alpha}$ is undefined, and on the other hand putting $\alpha = 2$ for the IHO gives $\bar{\alpha} = -1$ corresponding to the gravitational case as expected, and so does not seem to include the ISP-IHO duality as a possibility. The result given in equation (1) takes no account of the fact that the IHO is inverted but when this is done one can map hyperbolic trajectories between the gravitational and IHO potentials [84]. Proceeding in a slightly different way, Wu and Sprung considered the limiting procedure where $\alpha \rightarrow \pm\infty$ in classical mechanics in two dimensions and have shown that it can represent a hard wall well or hard sphere scattering and that the dual potential is the ISP [99]. However, the duality we study here is of a different nature since it maps between small and large distances (see figure 4) such that fall-to-the-centre in the ISP becomes fall-to-infinity in the IHO. Furthermore, the scale invariance which is such an important part of the quantum behaviour of the ISP is not replicated in the classical mechanics as the kinetic energy in this case does not scale as an inverse square length. We leave it as an open problem as to whether equation (1) can be re-interpreted in a creative way that includes the ISP-IHO duality to be detailed below.

3. The systems

This section gives a brief description of each of the three systems that are to be related.

3.1. IHO

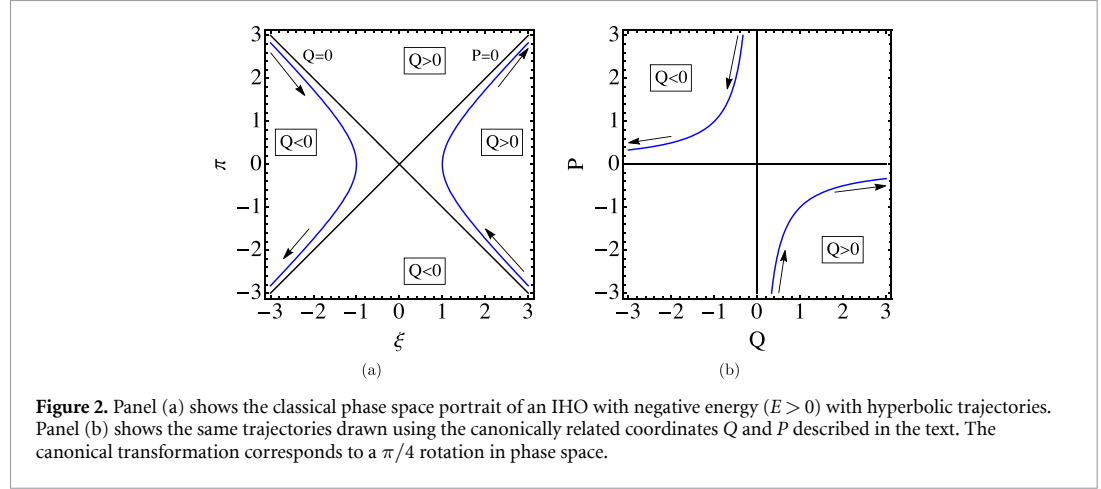
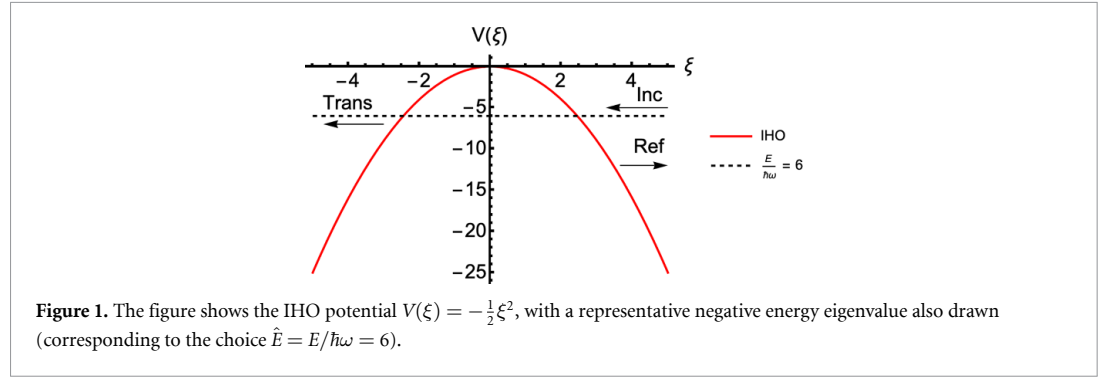
The IHO is defined by the Hamiltonian:

$$H(x, p) = \frac{p^2}{2m} - \frac{1}{2}m\omega^2 x^2 \quad (2)$$

and so the time-independent Schrödinger equation for energy eigenvalue⁴ $\mathcal{E} = -E$ written in the position representation is:

$$\left[\frac{-\hbar^2}{2m} \frac{\partial^2}{\partial x^2} - \frac{1}{2}m\omega^2 x^2 \right] \phi(x) = -E\phi(x). \quad (3)$$

⁴ Perversely, we denote the system energy by $-E$ so that $E > 0$ describes negative-energy states. We do this because for applications such as Schwinger pair production it is the tunnelling states that are required.



It is convenient to use the following dimensionless coordinate

$$\xi = \sqrt{\frac{m\omega}{\hbar}} x \quad (4)$$

in terms of which (3) becomes

$$\frac{\pi^2 - \xi^2}{2} \phi(\xi) = -\frac{E}{\hbar\omega} \phi(\xi) = -\hat{E} \quad (5)$$

where $\hat{E} := E/\hbar\omega$ and the canonical momentum $\pi = -i\partial/\partial\xi$ satisfies $[\xi, \pi] = i$.

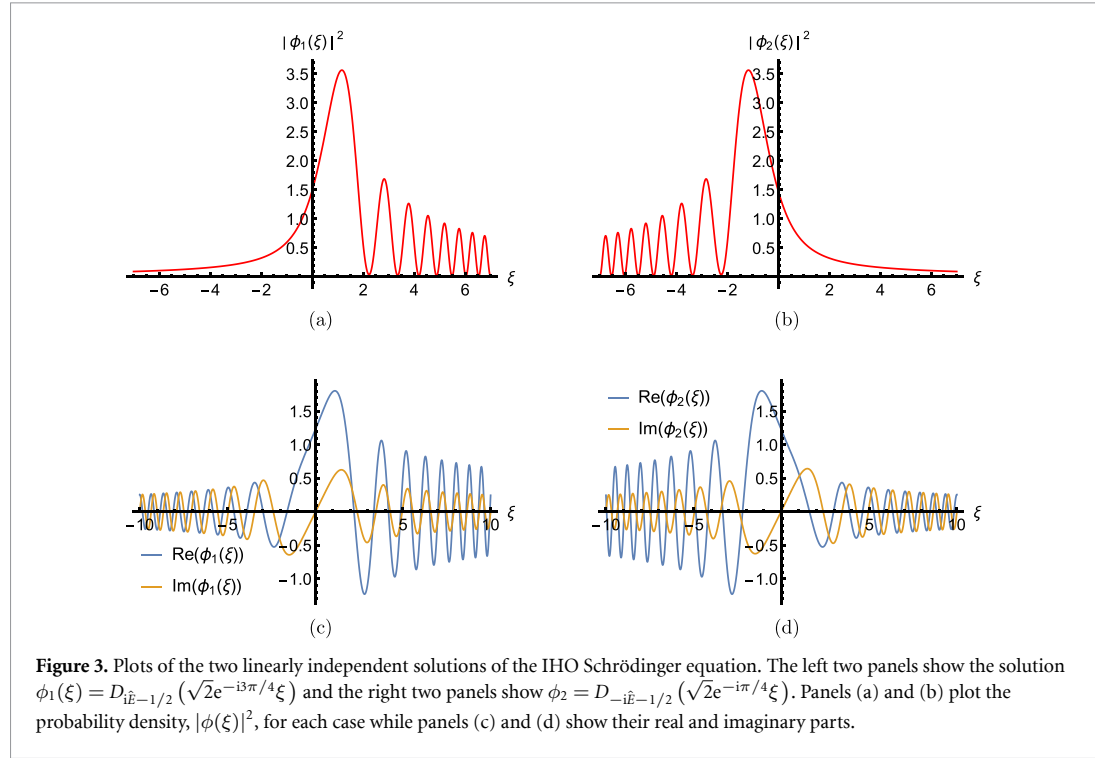
The IHO potential is shown in figure 1 together with a representative negative energy eigenvalue. Notice that both positive and negative energy eigenvalues are allowed and instability arises because the spectrum is not bounded from below. For negative energy states (i.e. $E > 0$ in our convention) evolution between large negative and positive positions is a tunnelling problem, while for positive energy states ($E < 0$) it is instead a classically allowed barrier scattering problem.

The classical turning points for negative energy ($E > 0$) are $\xi_0 = \pm\sqrt{2\hat{E}}$ and the classical negative-energy solutions are given by

$$\xi = \xi_0 \cosh(t - t_0), \quad (6)$$

where integration constants are fixed by specifying the turning point ξ_0 and the time t_0 when the trajectory reaches this turning point, $\xi(t_0) = \xi_0$. The only static solution is $\xi_0 = 0$ and is unstable. A typical classical phase-space portrait for the IHO with negative energy is drawn in panel (a) of figure 2. For each negative energy ($E > 0$) there are two distinct hyperbolic trajectories depending on whether the particle approaches from the right or left. The trajectory in the left-hand quadrant of the figure describes a particle approaching from the left, while the one in the right-hand quadrant corresponds to a particle approaching from the right.

The quantum mechanics of an IHO is well-posed mathematically—i.e. is essentially self-adjoint [7, 100, 101] on the real line—but is unstable because its Hamiltonian is unbounded from below. Parabolic cylinder functions are known to provide an energy eigenbasis, and the invariance of the Hamiltonian under parity



($\xi \rightarrow -\xi$) implies each energy level is doubly degenerate. A general solution to the Schrödinger equation with energy $\mathcal{E} = -E = -\hat{E}\hbar\omega$ can be written

$$\begin{aligned}\phi(\xi) &= C_1 \phi_1(\xi) + C_2 \phi_2(\xi) \\ &= C_1 D_{i\hat{E}-\frac{1}{2}}\left(\sqrt{2}e^{-i3\pi/4}\xi\right) + C_2 D_{-i\hat{E}-\frac{1}{2}}\left(\sqrt{2}e^{-i\pi/4}\xi\right)\end{aligned}\quad (7)$$

where $D_s(z)$ are parabolic cylinder functions [102] and C_1, C_2 are arbitrary constants that determine the choice of wavefunction. The eigenfunctions ϕ_1 and ϕ_2 are plotted as a function of ξ in figure 3.

Note that although it may seem as though the two eigenfunctions ϕ_1 and ϕ_2 in (7) correspond to different energies due to the $\pm i\hat{E}$ factors labelling their parabolic cylinder functions, this is actually not the case due to the effect of the different complex phases in their arguments. This point is spelled out in appendix A. Indeed, although we shall not use it, an alternative energy eigenbasis where both terms have the same $+i\hat{E}$ factors and makes the action of parity more manifest is

$$\tilde{\phi}_{\pm}(\xi) = C_{\pm} D_{i\hat{E}-\frac{1}{2}}\left(\pm\sqrt{2}e^{-i3\pi/4}\xi\right). \quad (8)$$

Because the wavefunctions are oscillatory at large $|\xi|$ the states are not normalisable even for negative energies. As is standard for continuum states, this means that normalisation of the state cannot determine one combination of C_1 and C_2 . One instead treats it as a scattering problem, such as by specifying an incoming flux at large positive or negative ξ and asking for the transmission and reflection probabilities per unit incident flux. For later purposes we remark that this implicitly means that states are chosen according to boundary information specified at large ξ .

3.2. BK system

Although not previously emphasised, the IHO Schrödinger system is part of a closed $\mathfrak{su}(1, 1)$ Lie algebra [7, 15, 103, 104] defined by the generators

$$K_1 = \frac{1}{2}(\pi^2 - \xi^2), \quad K_2 = \frac{1}{2}(\pi^2 + \xi^2), \quad K_3 = \frac{1}{2}(\xi \cdot \pi + \pi \cdot \xi) \quad (9)$$

since the commutation relations imply these satisfy

$$[K_1, K_2] = -iK_3, \quad [K_2, K_3] = iK_1, \quad [K_3, K_1] = iK_2. \quad (10)$$

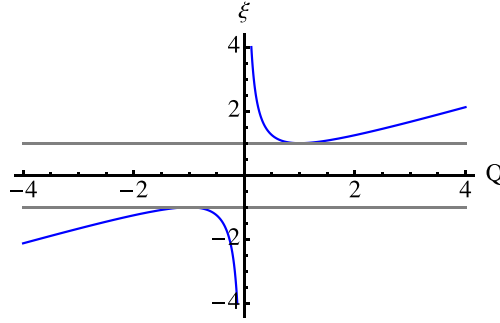


Figure 4. The figure shows the relation between the variables ξ and Q given by $\xi = \frac{\xi_0}{2} \left(Q + \frac{1}{Q} \right)$. The sectors $Q > 0$ and $Q < 0$ are disconnected classically. Although in general the relationship between ξ and Q is multivalued, we can see that for small Q we have the simple inverse relationship $\xi = \frac{\xi_0}{2} \frac{1}{Q}$ so that small distances in the BK and ISP systems are equivalent to large distances in the IHO.

The Casimir invariant $\hat{C} = K_3^2 - K_1^2 - K_2^2$ commutes with the IHO Hamiltonian (K_1), i.e. $[\hat{C}, K_1] = 0$, as well as with the other generators K_2 and K_3 . This is a spectrum-generating algebra because the generator K_1 is the IHO Hamiltonian and the other generators do not commute with it.

This observation suggests a canonical transformation that has the effect of swapping which of the K_i plays the role of Hamiltonian. In particular, we transform to BK variables for which K_3 becomes the Hamiltonian. This is done using the following canonical transformation to the new hermitian operators [3]

$$Q = \frac{\pi + \xi}{\sqrt{2}}, \quad P = \frac{\pi - \xi}{\sqrt{2}}, \quad (11)$$

which preserves the classical Poisson bracket, $\{Q, P\} = 1$, and hence the commutation relation, $[Q, P] = i$. In terms of these the IHO Hamiltonian becomes

$$H(Q, P) = \frac{Q \cdot P + P \cdot Q}{2}. \quad (12)$$

This quantum BK Hamiltonian is symmetric under the exchange of Q and P , like the simple harmonic oscillator Hamiltonian. Parity symmetry is realised in these variables as $(Q, P) \rightarrow (-Q, -P)$.

Hamilton's (classical) equations in the new variables are

$$\frac{dQ}{dt} = Q \quad \text{and} \quad \frac{dP}{dt} = -P \quad (13)$$

with solutions [8]

$$Q = Q_0 e^t \quad \text{and} \quad P = P_0 e^{-t}, \quad (14)$$

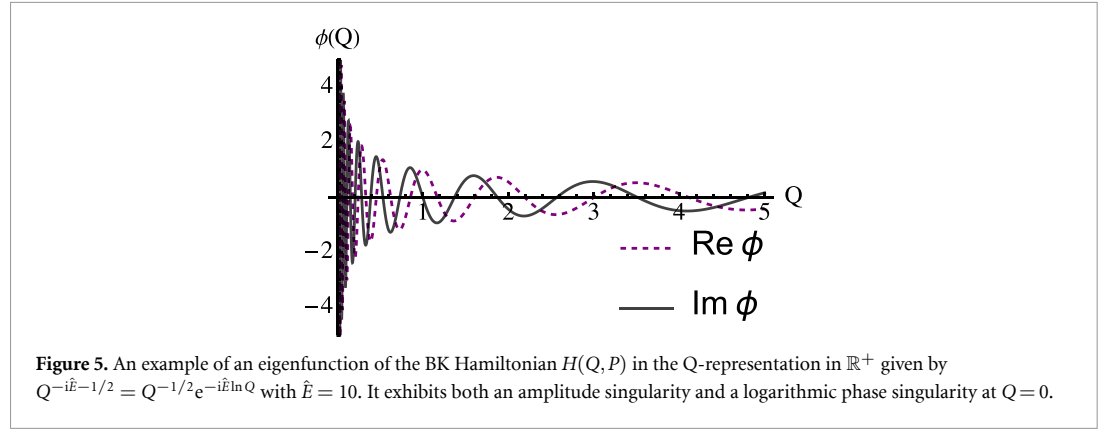
where Q_0 and P_0 are the initial conditions at $t = 0$ —see figure 2. (Notice in particular that $\frac{dQ}{dt}$ is *not* P .) These solutions show how time translation corresponds to rescalings of Q and P and so sheds light on the scale-invariance behind the algebra (9). Although the canonical transformation (11) acts on both position and momentum, it is possible to use the classical solutions to derive a relationship between the position variables ξ and Q alone. Comparing the solutions (6) and (14) leads to the relation

$$\xi = \frac{\xi_0}{2} \left(Q + \frac{1}{Q} \right), \quad (15)$$

a plot of which is given in figure 4. Although the relation between Q and ξ is multivalued, for small Q the relation is simply inverse so that small Q is mapped to large ξ .

The Schrödinger equation in these variables takes the form [4, 6–8]:

$$\frac{1}{2} (Q \cdot P + P \cdot Q) |\phi\rangle = -\frac{E}{\hbar\omega} |\phi\rangle \quad (16)$$



where we again write the energy eigenvalue as $\mathcal{E} = -E = -\hat{E}\hbar\omega$. In the position representation this becomes the following first-order equation for $\phi(Q)$,

$$Q \frac{\partial \phi}{\partial Q} = -\left(i\hat{E} + \frac{1}{2}\right) \phi \quad (17)$$

whose scale-invariance under $Q \rightarrow \zeta Q$ is manifest. This reflects the fact that the BK Hamiltonian is itself the generator of scale transformations, since

$$e^{i\zeta H(Q,P)} Q e^{-i\zeta H(Q,P)} = e^{\zeta} Q \quad \text{and} \quad e^{i\zeta H(Q,P)} P e^{-i\zeta H(Q,P)} = e^{-\zeta} P \quad (18)$$

for constant ζ , as expected from the classical result in (14).

The lone solution of (17) is

$$\phi(Q) = A Q^{-\frac{1}{2}-i\hat{E}} = A Q^{-\frac{1}{2}} e^{-i\hat{E}\ln Q}, \quad (19)$$

where A is a constant. Unusually, because the Schrödinger equation is first order there is not a second independent solution to this equation, which at face value seems to contradict the fact that the IHO has doubly degenerate energy eigenspaces. Since parity provides the secondary label for states within a given energy eigenspace we should ask what it implies for the solutions to (17). When doing so it is crucial that for general \hat{E} the solution (19) has a logarithmic branch point at $Q = 0$, leading to both an amplitude singularity and a logarithmic phase singularity at $Q = 0$ (as can be seen in figure 5). Such singularities are generic signatures of quantum catastrophes [105, 106], and appear in many other interesting physical systems like waves near black-hole event horizons, in accelerated frames, and so on [4, 7, 8, 107, 108].

What is important for present purposes is that the logarithmic branch point at $Q = 0$ makes the extrapolation of (19) from $Q > 0$ to $Q < 0$ non-unique. Starting with $Q > 0$ and navigating around different sides of the branch point—such as by multiplying by $e^{\pm i\pi}$ —leads to different sheets for $Q < 0$. These two distinct extensions of (19) to negative Q provide the two linearly independent energy eigenstates of the BK problem. More formally, the BK Hamiltonian can be shown to be essentially self-adjoint on the half real line (\mathbb{R}^{\pm}) but not on the full real line (\mathbb{R}) using von Neumann's theorem [74].

Because the two solutions share the same Q -dependence for positive Q (say) their difference is an energy eigenstate that vanishes for all $Q > 0$. A conventional choice for a basis of eigenstates is to ask one basis eigenstate to vanish for $Q > 0$ and the other to vanish for $Q < 0$. This leads to the following expression for the general energy eigenvector for the BK Hamiltonian [5]

$$\phi(Q) = |Q|^{-\frac{1}{2}-i\hat{E}} [A\Theta(Q) + B\Theta(-Q)], \quad (20)$$

where A and B are the integration constants and $\Theta(Q)$ is the Heaviside step function.

The existence of a canonical transformation between the IHO and BK systems implies the existence of a canonical map that relates their quantum states [4, 7, 8]. The mapping between the states presented in (7) and (20) is provided by a ‘quantum canonical transform’ (see B.1)

$$\phi(\xi) = \int_0^\infty dQ Q^{-\frac{1}{2}-i\hat{E}} e^{i(-\frac{1}{2}\xi^2 + \sqrt{2}\xi Q - \frac{1}{2}Q^2)} \quad (21)$$

which can be recognised as one of the integral representations of parabolic cylinder functions, and will be discussed in more detail in section 4.

3.3. ISP

The ISP problem has the Hamiltonian appropriate to an interaction potential whose strength falls off like the square of the distance from the origin

$$H = \frac{1}{2} P^2 - \frac{g}{Q^2}, \quad (22)$$

and our focus here is on attractive potentials for which $g > 0$. This Hamiltonian also enjoys a spectrum-generating scale invariance because $H \rightarrow \zeta^{-2} H$ under the scale transformation $Q \rightarrow \zeta Q$ [109]. Classically, the generator of the scale transformation is $D = QP$, which satisfies

$$\frac{dD}{dt} = 2H \quad (23)$$

and so is not conserved unless restricted to configurations with vanishing energy. Equation (23) is called an *almost* conservation law [110].

The quantum version of this problem has the time-independent Schrödinger equation

$$Q^2 \frac{\partial^2 \psi}{\partial Q^2} + (2g - \kappa^2 Q^2) \psi = 0, \quad (24)$$

for energy eigenvalue $\mathcal{E} = -E = -\frac{1}{2}\kappa^2$. The change of variables $\psi(z) = z^l e^{-z/2} u(z)$ for $z = 2\kappa Q$ and l satisfying $l = \frac{1}{2}(1 + \zeta)$ with

$$\zeta := \sqrt{1 - 8g}, \quad (25)$$

leads to a new dependent variable $u(z)$ that satisfies the confluent hypergeometric equation. Notice that ζ changes from real to imaginary at what is called the critical coupling $g_c = \frac{1}{8}$.

The two linearly independent solutions of equation (24) are

$$\psi_{\pm}(Q) = (2\kappa Q)^{\frac{1}{2}(1 \pm \zeta)} e^{-\kappa Q} M\left[\frac{1}{2}(1 \pm \zeta), 1 \pm \zeta; 2\kappa Q\right], \quad (26)$$

provided $1 \pm \zeta$ is not a nonpositive integer, where $M(a, b; z) = 1 + (a/b)z + \dots$ is the confluent hypergeometric function.

Famously, when $g > 0$ both of the solutions (26) can be singular at $Q = 0$ and so (unlike for the Coulomb problem) one cannot use the regularity of the solution at the origin as a criterion for selecting one or the other. Instead the eigenvalue problem for this Hamiltonian is not well-posed without specifying a boundary condition [109] at $Q = 0$. Physically this conveys how the solutions depend on the properties of whatever the object is that sits at $Q = 0$ (and so is ultimately responsible for the existence of the $1/Q^2$ potential). Although this boundary condition is often chosen to ensure the Hamiltonian is self-adjoint, this need not be what is required by specific physical situations (such as when the origin is a source or sink of probability [33]).

In practice the divergence of solutions at $Q = 0$ usually means any boundary condition is actually imposed at a small but nonzero $Q = \epsilon$. This boundary condition is often linear (Robin-type boundary condition) and when it is it can be written

$$\left. \frac{\partial \psi}{\partial Q} \right|_{Q=\epsilon} = \lambda \psi(\epsilon), \quad (27)$$

for some constant λ . Conditions of this form are sometimes also referred to as Bethe–Peierls boundary conditions following their early application in nuclear physics [111]. A modern systematic method for determining boundary conditions at small distances is provided by PPEFT wherein the boundary condition can be related to an effective action describing the object at the origin and because of this dimensional arguments can be applied that typically lead to (27) at low energy [112]. In the present context of the scale invariant ISP, imposing a boundary condition at nonzero Q breaks scale invariance and this ultimately causes anomaly-type quantum breaking of the classical scale invariance. Furthermore, because the regularisation scale ϵ is arbitrary it cannot appear in physical predictions. This turns out to be ensured by an implicit ϵ -dependence carried by the parameter λ , which adjusts as a function of ϵ in a way that keeps physical observables fixed; an adjustment that is captured by an RG flow $\lambda = \lambda(\epsilon)$ [112]. Comparison with well-understood systems (such as atoms) with small objects at the origin (nuclei) shows that the physical scale associated with the physics at $Q = 0$ is ultimately an RG invariant of this flow [113–116].

4. Mapping between the IHO and the ISP system

We now construct the mapping between the IHO/BK system and the ISP system. We remind the reader that our convention for the energy eigenvalue for the IHO and BK systems is $-E = -\hat{E}\hbar\omega$ so that positive E describes negative energy states. However, as we shall see in this section, this choice makes little difference to the ISP system due to the squaring step.

4.1. Mapping of the Hamiltonian

The main construction in the duality mapping relates the *square* of the BK Hamiltonian to the ISP Hamiltonian. The eigenstates $\phi(Q)$ of the BK Hamiltonian are also eigenstates of its square but with a squared eigenvalue

$$\left(\frac{Q \cdot P + P \cdot Q}{2}\right)^2 \phi(Q) = \hat{E}^2 \phi(Q). \quad (28)$$

In the position representation this equation for the squared BK Hamiltonian can easily be seen to take the form

$$\left[Q^2 \frac{\partial^2}{\partial Q^2} + 2Q \frac{\partial}{\partial Q} + \left(\hat{E}^2 + \frac{1}{4}\right)\right] \phi(Q) = 0. \quad (29)$$

Using the integrating factor

$$\phi(Q) = \frac{\chi(Q)}{Q}, \quad (30)$$

then gives

$$-\frac{\partial^2 \chi(Q)}{\partial Q^2} - \frac{(\hat{E}^2 + \frac{1}{4})}{Q^2} \chi(Q) = 0, \quad (31)$$

which with the definition

$$2g = \hat{E}^2 + \frac{1}{4} \geq \frac{1}{4}, \quad (32)$$

is the ISP Schrödinger equation (24) restricted to the case of zero energy ($\kappa^2 = 0$). Notice that the restriction to $\kappa^2 = 0$ ensures that the condition (23) becomes a conservation rule. The condition $2g > \frac{1}{4}$ means $g > g_c = \frac{1}{8}$ and so the coupling given by our mapping is always super-critical.

The solution $\chi(Q)$ for the ISP Schrödinger equation specialised to zero energy is particularly simple because the confluent hypergeometric equation degenerates to the Euler equation, which has power-law solutions. The most general solution is

$$\chi(Q) = \alpha Q^{\frac{1}{2} - i\hat{E}} + \beta Q^{\frac{1}{2} + i\hat{E}} \quad (33)$$

where α and β are integration constants. These two basis solutions are linearly independent if $\hat{E} \neq 0$. They both exhibit logarithmic phase singularities as did the solutions in equation (20) for the BK Hamiltonian. We see that the effect of the squaring is to allow $\pm\hat{E}$ states (these do *not* correspond to energy on the ISP side of the mapping).

From this point of view the boundary-condition ambiguity at the origin in the ISP system maps directly onto the boundary condition ambiguity of the IHO problem; in both cases normalisability cannot be used to choose a preferred state and a boundary condition is instead required near a singular point (at Q near zero for the ISP problem and at large ξ for the IHO problem). This implies in particular that the entire RG description for the ISP problem [33, 112] can be directly mapped across to the IHO (and its applications).

4.2. Mapping the states

Equation (30) shows explicitly how zero-energy states $\chi(Q)$ for an attractive ISP with super-critical coupling g are mapped to energy eigenstates $\phi(Q)$ of the BK system with energy $E(g)$ given by (32). The quantum canonical transformation described in (21) then maps the result onto an IHO state $\phi(\xi)$.

In this language the zero-energy ISP solution

$$\chi(Q) = \alpha Q^{\frac{1}{2} - i\hat{E}} \quad (34)$$

becomes the BK solution

$$\phi(Q) = \alpha Q^{-\frac{1}{2} - i\hat{E}} \quad (35)$$

and this in turn maps over to the following IHO eigenstate via [4]

$$\phi_1(\xi) = \alpha \int_0^\infty dQ Q^{-i\hat{E} - \frac{1}{2}} e^{i(-\frac{1}{2}\xi^2 + \sqrt{2}\xi Q - \frac{1}{2}Q^2)}. \quad (36)$$

Noting that parabolic cylinder functions $D_s(z)$ have the integral representation [8]

$$D_s\left(\frac{b}{\sqrt{2a}}\right) = \frac{(2a)^{-s/2}}{\Gamma(-s)} \int_0^\infty dQ Q^{-s-1} e^{-aQ^2 - bQ - \frac{b^2}{8a}} \quad (37)$$

and putting $a = i/2$, $b = -\sqrt{2}i\xi$, $s = i\hat{E} - \frac{1}{2}$, the integral in (36) becomes

$$\phi_1(\xi) = \alpha e^{-\frac{\pi\hat{E}}{4}} e^{-i\pi/8} \Gamma\left(\frac{1}{2} - i\hat{E}\right) D_{i\hat{E} - \frac{1}{2}}\left(\sqrt{2}e^{-i3\pi/4}\xi\right) \quad (38)$$

which is the first of the IHO wavefunctions. Its coefficient α maps over directly from the first ISP solution since the mapping does not mix in any of the second IHO wavefunction $\phi_2(\xi)$. A similar construction applies to the second ISP solution $\beta Q^{i\hat{E} - \frac{1}{2}}$, which maps across to the IHO state

$$\phi_2(\xi) = \beta \int_0^\infty dQ Q^{i\hat{E} - \frac{1}{2}} e^{i(\frac{1}{2}\xi^2 + \sqrt{2}\xi Q + \frac{1}{2}Q^2)}. \quad (39)$$

See appendix B.2 for details on how to obtain the above form of kernel that generates the second IHO state. Using (37) again, but with $a = -\frac{i}{2}$, $b = -\sqrt{2}i\xi$ and $s = -\frac{1}{2} - i\hat{E}$, allows the second solution on the IHO side to be written

$$\phi_2(\xi) = \beta e^{-\frac{\pi\hat{E}}{4}} e^{i\pi/8} \Gamma\left(\frac{1}{2} + i\hat{E}\right) D_{-i\hat{E} - \frac{1}{2}}\left(\sqrt{2}e^{-i\pi/4}\xi\right). \quad (40)$$

It follows that the general zero-energy ISP eigenstate $[\chi(Q) = \alpha Q^{\frac{1}{2} - i\hat{E}} + \beta Q^{\frac{1}{2} + i\hat{E}}]$ given in (33) maps over to the IHO state $[\phi(\xi) = C_1 D_{i\hat{E} - \frac{1}{2}}(\sqrt{2}e^{-i3\pi/4}\xi) + C_2 D_{-i\hat{E} - \frac{1}{2}}(\sqrt{2}e^{-i\pi/4}\xi)]$ given in (7) where the constants C_1 and C_2 are expressed in terms of α and β by

$$C_1 = \alpha e^{-\frac{\pi\hat{E}}{4}} e^{-i\pi/8} \Gamma\left(\frac{1}{2} - i\hat{E}\right), \quad C_2 = \beta e^{-\frac{\pi\hat{E}}{4}} e^{i\pi/8} \Gamma\left(\frac{1}{2} + i\hat{E}\right). \quad (41)$$

Physical predictions depend only on the ratios α/β and C_1/C_2 and so are related by

$$\frac{C_1}{C_2} = \left(\frac{\alpha}{\beta}\right) \frac{\Gamma\left(\frac{1}{2} - i\hat{E}\right)}{\Gamma\left(\frac{1}{2} + i\hat{E}\right)} e^{-i\pi/4}. \quad (42)$$

4.3. Mapping the boundary condition

The previous sections show in detail how the zero-energy states of the super-critical ISP system are mapped onto the states of the IHO system. Expression (42) is the core of a complete solution to the question of how to map observables (like scattering rates) in the IHO onto similar observables in the ISP system. Once the observable is known as a function of α/β or C_1/C_2 then this map can be used to relate observables directly to one another.

It can be more useful to directly relate the boundary condition that makes the ISP well-defined with the boundary condition used for the IHO. That is, suppose the ISP imposes the linear boundary condition (27) with constant λ_{ISP} at $Q = \epsilon$ and the IHO involves a similar boundary condition at large $\xi = L$ (with constant λ_{IHO}). How are the parameters λ_{ISP} and λ_{IHO} related by the map between these two systems? Finding this relation is our purpose in the present section. We do so by using (42) together with the predictions for α/β as a function of the pair $(\lambda_{\text{ISP}}, \epsilon)$ and for C_1/C_2 as function of $(\lambda_{\text{IHO}}, L)$.

An important complication arises because the mapping from the pair (λ, ϵ) to a ratio like C_1/C_2 is many to one. It is many to one because the scale ϵ is arbitrary and so λ necessarily varies as ϵ does, in precisely the way required to ensure that observables (and so also ratios like α/β and C_1/C_2) remain ϵ -independent. Because of this the prediction for observables from boundary conditions proceeds in two steps. First, one identifies the RG-invariant quantities that characterise the curve $\lambda(\epsilon)$. Second, a formula is derived for α/β

or C_1/C_2 as a function of these RG invariants (see [112] for details). We therefore pause briefly to recap how λ_{ISP} and λ_{IHO} run.

ISP case: we start by reviewing the zero-energy ISP case [112], for which the energy eigenstates are

$$\chi(Q) = \alpha Q^{\frac{1}{2}-i\hat{E}} + \beta Q^{\frac{1}{2}+i\hat{E}}, \quad (43)$$

where $\hat{E} := E/\hbar\omega$ is computed from the ISP coupling g using (32). We wish to determine the ratio α/β that follows from (27), which we rewrite in the equivalent form

$$\lambda_{\text{ISP}} = \frac{1}{\chi(\epsilon)} \left(\frac{\partial \chi}{\partial Q} \right)_{Q=\epsilon}. \quad (44)$$

The relation between λ_{ISP} and α/β is found by substituting in (43) for $\chi(Q)$. The result is

$$\frac{\lambda_{\text{ISP}}}{i\hat{E}} = \frac{1 - (\alpha/\beta) \epsilon^{-2i\hat{E}}}{1 + (\alpha/\beta) \epsilon^{-2i\hat{E}}}, \quad (45)$$

where

$$\Lambda_{\text{ISP}} := \epsilon \lambda_{\text{ISP}} - \frac{1}{2}. \quad (46)$$

There are two ways to read these last two expressions. First they can be solved for α/β , giving the solution for the integration constants as a function of the boundary data (λ, ϵ)

$$\frac{\alpha}{\beta} = \frac{1 + i(\Lambda_{\text{ISP}}/\hat{E})}{1 - i(\Lambda_{\text{ISP}}/\hat{E})} e^{2i\hat{E}}. \quad (47)$$

The second way to read (45) and (46) is as a solution to the question of how λ_{ISP} must vary as a function of ϵ if changes to ϵ are to not change α/β (which controls the size of observables). This defines an RG running to the extent that it dictates how λ must depend on ϵ in order for the precise value of ϵ not to matter for physical predictions. In this view the ϵ -dependence of (47) is telling us that physics depends only on the curve $\{\lambda(\epsilon), \epsilon\}$, and so α/β depends only on the properties that specify this curve—perhaps an initial condition $\lambda(\epsilon_0) = \lambda_0$, though any other RG-invariant characterisation works equally well. In fact, for the ISP system it is known that RG flow in the super-critical regime gives rise to curves $\lambda(\epsilon)$ that are generically limit cycles which encircle but never reach one of two fixed points in the complex λ -plane (the fixed points are complex conjugates of each other) [66–69]. Complex λ indicates that the theory is not self-adjoint and can describe the absorption or emission of particles at the origin. In fact, the behaviour of the fixed points of the boundary condition in the super-critical ISP case is an example of a \mathcal{PT} symmetry breaking transition [70] that is more commonly studied in the eigenvectors of non-hermitian quantum mechanical systems [117]. The flow around a limit cycle gives rise to log-periodic behaviour of physical observables (such as elastic and non-elastic scattering cross-sections) as a functions of experimentally tuneable parameters like incident energy [33, 112].

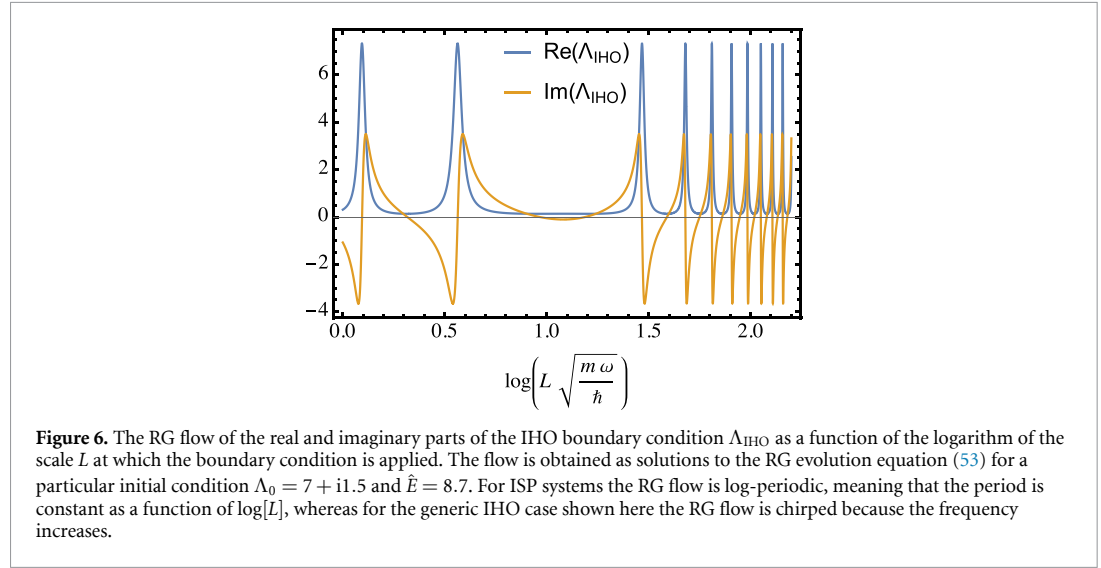
A convenient choice for the RG-invariant characterisation of $\Lambda_{\text{ISP}}(\epsilon)$ is given by the pair (ϵ_*, γ_*) , where $\epsilon = \epsilon_*$ is the scale where the trajectory $\Lambda_{\text{ISP}}(\epsilon)$ crosses the imaginary axis, taking the value $\Lambda_{\text{ISP}}(\epsilon_*) = i\gamma_*$. This is convenient because the RG-invariant scale ϵ_* corresponds to the physical scattering length once α/β is computed and converted into a scattering cross section. The differential version of the running is easier if (47) is differentiated holding α/β and \hat{E} fixed, and implies

$$\epsilon \frac{d}{d\epsilon} \left(\frac{\Lambda_{\text{ISP}}}{i\hat{E}} \right) = i\hat{E} \left[1 - \left(\frac{\Lambda_{\text{ISP}}}{i\hat{E}} \right)^2 \right]. \quad (48)$$

This shows how the pure imaginary choices $\Lambda_{\text{ISP}} = \pm i\hat{E}$ are the only fixed points. Using these in (47) shows that these fixed points correspond to boundary conditions that set either α or β to zero, corresponding to purely incoming or outgoing waves [33, 56]. Notice also that the flow (48) maps the real axis to itself and so preserves the reality of Λ_{ISP} in the special case where the initial condition is real.

IHO case: a similar story goes through for the IHO. For large ξ the asymptotics of the parabolic cylinder functions imply the energy eigenstates of the IHO are given by [102]

$$\phi(\xi) \sim \frac{C_1}{\sqrt{\xi}} e^{i(\frac{1}{2}\xi^2 - \hat{E}\ln(\sqrt{2\xi}) + \frac{1}{2}\theta + \frac{\pi}{4})} + \frac{C_2}{\sqrt{\xi}} e^{-i(\frac{1}{2}\xi^2 - \hat{E}\ln(\sqrt{2\xi}) + \frac{1}{2}\theta + \frac{\pi}{4})} \quad (49)$$



where C_1 and C_2 are the integration constants in (7). Here $\theta = \arg \Gamma(\frac{1}{2} + i\hat{E})$.

The choices $C_1 = 0$ or $C_2 = 0$ correspond to waves asymptotically propagating only in one direction, as can be seen by combining (49) with the time-dependence $e^{-i\mathcal{E}t/\hbar} = e^{+iEt/\hbar}$ and noting that the direction of propagation for the wavefunction can be evaluated using the group velocity obtained from the total phase of the wavefunction $\Phi(\xi) = \text{Arg}[\phi(\xi)]$ [9]. If the definition of the local wavenumber is defined to be $K(\xi) = \frac{\partial \Phi}{\partial \xi}$ then the definition of the group velocity is $v_g = (\frac{\partial K}{\partial E})^{-1}$.

If the ratio C_1/C_2 is determined by a boundary condition of the type (27) then using (49) in $\lambda_{\text{IHO}} = \phi^{-1}(\partial \phi / \partial \xi)_{\xi=L}$ gives an explicit relation

$$\Lambda_{\text{IHO}} = i \frac{1 - (C_1/C_2) e^{2i\Omega(L)}}{1 + (C_1/C_2) e^{2i\Omega(L)}}, \quad (50)$$

where the dimensionless quantity Λ_{IHO} is a rescaled version of λ_{IHO} and is defined to be

$$\Lambda_{\text{IHO}} := \frac{\sqrt{m\omega/\hbar} L \lambda_{\text{IHO}} + 1/2}{[\hat{E} - (m\omega L^2/\hbar)]}, \quad (51)$$

and the phase $\Omega(L)$ is defined as

$$\Omega(L) := \frac{m\omega L^2}{2\hbar} - \hat{E} \ln \left(\sqrt{\frac{2m\omega}{\hbar}} L \right) + \frac{\theta}{2} + \frac{\pi}{4}. \quad (52)$$

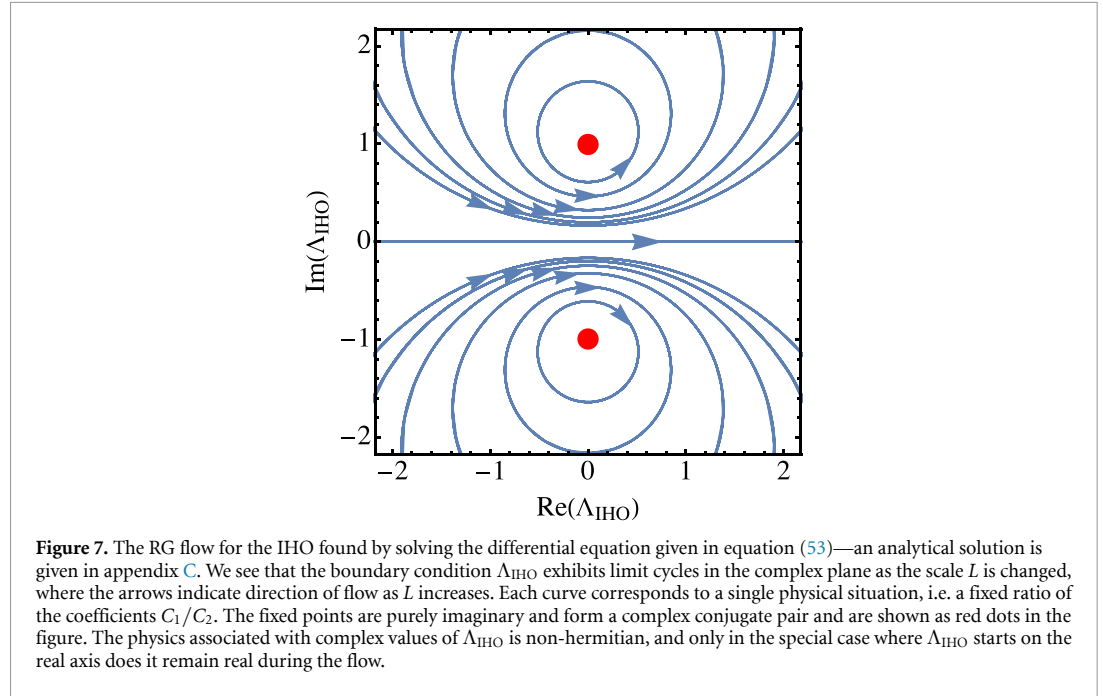
Similarly to the ISP case, these expressions can be read as defining how λ_{IHO} must depend on L in order to ensure that C_1/C_2 is L -independent, as well as giving an explicit formula for C_1/C_2 as a function of the curve $\lambda_{\text{IHO}}(L)$.

The differential evolution of Λ_{IHO} can be written as

$$L \frac{d\Lambda_{\text{IHO}}}{dL} = \left(\frac{m\omega L^2}{\hbar} - \hat{E} \right) (\Lambda_{\text{IHO}}^2 + 1) \quad (53)$$

which reveals fixed points at $\Lambda_{\text{IHO}} = \pm i$. A sample solution to this equation (the analytical solution is given in appendix C) is shown in figure 6 where we see that the RG flow of the real and imaginary parts of Λ_{IHO} as the length scale L is varied is reminiscent of the log-periodic behaviour of the ISP problem, compare with figure 2 in [33]. Log-periodic behaviour indicates that the continuous scaling symmetry of the classical problem is broken down to a discrete scaling symmetry by a quantum anomaly. The trajectories in the complex Λ_{IHO} plane are limit cycles as shown in figure 7, i.e. their geometry in the complex plane is just like that in the ISP. However, the flow along these limit cycles is *faster* than log periodic; the frequency gradually increases as $\log(L)$ increases giving rise to a chirped behaviour as seen in figure 6.

Whereas continuous scaling symmetry is explicit in the Hamiltonian of the ISP problem, i.e. the Hamiltonian commutes with the scaling operator, the IHO system does not appear to have scaling symmetry.



The question is then what continuous symmetry is being broken to give rise to the limit cycles in its RG flow? The answer is that the IHO Hamiltonian is part of a larger symmetry group, namely the $SU(1,1)$ group associated with the spectrum generating algebra discussed in section 3.2 (equation (10)). Following [103], we therefore refer to this as a *hidden* symmetry of the IHO and the limit cycles indicate an anomalous breaking of this hidden symmetry by the linear boundary condition imposed at long distances.

Clearly the map (42) between α/β and C_1/C_2 together with expressions like (45) and (50) allow boundary condition parameters like λ_{ISP} and λ_{IHO} to be related to one another. This is most usefully done by relating the RG-invariant characterisation of these couplings on either side of the mapping.

5. Conclusions

It has been known for some time that the IHO problem is equivalent to the BK problem through an explicit canonical transformation. In this paper we provide a precise mapping between this joint system and a particle in an ISP with a super-critical attractive coupling. The map relates the zero-energy subspace of the ISP problem to the eigenstates of the IHO/BK system, with the square of the IHO energy $\mathcal{E} = -E = -\tilde{E}\hbar\omega$ being mapped into the *strength* of the ISP $-g/Q^2$ through expression (32).

There are a number of symmetries connecting the IHO, BK and ISP systems. The BK and ISP Hamiltonians have scaling symmetry such that the generator of scale transformations commutes with their Hamiltonians. The IHO Hamiltonian does not have such a scaling symmetry, but a spectrum generating symmetry is still present through an $su(1,1)$ spectrum generating Lie algebra as recorded in equation (9) that links the IHO, BK and simple harmonic oscillator Hamiltonians. Thus, we say that the IHO has hidden symmetry. The ISP Hamiltonian is linked to this algebra because it is given by the square of the BK Hamiltonian. The breaking of scaling symmetry by the introduction of a regulator corresponds to an opening of this algebra [62] and the appearance of a quantum anomaly.

Besides showing how the Hamiltonians of these systems are related we also explicitly identify how a convenient basis of energy eigenstates are mapped into one another. Physical applications in both systems rely on the specification of boundary conditions and we use our knowledge of how the states are mapped to see how the boundary conditions are also related (in the typical case where the boundary condition is linear, as defined in equation (27), which can be justified using PPEFT [112]). On both the IHO and ISP sides of the duality the boundary condition coefficient λ undergoes an RG flow as the length scales (L and ϵ , respectively) at which the boundary conditions are applied are varied. The flows take the characteristic form of limit cycles in the complex plane around a pair of fixed points which are complex conjugates of each other. The fact that these fixed points are complex indicates a \mathcal{PT} symmetry breaking transition and physically corresponds to the emission or absorption of particles.

Having these systems be explicitly related explains why they share distinctive features such as classical scale invariance with quantum anomalies. Many systems reduce to these models in particular limits (e.g. Schwinger pair-production can be related to solutions of the IHO problem) and one hopes the mapping described here will help find new connections amongst these ancillary systems.

Data availability statement

No new data were created or analysed in this study.

Acknowledgments

C B and D O acknowledge funding from the Natural Sciences and Engineering Research Council of Canada through Discovery Grants. Research at the Perimeter Institute is supported in part by the Government of Canada through the Department of Innovation, Science and Economic Development and by the Province of Ontario through the Ministry of Colleges and Universities. S S dedicates this paper to the memory of his beloved mother Chithra Narayanan.

Appendix A. Verification that the two solutions $\phi_1(\xi)$ and $\phi_2(\xi)$ of the IHO have the same energy

In section 3.1 of the main body of the paper we started off with an inverted harmonic oscillator Schrödinger equation in the form

$$\frac{\pi^2 - \xi^2}{2} \phi(\xi) = -\hat{E} \phi(\xi). \quad (\text{A.1})$$

In the ξ representation this can be written as

$$\left(-\frac{1}{2} \frac{d^2}{d\xi^2} - \frac{1}{2} \xi^2 \right) \phi = -\hat{E} \phi. \quad (\text{A.2})$$

We shall now check if both the solutions $\phi_1(\xi)$ and $\phi_2(\xi)$ of the IHO given in equation (7) are states with the same energy as claimed.

- (i) We first note that the standard parabolic cylinder differential equation that is satisfied by $\phi = D_\nu(z)$ is given in [102] as

$$\frac{d^2 \phi}{dz^2} + \left(\nu + \frac{1}{2} - \frac{z^2}{4} \right) \phi = 0. \quad (\text{A.3})$$

- (ii) To find the differential equation whose solution is $\phi_1(\xi) = D_{i\hat{E}-\frac{1}{2}}(\sqrt{2}e^{-i3\pi/4}\xi)$, we put

$$z = \sqrt{2}e^{-i3\pi/4}\xi \quad (\text{A.4})$$

which means that $\frac{z^2}{4} = \frac{i}{2}\xi^2$. We also write the index as $\nu = i\hat{E} - \frac{1}{2}$. The parabolic cylinder differential equation in equation (A.3) then becomes

$$\left(-\frac{i}{2} \frac{d^2}{d\xi^2} + i\hat{E} - \frac{i}{2} \xi^2 \right) \phi_1 = 0 \quad (\text{A.5})$$

which can be written as

$$\left(-\frac{1}{2} \frac{d^2}{d\xi^2} - \frac{1}{2} \xi^2 \right) \phi_1 = -\hat{E} \phi_1 \quad (\text{A.6})$$

which is same as equation (A.2).

- (iii) Next we find the underlying differential equation for the second solution $\phi_2(\xi) = D_{-i\hat{E}-\frac{1}{2}}(\sqrt{2}e^{-i\pi/4}\xi)$. This time we put

$$z = \sqrt{2}e^{-i\pi/4}\xi \quad (\text{A.7})$$

which implies that $\frac{z^2}{4} = -\frac{i}{2}\xi^2$. Writing the index as $\nu = -i\hat{E} - \frac{1}{2}$ the same parabolic cylinder equation equation (A.3) now becomes

$$\left(\frac{i}{2} \frac{d^2}{d\xi^2} - iE + \frac{i}{2}\xi^2\right) \phi_2 = 0 \quad (\text{A.8})$$

which upon simplification yields

$$\left(-\frac{1}{2} \frac{d^2}{d\xi^2} - \frac{1}{2}\xi^2\right) \phi_2 = -\hat{E}\phi_2 \quad (\text{A.9})$$

which is equation (A.2) again.

Thus, we have shown that both $\phi_1(\xi)$ and $\phi_2(\xi)$ are solutions of the IHO equation with the same energy, and the claim is proved. Furthermore, these two solutions are linearly independent as their Wronskian is non-zero [102]

$$\mathcal{W}\left(D_{i\hat{E}-\frac{1}{2}}\left(\sqrt{2}e^{-i3\pi/4}\xi\right), D_{-i\hat{E}-\frac{1}{2}}\left(\sqrt{2}e^{-i\pi/4}\xi\right)\right) = -ie^{-\pi\hat{E}/2}, \quad (\text{A.10})$$

and so the solution given in equation (7) is indeed the general solution to the IHO Schrödinger equation (5) with energy $-\hat{E}$.

Appendix B. The quantum canonical transform from wavefunctions in Q to wavefunctions in ξ

In this appendix we explain the basic idea behind quantum canonical transforms and also derive the two specific transforms given in the main text in equations (36) and (39). The quantum canonical transforms used in this paper take wavefunctions in the Q variable and map them to wavefunctions in the ξ variable. Both the ISP and BK wavefunctions are functions of Q , whereas the IHO wavefunctions are functions of ξ . It is perhaps surprising that two different transforms are needed, but this can ultimately be traced back to the fact that the BK wavefunctions live in two disconnected half-spaces as summarised in equation (20). This means that the BK system is governed by a first order differential equation with only a single solution (in each half space) whereas the ISP and IHO systems are governed by second order differential equations with two independent solutions. To map between these different systems therefore requires some ingenuity; in [4] they solve the problem of mapping between the BK and IHO systems by obtaining their second solution from the momentum space representation of the BK Hamiltonian, whereas we prefer to remain in a single representation and instead solve the problem by squaring the BK Hamiltonian which has the added bonus of straightforwardly connecting to the ISP system. One interpretation of the squaring is that by allowing both energies $\pm\hat{E}$ it in some sense includes both particle and antiparticle type solutions on an equal footing. Equivalently, we note that the BK Hamiltonian breaks time reversal symmetry since it is not invariant under $P \rightarrow -P$, but squaring restores this symmetry.

B.1. From Berry–Keating states to inverted harmonic oscillator states

References [4, 8] describe the mapping of the BK states to parabolic cylinder states which we now discuss in detail. The classical version of this mapping is a canonical transformation and it is worthwhile recalling the theory of canonical transformations via generating functions in classical mechanics [118]. There are four classes of generating functions but for the first transform (as given in equation (36)) we need the first class $F_1 = F_1(\xi, Q, t)$. This generates a transformation via the relations $P = -\partial F_1 / \partial Q$ and $\pi = \partial F_1 / \partial \xi$ where (ξ, π) and (Q, P) are the old and new phase space variables, respectively. Taking

$$F_1(\xi, Q) = -\frac{\xi^2}{2} + \sqrt{2}\xi Q - \frac{Q^2}{2}, \quad (\text{B.1})$$

it can be readily verified that F_1 gives the required BK \leftrightarrow IHO canonical transformation $Q = \frac{\pi+\xi}{\sqrt{2}}, P = \frac{\pi-\xi}{\sqrt{2}}$.

Coming now to the quantum case, the BK Schrödinger equation in the Q representation is (equation (17) in the main text)

$$Q \frac{\partial \phi}{\partial Q} = \left(-i\hat{E} - \frac{1}{2}\right) \phi(Q), \quad (\text{B.2})$$

and its solution is given by

$$\phi(Q) = Q^{-i\hat{E}-1/2}. \quad (\text{B.3})$$

To map this to the ξ representation we apply a *quantum canonical transform* [119–121]

$$\phi(\xi) = \int dQ \langle \xi | Q \rangle \langle Q | \phi \rangle = \int_0^\infty dQ \underbrace{e^{iF_1(\xi, Q)}}_{\langle \xi | Q \rangle} \underbrace{\phi(Q)}_{\langle Q | \phi \rangle}. \quad (\text{B.4})$$

The function $F_1(\xi, Q)$ in the kernel $\langle \xi | Q \rangle = e^{iF_1(\xi, Q)/\hbar}$ can be derived following Dirac [119]

$$\langle \xi | \pi | Q \rangle = -i\hbar \frac{\partial}{\partial \xi} \langle \xi | Q \rangle = \left(\frac{\partial F_1}{\partial \xi} \right) \langle \xi | Q \rangle = \langle \xi | \frac{\partial F_1}{\partial \xi} | Q \rangle \quad (\text{B.5})$$

which implies

$$\pi = \frac{\partial F_1}{\partial \xi}. \quad (\text{B.6})$$

Similarly,

$$\langle \xi | P | Q \rangle = i \frac{\partial}{\partial Q} \langle \xi | Q \rangle = -\frac{\partial F_1}{\partial Q} \langle \xi | Q \rangle = -\langle \xi | \frac{\partial F_1}{\partial Q} | Q \rangle \quad (\text{B.7})$$

which implies

$$P = -\frac{\partial F_1}{\partial Q}. \quad (\text{B.8})$$

Together these yield

$$\langle \xi | Q \rangle = e^{iF_1(\xi, Q)} = e^{i\left(-\frac{\xi^2}{2} + \sqrt{2}\xi Q - \frac{Q^2}{2}\right)}. \quad (\text{B.9})$$

The quantum canonical transform to the ξ representation is therefore

$$\phi(\xi) = \int_0^\infty dQ Q^{-i\hat{E}-1/2} e^{i\left(-\frac{\xi^2}{2} + \sqrt{2}\xi Q - \frac{Q^2}{2}\right)} \quad (\text{B.10})$$

which is also an example of a Mellin transform [74]. Making use of the representation of the parabolic cylinder function $D_s(\xi)$ given in equation (B6) in [8]

$$D_s\left(\frac{b}{\sqrt{2a}}\right) = \frac{(2a)^{-s/2}}{\Gamma(-s)} e^{-\frac{b^2}{8a}} \int_0^\infty dQ Q^{-s-1} e^{-aQ^2 - bQ}, \quad (\text{B.11})$$

and putting

$$a = i/2 \quad (\text{B.12})$$

$$s = i\hat{E} - 1/2 \quad (\text{B.13})$$

$$b = -\sqrt{2}i\xi \quad (\text{B.14})$$

one recognises that the wavefunction $\phi(\xi)$ in equation (B.10) can be written in terms of parabolic cylinder functions as

$$\phi(\xi) = e^{-\pi\hat{E}/4} e^{-i\pi/8} \Gamma\left(\frac{1}{2} - i\hat{E}\right) D_{i\hat{E}-1/2}\left(\sqrt{2}e^{-i3\pi/4}\xi\right) \quad (\text{B.15})$$

which is equation (38) for $\phi_1(\xi)$ in the main text (apart from the coefficient α).

How do we find the second solution $\phi_2(\xi)$? At first sight it seems that there is only a single solution $\phi(Q)$, as given in equation (B.3), available on the BK side to transform over to the IHO side. One way to get a second solution is to change into the momentum representation for the BK Schrödinger equation

$$P \frac{\partial \psi}{\partial P} = \left(i\hat{E} - \frac{1}{2} \right) \psi(P), \quad (\text{B.16})$$

which has the solution $\psi(P) = P^{+i\hat{E}-1/2} = [\phi(P)]^*$. This has the same structure as the Q -space solution but is complex conjugated [5]. Complex conjugation effectively changes the sign of \hat{E} and can be interpreted as a time reversal operation, as is also evident by comparing the classical solutions for the position and momentum variables given in equation (14). A quantum canonical transformation of $\psi(P)$ with the kernel [4]

$$F_2(\xi, P) = \frac{\xi^2}{2} + \sqrt{2}\xi P + \frac{P^2}{2} \quad (\text{B.17})$$

gives the second IHO solution. As the notation indicates, $F_2(\xi, P)$ is a member of the second class of generating functions [118].

However, in this paper we prefer to remain in the Q -representation and will not follow this route. Instead we shall show in the next section that when the BK Hamiltonian is squared (which is a step in the full mapping from ISP to IHO) a second spatial BK solution $Q^{+i\hat{E}-1/2}$ becomes allowed because both energies $\pm\hat{E}$ give the same eigenvalue \hat{E}^2 . This provides the second solution without the need to invoke the momentum space solution.

B.2. From inverse square potential states to inverted harmonic oscillator states

The zero energy ISP Schrödinger equation (equation (31) in the main text) is

$$\left(-\frac{\partial^2}{\partial Q^2} - \frac{\hat{E}^2 + 1/4}{Q^2} \right) \chi(Q) = 0, \quad (\text{B.18})$$

where $-\hat{E}$ is the dimensionless energy of the IHO and BK Hamiltonians that here determines the depth of the ISP (we recall that the zero-energy ISP system is directly related to square of the BK system). If $\hat{E} \neq 0$ we have an unbounded-from-below ('super-critical') ISP system, and there is an ambiguity in the boundary condition at $Q = 0$. The general solution to the zero energy ISP Schrödinger equation takes the form

$$\chi(Q) = \alpha Q^{\frac{1}{2}-i\hat{E}} + \beta Q^{\frac{1}{2}+i\hat{E}} \quad (\text{B.19})$$

which is equation (33) in the main text. The two terms in this wavefunction are linearly independent with Wronskian non-zero if $\hat{E} \neq 0$.

One can perform a quantum canonical transform integral directly from the ISP states to the IHO states $\phi(\xi)$ because the ISP states are in the same variable Q as the BK states [according to equation (30) the relationship between the BK states $\phi(Q)$ and the ISP states $\chi(Q)$ is $\phi(Q) = \chi(Q)/Q$] which are in turn related to the IHO states by the canonical transformation discussed in appendix B.1. However, the kernel needed in the quantum canonical transform is different for the two ISP states. For the first ISP state, $\alpha Q^{\frac{1}{2}-i\hat{E}}$, which maps to the BK state $\alpha Q^{-\frac{1}{2}-i\hat{E}}$, the kernel has already been derived in appendix B.1, namely $e^{iF_1(\xi, Q)}$, as given in equation (B.9). Hence, the first ISP solution can be mapped directly to the first IHO solution as

$$\phi_1(\xi) = \int_0^\infty dQ \alpha Q^{-i\hat{E}-1/2} e^{i\left(-\frac{\xi^2}{2} + \sqrt{2}\xi Q - \frac{Q^2}{2}\right)} \quad (\text{B.20})$$

which upon using the integral representation of the parabolic cylinder function $D_s(\xi)$ given in equation (B.11) with $a = i/2$, $s = i\hat{E} - 1/2$, $b = -\sqrt{2}i\xi$ yields

$$\phi_1(\xi) = \alpha e^{-\pi\hat{E}/4} e^{-i\pi/8} \Gamma\left(\frac{1}{2} - i\hat{E}\right) D_{i\hat{E}-1/2}\left(\sqrt{2}e^{-i3\pi/4}\xi\right), \quad (\text{B.21})$$

like in equation (B.15) above and also in equation (38) in the main text. The second ISP solution $\beta Q^{i\hat{E}+1/2}$ gives the second IHO solution via a different quantum canonical transform (to be derived below)

$$\phi_2(\xi) = \int_0^\infty dQ \beta Q^{i\hat{E}-1/2} e^{iG(\xi, Q)} = \int_0^\infty dQ \beta Q^{i\hat{E}-1/2} e^{i\left(\frac{\xi^2}{2} + \sqrt{2}\xi Q + \frac{Q^2}{2}\right)}. \quad (\text{B.22})$$

As before, we can use the integral representation of the parabolic cylinder function in equation (B.11) to write this integral in terms of $D_s(\xi)$ as

$$\phi_2(\xi) = \beta e^{-\pi\hat{E}/4} e^{i\pi/8} \Gamma\left(\frac{1}{2} + i\hat{E}\right) D_{-i\hat{E}-1/2}\left(\sqrt{2}e^{-i\pi/4}\xi\right) \quad (\text{B.23})$$

where this time we have put $a = -i/2$, $s = -i\hat{E} - 1/2$, $b = -\sqrt{2}i\xi$. This is equation (40) in the main text. To derive the generating function $G(\xi, Q) = \xi^2/2 + \sqrt{2}\xi Q + Q^2/2$ used in the second quantum canonical

transform we can use the following symmetry of the squared Berry–Keating equation: $Q \rightarrow P$, $P \rightarrow -Q$. This transformation is canonical because it preserves the commutation relation $[Q, P] = i$. Under this transformation the BK Hamiltonian transforms as $H_{\text{BK}} \rightarrow -H_{\text{BK}}$, and we note the second ‘BK state’ $\beta Q^{i\hat{E}-1/2}$ is an eigenfunction $-H_{\text{BK}}$. Because of the squaring step this transformation is a symmetry of the squared BK equation of motion. Hence one can use the generating function $G(\xi, Q) = \frac{\xi^2}{2} + \sqrt{2}\xi Q + \frac{Q^2}{2}$ that generates the following canonical transformation

$$Q \rightarrow P \quad \text{implies} \quad Q = \frac{\pi - \xi}{\sqrt{2}} \quad (\text{B.24})$$

$$P \rightarrow -Q \quad \text{implies} \quad P = -\left(\frac{\pi + \xi}{\sqrt{2}}\right) \quad (\text{B.25})$$

to build the second linearly independent IHO state using the squared BK state. Comparing the function $G(\xi, Q)$ with $F_2(\xi, P)$ in equation (B.17) we see they have an identical structure except for exchanging Q and P .

Finally we note that the Wronskian for these two parabolic cylinder states is non-zero [102]

$$\mathcal{W}\left(D_{i\hat{E}-1/2}\left(\sqrt{2}e^{-i3\pi/4}\xi\right), D_{-i\hat{E}-1/2}\left(\sqrt{2}e^{-i\pi/4}\xi\right)\right) = -ie^{-\pi\hat{E}/2} \quad (\text{B.26})$$

which means they are linearly independent. So we get two linearly independent solutions (parabolic cylinder functions) to the IHO in the ξ variables from the inverse square solutions in the Q variables.

Appendix C. Solutions to the RG differential equation for the IHO system

In the main body of the paper, equation (53) gives the differential equation for the RG flow for the IHO system

$$L \frac{d\Lambda_{\text{IHO}}}{dL} = \left(\frac{m\omega L^2}{\hbar} - \hat{E}\right) (\Lambda_{\text{IHO}}^2 + 1). \quad (\text{C.1})$$

By integrating the above equation for a given initial condition Λ_0 we find the solution

$$\Lambda_{\text{IHO}} = \frac{\Lambda_0 + \tan\left(m\omega/2\hbar L^2 - \hat{E} \ln\left(\sqrt{2m\omega/\hbar}L\right)\right)}{1 - \Lambda_0 \tan\left(m\omega/2\hbar L^2 - \hat{E} \ln\left(\sqrt{2m\omega/\hbar}L\right)\right)}. \quad (\text{C.2})$$

The plot given in figure 6 shows the real and imaginary parts of this solution as a function of $\ln(\sqrt{m\omega/\hbar}L)$. The phase portrait in the complex plane is given in figure 7 which exhibits limit cycles like in the ISP system, however the flow of the IHO system is faster than the log periodic behaviour found in the ISP and is discussed in detail in section 4.

ORCID iD

D H J O’Dell  <https://orcid.org/0000-0003-1463-1527>

References

- [1] Landau L D and Lifshitz E M 1965 *Quantum Mechanics (Non-Relativistic Theory)* (Pergamon)
- [2] Perelomov A M and Popov V S 1970 *Theor. Math. Phys.* **4** 664–77
- [3] Balazs N L and Voros A 1990 *Ann. Phys., NY* **199** 123–40
- [4] Brout R, Massar S, Parentani R and Spindel P 1995 *Phys. Rep.* **260** 329–446
- [5] Berry M V and Keating J P 1999 $H = xp$ and the Riemann Zeros *Supersymmetry and Trace Formulae: Chaos and Disorder* ed I V Lerner, J P Keating and D E Khmelnitskii (Springer) pp 355–67
- [6] Chruściński D 2003 *J. Math. Phys.* **44** 3718–33
- [7] Subramanyan V, Hegde S S, Vishveshwara S and Bradlyn B 2021 *Ann. Phys., NY* **435** 168470
- [8] Ullinger F, Zimmermann M and Schleich W P 2022 *AVS Quantum Sci.* **4** 1–19
- [9] Barton G 1986 *Ann. Phys., NY* **166** 322–63
- [10] Yuce C, Kilic A and Coruh A 2006 *Phys. Scr.* **74** 114
- [11] Bhattacharyya A, Chemissany W, Haque S S, Murugan J and Yan B 2021 *SciPost Phys. Core* **4** 002
- [12] Landau L 1932 *Phys. Z. Sov. Union* **2** 46–51
- [13] Zener C 1932 *Proc. R. Soc. A* **137** 696–702
- [14] Yurke B, McCall S L and Klauder J R 1986 *Phys. Rev. A* **33** 4033
- [15] Prakash G S and Agarwal G S 1994 *Phys. Rev. A* **50** 4258
- [16] Glauber R J 1986 *Ann. New York Acad. Sci.* **480** 336–72

- [17] Gentilini S, Braidotti M C, Marcucci G, DelRe E and Conti C 2015 *Sci. Rep.* **5** 15816
- [18] Gietka K and Busch T 2021 *Phys. Rev. E* **104** 034132
- [19] Qu L C, Chen J and Liu Y X 2022 *Phys. Rev. D* **105** 126015
- [20] Hashimoto K, Huh K B, Kim K Y and Watanabe R 2020 *J. High Energy Phys.* **JHEP11(2020)068**
- [21] Bhaduri R K, Khare A, Reimann S M and Tomusiak E L 1997 *Ann. Phys., NY* **254** 25–40
- [22] Srinivasan K and Padmanabhan T 1999 *Phys. Rev. D* **60** 024007
- [23] Schützhold R and Unruh W G 2013 *Phys. Rev. D* **88** 124009
- [24] Albrecht A, Ferreira P, Joyce M and Prokopec T 1994 *Phys. Rev. D* **50** 4807
- [25] Das A, Panda S and Roy S 2008 *Phys. Rev. D* **78** 061901
- [26] Dhar A, Mandal G and Wadia S R 1995 *Nucl. Phys. B* **454** 541–60
- [27] Klebanov I R, Maldacena J and Seiberg N 2003 *J. High Energy Phys.* **JHEP07(2003)045**
- [28] Maldacena J and Seiberg N 2005 *J. High Energy Phys.* **JHEP09(2005)077**
- [29] Sen A 2023 *J. High Energy Phys.* **JHEP04(2023)101**
- [30] Lévy-Leblond J M 1967 *Phys. Rev.* **153** 1–4
- [31] Camblong H E, Epele L N, Fanchiotti H and García C C A 2001 *Phys. Rev. Lett.* **87** 220402
- [32] Denschlag J, Umshaus G and Schmiedmayer J 1998 *Phys. Rev. Lett.* **81** 737
- [33] Plestid R, Burgess C P and O'Dell D H J 2018 *J. High Energy Phys.* **JHEP08(2018)059**
- [34] Efimov V 1970 *Phys. Lett. B* **33** 563–4
- [35] Efimov V 1973 *Nucl. Phys. A* **210** 157–88
- [36] Werner F and Castin Y 2006 *Phys. Rev. Lett.* **97** 150401
- [37] Braaten E and Hammer H W 2006 *Phys. Rep.* **428** 259–390
- [38] Bhaduri R K, Chatterjee A and van Zyl B P 2011 *Am. J. Phys.* **79** 274–81
- [39] Moroz S, D'Incao J P and Petrov D S 2015 *Phys. Rev. Lett.* **115** 180406
- [40] Kraemer T et al 2006 *Nature* **440** 315–8
- [41] Williams J R, Hazlett E L, Huckans J H, Stites R W, Zhang Y and O'Hara K M 2009 *Phys. Rev. Lett.* **103** 130404
- [42] Pollack S E, Dries D and Hulet R G 2009 *Science* **326** 1683
- [43] Huang B, Sidorenkov L A, Grimm R and Hutson J M 2014 *Phys. Rev. Lett.* **112** 190401
- [44] Tung S K, Jiménez-García K, Johansen J, Parker C V and Chin C 2014 *Phys. Rev. Lett.* **113** 240402
- [45] Calogero F 1969 *J. Math. Phys.* **10** 2191–6
- [46] Sutherland B 1971 *Phys. Rev. A* **4** 2019–21
- [47] Gurappa N and Panigrahi P K 1999 *Phys. Rev. B* **59** R2490
- [48] Gurappa N and Panigrahi P K 2000 *Phys. Rev. B* **62** 1943
- [49] Nisoli C and Bishop A R 2014 *Phys. Rev. Lett.* **112** 070401
- [50] Sundaram S and Panigrahi P K 2016 *Opt. Lett.* **41** 4222–4
- [51] Gangopadhyaya A, Panigrahi P K and Sukhatme U P 1994 *J. Phys. A: Math. Gen.* **27** 4295
- [52] Scursulim J V S, Lima A A, da Silva U C and Sotkov G M 2020 *Phys. Rev. A* **101** 032105
- [53] Moroz S 2010 *Phys. Rev. D* **81** 066002
- [54] Birmingham D, Gupta K S and Sen S 2001 *Phys. Lett. B* **505** 191–6
- [55] Camblong H E and Ordóñez C R 2003 *Phys. Rev. D* **68** 125013
- [56] Burgess C P, Plestid R and Rummel M 2018 *J. High Energy Phys.* **JHEP09(2018)113**
- [57] Zhao Q L, Zhang P M and Horvathy P A 2024 arXiv:2403.02230
- [58] Callan J C G Coleman S and Jackiw R 1970 *Ann. Phys., NY* **59** 42
- [59] Coleman S 1988 *Aspects of Symmetry: Selected Erice Lectures* (Cambridge University Press)
- [60] Coon S A and Holstein B R 2002 *Am. J. Phys.* **70** 513–9
- [61] Essin A M and Griffiths D J 2006 *Am. J. Phys.* **74** 109–17
- [62] Olshanii M, Perrin H and Lorent V 2010 *Phys. Rev. Lett.* **105** 095302
- [63] da Silva U C 2018 *Ann. Phys., NY* **398** 38–54
- [64] da Silva U C, Pereira C F and Lima A A 2024 *Ann. Phys., NY* **460** 169549
- [65] Gupta K S and Rajeev S G 1993 *Phys. Rev. D* **48** 5940
- [66] Bawin M and Coon S A 2003 *Phys. Rev. A* **67** 042712
- [67] Mueller E J and Ho T L 2004 arXiv:cond-mat/0403283
- [68] Kaplan D B, Lee J W, Son D T and Stephanov M A 2009 *Phys. Rev. D* **80** 125005
- [69] Moroz S and Schmidt R 2010 *Ann. Phys., NY* **325** 491–513
- [70] Sundaram S, Burgess C P and O'Dell D H J 2021 *J. Phys.: Conf. Ser.* **2038** 012024
- [71] Stålhammar M, Larana-Aragon J, Rødland L and Kunst F K 2023 *New J. Phys.* **25** 043012
- [72] Berry M V 1986 Riemann's Zeta function: a model for quantum chaos? *Quantum Chaos and Statistical Nuclear Physics* ed T H Seligman and H Nishioka (Springer) pp 1–17
- [73] Connes A 1999 *Sel. Math. New Ser.* **5** 29
- [74] Twamley J and Milburn G J 2006 *New J. Phys.* **8** 328
- [75] Srednicki M 2011 *J. Phys. A: Math. Theor.* **44** 305202
- [76] Bender C M, Brody D C and Müller M P 2017 *Phys. Rev. Lett.* **118** 130201
- [77] Sierra G 2019 *Symmetry* **11** 494
- [78] Sierra G 2005 *J. Stat. Mech.* **2005** 12006
- [79] Dalui S and Majhi B R 2020 *Phys. Rev. D* **102** 124047
- [80] Dalui S, Majhi B R and Mishra P 2019 *Phys. Lett. B* **788** 486–93
- [81] Gupta K S, Harikumar E and de Queiroz A R 2013 *Europhys. Lett.* **102** 10006
- [82] Ovdad O, Mao J, Jiang Y, Andrei E Y and Akkermans E 2017 *Nat. Commun.* **8** 1–6
- [83] Arnold V I 1990 *Huygens and Barrow, Newton and Hooke: Pioneers in Mathematical Analysis and Catastrophe Theory From Evolvents to Quasicrystals* (Birkhäuser Verlag)
- [84] Needham T 1993 *Am. Math. Mon.* **100** 119–37
- [85] Bohlin K 1911 *Bull. Astron.* **28** 113–9
- [86] Horvathy P A and Zhang P M 2020 *Phys. Educ.* **36** 1–14
- [87] Kasner E 1913 *Colloquium Publications* vol 3 (AMS)

- [88] Arnold V I and Vasil'ev V A 1989 *Not. Am. Math. Soc.* **36** 1148–54
- [89] Grant A K and Rosner J L 1994 *Am. J. Phys.* **62** 310–5
- [90] Albouy A and Zhao L 2022 *Regul. Chaot. Dyn.* **27** 253–80
- [91] Newton I 1687 *Philosophiæ Naturalis Principia Mathematica* (Jussu Societatis Regiæ ac Typis Josephi Streater)
- [92] Newton I 1999 *The Principia: Mathematical Principles of Natural Philosophy* (University of California Press)
- [93] Chandrasekhar S 2003 *Newton's Principia for the Common Reader* (Oxford University Press)
- [94] Faure R 1953 *C. R. Acad. Sci., Paris* **237** 603–5
- [95] Bateman D S, Boyd C and Dutta-Roy B 1992 *Am. J. Phys.* **60** 833–6
- [96] Inomata A and Junker G 2021 *Symmetry* **13** 409
- [97] Niederer U 1973 *Helv. Phys. Acta* **46** 191–200
- [98] Steuernagel O 2014 *Eur. Phys. J. Plus* **129** 114
- [99] Wu H and Sprung D W L 1995 *Am. J. Phys.* **63** 564–7
- [100] Reed M and Simon B 1975 Fourier analysis, self-adjointness *Methods of Modern Mathematical Physics* vol 2 (Elsevier)
- [101] Finster F and Isidro J M 2017 *J. Math. Phys.* **58** 092104
- [102] NIST Digital Library of Mathematical Functions *Release 1.1.12 of 2023-12-15 f* ed W J Olver, A B O Daalhuis, D W Lozier, B I Schneider, R F Boisvert, C W Clark, B R Miller, B V Saunders, H S Cohl and M A McClain
- [103] Pitaevskii L P and Rosch A 1997 *Phys. Rev. A* **55** R853
- [104] Gurappa N and Panigrahi P K 2003 *Phys. Rev. B* **67** 155323
- [105] Leonhardt U 2002 *Phys. Rev. A* **65** 043818
- [106] Kiss T and Leonhardt U 2004 *J. Opt. A: Pure Appl. Opt.* **6** S246
- [107] Coutant A and Parentani R 2014 *Phys. Rev. D* **90** 121501
- [108] Farrell L M, Howls C J and O'Dell D H J 2023 *J. Phys. A: Math. Gen.* **56** 044001
- [109] Case K M 1950 *Phys. Rev.* **80** 797
- [110] Rajeev S G 2013 *Advanced Mechanics: From Euler's Determinism to Arnold's Chaos* (OUP Oxford)
- [111] Bethe H and Peierls R 1935 *Proc. R. Soc. A* **148** 146–56
- [112] Burgess C P, Hayman P, Williams M and Zalavári L 2017 *J. High Energy Phys.* **JHEP04(2017)106**
- [113] Burgess C P, Hayman P, Rummel M, Williams M and Zalavári L 2017 *J. High Energy Phys.* **JHEP07(2017)072**
- [114] Burgess C P, Hayman P, Rummel M and Zalavári L 2017 *J. High Energy Phys.* **JHEP09(2017)007**
- [115] Burgess C P, Hayman P, Rummel M and Zalavári L 2018 *Phys. Rev. A* **98** 052510
- [116] Burgess C P, Hayman P, Rummel M and Zalavári L 2021 *Phys. Lett. A* **390** 127105
- [117] Bender C M 2007 *Rep. Prog. Phys.* **70** 947
- [118] Goldstein H, Poole C and Saffo J 2001 *Classical Mechanics* (Addison Wesley)
- [119] Dirac P A M 1945 *Rev. Mod. Phys.* **17** 195
- [120] Leacock R A and Padgett M J 1983 *Phys. Rev. D* **28** 2491
- [121] Kim J H and Lee H W 1999 *Can. J. Phys.* **77** 411–25

SCHWINGER PAIR PRODUCTION: A NON-HERMITIAN QUANTUM MECHANICS PERSPECTIVE

Sriram Sundaram, C. P. Burgess, and D. H. J. O'Dell

EFT of finite-size effects in Schwinger pair production: Scale Anomaly and \mathcal{PT} symmetry breaking

Manuscript in preparation.

In this chapter we study the classical field theory of Schwinger pair creation using non-hermitian quantum mechanics of the IHO. The instability of the vacuum in the presence of an external constant electric field that creates particle-antiparticle pairs is termed as Schwinger pair creation. It is known that the Klein-Gordon equation in $1+1$ dimensions in the presence of a static electric field \mathcal{E} can be mapped to a time independent Schrödinger equation with an IHO potential which is Hermitian and \mathcal{PT} symmetric. However, the IHO Hamiltonian is unbounded from below. We use the methods of EFT to implement appropriate non-hermitian linear (Robin) boundary conditions at finite but long distances that describe pair creation. We further renormalize the boundary coupling so that physical predictions are only functions of the invariants of the RG flow. We show that the constant field Schwinger pair production probability emerges at the fixed point which is the scale invariant region of the RG flow, and that breaks \mathcal{PT} symmetry. The limit cycle behaviour of the boundary coupling when one is away from the fixed point is suggestive that certain physical observables such as the

current correlation function can exhibit periodic (faster than log periodic) behaviour as a function of system size or electric field strength.

EFT of finite-size effects in Schwinger pair production: Scale Anomaly and \mathcal{PT} symmetry breaking

Sriram Sundaram¹, C.P. Burgess^{1,2,3} and D.H.J. O'Dell¹

¹Department of Physics and Astronomy, McMaster University,
1280 Main Street W., Hamilton ON, Canada L8S 4M1

²Perimeter Institute for Theoretical Physics,
31 Caroline Street N., Waterloo, ON, Canada, N2L 2Y5

³School of Theoretical Physics, Dublin Institute for Advanced Studies,
10 Burlington Rd., Dublin, Co. Dublin, Ireland

E-mail: sundas1@mcmaster.ca, cburgess@perimeterinstitute.ca,
dodell@mcmaster.ca

Abstract. We describe Schwinger pair creation of spinless particles using non-hermitian quantum mechanics with a particular focus on finite size effects that are relevant to experimental observations. We follow earlier workers and map the Klein-Gordon equation in 1+1 dimensions in a constant electric field \mathcal{E} to the time-independent Schrödinger equation with an inverted harmonic oscillator (IHO) potential which at face value is Hermitian and is \mathcal{PT} symmetric but unbounded from below. We use effective field theory (EFT) methods to identify the universal non-self-adjoint extension that describes pair production when the region of constant electric field is large compared to other scales. The leading \mathcal{PT} -breaking effects are captured by linear (Robin) boundary conditions that apply to the IHO at long distances. EFT methods also allow a renormalization-group (RG) treatment of how the required boundary conditions depend on the size of the region of constant field, with physical quantities emerging as invariants of the RG flow. We show that the RG flow exhibits limit cycles around complex fixed points, which is a signature of a scale anomaly. The standard Schwinger result emerges as the scale invariant limit at the fixed point describing pure emission, whereas the limit-cycle behaviour away from the fixed point implies observables exhibit periodic behaviour (faster than log periodic) as a function of physical parameters. Our approach is universal in the sense that it does not assume a specific form of high energy cut-off or regulator and so can be equally applied to the case of an electric field confined between two condenser plates which apply abrupt spatial cut-offs and the Sauter potential where the electric field switches on and off smoothly.

Keywords: inverted harmonic oscillator, non-hermitian boundary condition, renormalization group.

1. Introduction

The generation of charged particle-antiparticle pairs from the vacuum due to the presence of an externally imposed electric field is often referred to as Schwinger pair production. Although this process was treated long ago using fully fledged quantum field theory [1, 2], the aim of the present paper is to give a simpler and more intuitive description in terms of non-hermitian quantum mechanics that can be more readily applied to possible future experiments where the field is confined to a finite region of space, rather than extending to infinity like in the most basic formulation. Particle creation and annihilation are not possible in standard non-relativistic quantum mechanics, but upon generalizing to the non-hermitian case one can include non-unitary behaviour that violates conservation of particle number. In common with many other treatments of Schwinger pair production [3–6], we represent each mode of the matter field by a quantum inverted harmonic oscillator (IHO) which models the instability of the vacuum to pair creation. The breaking of hermiticity can then be implemented by applying complex boundary conditions to the IHO, which we do within the framework of point particle effective field theory (PPEFT) [7–11]. The problem we formulate and solve in this paper is the question of what the correct boundary conditions should be in order to describe pair production in *finite* systems [12–14]. Crucially, our approach does not impose a specific high energy cut-off or regularization, and can therefore equally deal with sharp cut-offs such as an electric field confined between condenser plates [12], or extended smooth cut-offs like the original Sauter case [15, 16], and related cases of inhomogeneous fields [17, 18]. We therefore consider our treatment to be universal in the sense that it can be applied to a broad range of different physical scenarios.

In 1931 F. Sauter used the Dirac equation to derive a nonperturbative expression for the probability of pair production in an electric field of strength \mathcal{E} [15, 16]. Sauter’s result leads to the following pair production rate per unit volume (in three spatial dimensions)

$$w = \frac{(2s+1)(q\mathcal{E})^2}{(2\pi)^3\hbar^2c} \exp\left(-\frac{\pi m^2c^3}{q\mathcal{E}\hbar}\right) \quad (1)$$

where s is the spin, q the charge and m the mass of the produced particles. This result was later confirmed to be the dominant contribution in a fully quantum electrodynamical calculation by J. Schwinger [1]. However, the fields required to obtain detectable particle production are so large, of the order of $\mathcal{E} = 10^{18}\text{V/m}$, that Schwinger pair production has not yet been seen experimentally in its original setting, although there is promising progress using superstrong laser fields [19–21]. The absence of experimental studies of such a fundamental process in quantum electrodynamics has stimulated experiments in analogue systems that perform quantum simulations of Schwinger pair production, including with trapped ions [22], cold atoms [23, 24] and graphene [25, 26]. These experiments have been informed by a large body of theoretical work, especially on cold atom systems [27–40], ions [41–43], and superconducting quantum circuits [44, 45], as well as studies on closely allied effects such as the dynamical Schwinger effect [46–50].

Dielectric breakdown (also known as Zener breakdown) [51], where electron-hole pairs are created in a semiconductor due to the application of a voltage across the sample, and the Mott metal-insulator transition in strongly correlated materials such as the cuprates [52], are examples of Schwinger pair production-type physics in a condensed matter physics context and in fact descriptions based on the same Heisenberg-Euler-Schwinger effective Lagrangian [53] are used to study these processes [54–57].

In a recent paper we showed that there is a duality between the IHO and a quantum particle in an attractive inverse square potential (ISP) $V(x) = -g/x^2$ [58] (in fact, the IHO, ISP and the Berry-Keating Hamiltonian $H = (xp + px)/2$ together form a closed $\mathfrak{su}(1,1)$ spectrum generating algebra). The duality establishes a map between both the hamiltonians and states of the two systems which reveals they give alternative descriptions of the same physics. At first sight this is surprising because the ISP diverges at the origin and the IHO diverges at infinity, but on the other hand both have energies that are unbounded from below. In the present context, the duality reveals a hidden scaling symmetry in Schwinger pair production because the dual Schrödinger equation with an ISP is scale invariant: both the kinetic energy and potential scale as length^{-2} . The ISP is also notorious for leading to ‘fall to the centre’ [59, 60], and we can similarly think of the IHO as leading to ‘fall to infinity’ since, roughly speaking, the duality maps a singularity at the origin to a singularity at infinity. We note in passing that the ISP has been used as an effective model for a great variety of physical situations involving scale invariance including the interaction between an electron and a neutral polarizable molecule [61, 62] (as well as the related problem of a neutral atom and a charged wire [63, 64]), the Efimov effect in nuclear physics [65–67] (which has been explored experimentally using ultracold atoms [68–72]), as a model for winding transitions in polymer physics [73], the exactly solvable Calogero-Sutherland model [74–77], the AdS/CFT correspondence [78], and the near horizon physics of black holes [5, 79–81]. The IHO has likewise been widely used as a simple solvable model for unstable quantum systems [82–85] and so in hindsight it is perhaps natural that the two should be related. In the present paper pair production is modelled via tunnelling through a parabolic barrier and the use of the IHO in such a way dates back at least to the celebrated Landau–Zener model [86, 87].

The divergence at the origin of the ISP is not physically real as some microscopic physics in all the problems listed above is expected to regulate it. In effective models the divergence is therefore typically handled by applying a cut-off or boundary condition at a short distance ϵ that lies between the even smaller microscopic scale and the much larger scale where our observables act. The choice of ϵ is otherwise arbitrary and the requirement that the observables do not depend upon it leads to a renormalization group (RG) flow of the boundary condition such that physically meaningful length scales instead appear as RG invariants of the flow. It is of considerable importance to the present work is that the RG flow for the ISP is well known to follow limit cycles [88–90]. Although flow around limit cycles (where the fixed point is never reached) may be less familiar than flow towards a fixed point, it was in fact envisaged in Wilson’s original work

on RG [91,92]. The physical significance of limit cycles for the ISP is that, because the boundary conditions repeat cyclically, they describe the breaking of continuous classical scale invariance down to a discrete series of values in a simple example of a quantum anomaly [93–98].

The duality between the IHO and the ISP means that the RG flow for the IHO also obeys limit cycles that give rise to a quantum anomaly [58]. In this paper we will examine the implications of this for Schwinger pair production. We shall not rely on the duality but instead derive it from scratch from the IHO. Our main result is that in a finite size system there is cyclical variation in the Schwinger pair production rate as the strength of the electric field \mathcal{E} or system size D is varied, in contrast to the monotonic behaviour predicted by Eq. (1). The result in Eq. (1) is recovered at the fixed point, which corresponds to an infinite system and is where scale invariance is restored. In fact there are two fixed points which both lie in the complex plane and are complex conjugates of each other. One corresponds to a pure emitter and the other to a pure absorber; the one relevant to Schwinger pair production is the pure emitter as one would expect. Complex valued fixed points are a consequence of the non-hermitian nature of the problem and the fact that we are in the “super-critical” \mathcal{PT} symmetry broken phase [99,100], where the two fixed points are the time reversals of each other [101,102]. Complex coupling constants have been discussed in field theory for a long time, such as in the Lee model [103–105] where states with negative norms (“ghosts”) can appear [106–108], and have more recently come back into focus [109–112], particularly in the context of phase transitions in non-hermitian systems and also weakly first order phase transitions [113–118]. In this paper we show that elementary processes in quantum field theory such as Schwinger pair production fall into the same family of problems.

The structure of the rest of this paper is as follows. In Section 2 we introduce the Klein-Gordon equation describing spinless particles in an external electric field. In the purely spatial (Coulomb) gauge each mode maps to an IHO. The exact eigenfunctions of the IHO are well known (parabolic cylinder functions) and the real problem to solve is to find the correct boundary conditions to describe particle production. Motivated by PPEFT, we apply Robin boundary conditions which allow for the possibility of non-hermitian physics that breaks \mathcal{PT} symmetry and this is an important feature for particle production in our scheme. The precise position where the boundary conditions are applied is arbitrary and should not affect the physical observables. Hence, in Section 3 we take account of this fact and apply RG methods to the boundary conditions. We find and solve the RG flow equations, and in Section 4 show how the fixed points and RG trajectories are connected to pair production, giving the standard Schwinger result. Section 5 considers finite systems where we need to go beyond the fixed points and how this might affect Schwinger’s result. In Section 6 we discuss the application of the RG theory to two particular cases: i) an electric field confined inside a condenser and ii) the Sauter problem. We give our conclusions in Section 7. In Appendix A we summarize the connection between the first quantized and second quantized descriptions of Schwinger

pair production.

2. Pair production and the inverted harmonic oscillator

This section reviews the connection between Schwinger pair production and inverse-harmonic-oscillator physics, introducing along the way some EFT and renormalization-group ideas for later use.

2.1. Klein-Gordon mode functions

Consider a charged scalar field $\phi(x, t)$ which for simplicity we limit to one spatial dimension. In the presence of a constant background electric field \mathcal{E} the field $\phi(x, t)$ obeys the Klein-Gordon equation[‡]

$$\left[\frac{\partial^2}{\partial x^2} - \left(\frac{\partial}{\partial t} - iq\mathcal{E}x \right)^2 \right] \phi = m^2 \phi, \quad (2)$$

where we adopt the gauge choice $A_0 = \mathcal{E}x$, $A_x = 0$ [3, 4]. This corresponds to an electric field pointing in the positive x direction[§]. The quantum field $\phi(x, t)$ can be expanded in a basis of mode functions $u_n(x)$ as

$$\phi(x, t) = \sum_n \left[u_n(x) a_n e^{-i\omega_n t} + u_n^*(x) \bar{a}_n^* e^{+i\omega_n t} \right] \quad (3)$$

where ‘ n ’ collectively denotes the quantum numbers needed to completely specify a single-particle state of energy ω_n . In this expansion a_n and \bar{a}_n are particle and antiparticle annihilation operators satisfying $[a_n, a_m^*] = \delta_{mn}$ and $[\bar{a}_n, \bar{a}_m^*] = \delta_{mn}$, respectively, so ϕ destroys particles with mass m and charge q and creates antiparticles with mass m and charge $-q$.

The mode functions $u_n(x)$ satisfy the time-independent Klein-Gordon equation

$$\left[\frac{\partial^2}{\partial x^2} + (\omega_n + q\mathcal{E}x)^2 \right] u_n(x) = m^2 u_n(x) \quad (4)$$

which has the form of the time-independent Schrödinger equation for the inverse-harmonic oscillator (IHO). This can be made explicit by redefining coordinates from x to

$$\xi := \sqrt{q\mathcal{E}} \left(x + \frac{\omega_n}{q\mathcal{E}} \right) \quad (5)$$

and we assume $q\mathcal{E} > 0$. In this case (4) becomes

$$H u_n(\xi) = \frac{1}{2} (p_\xi^2 - \xi^2) u_n(\xi) = -E u_n(\xi) \quad (6)$$

where $p_\xi = -i\partial/\partial\xi$ and so $[\xi, p_\xi] = i$ and the energy eigenvalue is denoted $-E$ where

$$E := \frac{m^2}{2q\mathcal{E}}, \quad (7)$$

[‡] Unless stated explicitly otherwise we use units for which $\hbar = c = 1$.

[§] We recall that the usual electric potential φ is given by $\varphi = A^0 = -A_0$ where $\mathcal{E} = -\partial\vec{A}/\partial t - \nabla\varphi$.

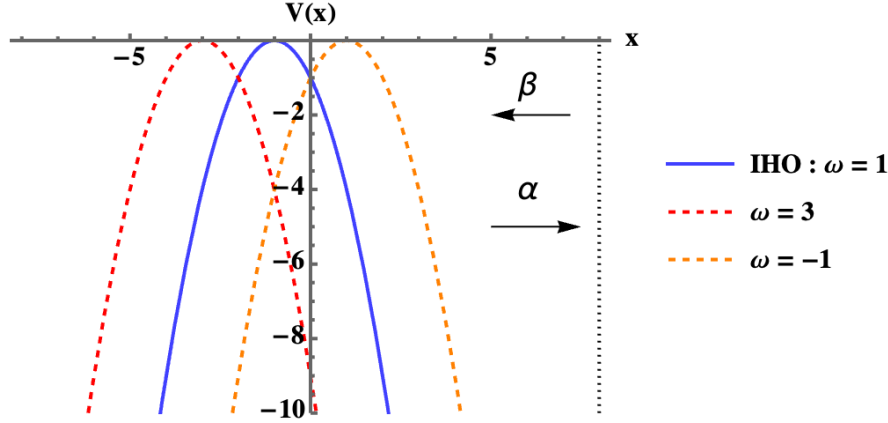


Figure 1: A plot of the IHO potential obtained from the Klein-Gordon equation in the guise of Eq. (4). The Klein-Gordon problem maps onto an energy eigenvalue that is always negative, so that Schwinger pair production can be viewed as a quantum mechanical tunnelling problem. The position of the potential's maximum varies for different values of ω , as depicted here by dashed curves, but the width of the barrier at any fixed energy $E = m^2/q\mathcal{E}$ is independent of ω . For a truly constant electric field the IHO potential continues to $x = \pm\infty$ in both directions, so that the Hamiltonian is not bounded below. The exact solutions are parabolic cylinder functions; for a given E there are two linearly independent parabolic cylinder functions whose precise combination needs to be fixed by a boundary condition. As will be explained in Sec. 2.3, we apply a boundary condition at a fictitious boundary on the far right (represented by the vertical dotted line) where the solution can be asymptotically decomposed into two propagating waves with quantum amplitudes α and β .

is a positive number and so the energy is strictly negative. Notice that the Hamiltonian is not bounded below and the coordinate position $\xi = 0$ of the potential's maximum corresponds to $x = -\omega_n/(q\mathcal{E})$ and so is displaced by an ω_n - and \mathcal{E} -dependent amount – see Fig. 1.

Due to the negative eigenvalue, the analogue Schrödinger problem contained in Eq. (6) is a tunnelling problem and so there are always classical turning points ξ_{\pm} for which $p_{\xi} = 0$. These turning points occur at the positions $\xi_{\pm} = \pm\sqrt{2E}$, or in terms of the original coordinate they are located at x_{\pm} , where

$$x_{\pm} = \pm \frac{m}{q\mathcal{E}} - \frac{\omega_n}{q\mathcal{E}}. \quad (8)$$

It is significant that the distance $\Delta x := x_+ - x_- = 2m/(q\mathcal{E})$ is *independent* of ω_n and equals the distance over which the work done by the electric field $q\mathcal{E}\Delta x$ equals the energy $2m$ required for pair production.

The transmission amplitude through the barrier in the WKB approximation is

$$T = \exp \left[i \int_{\xi_-}^{\xi_+} p_{\xi}(\xi) d\xi \right] = \exp \left[- \int_{-\sqrt{2E}}^{\sqrt{2E}} \sqrt{2E - \xi^2} d\xi \right] = e^{-\pi E} \quad (9)$$

and hence the tunnelling probability becomes

$$|T|^2 = e^{-2\pi E} = \exp[-\pi m^2/(q\mathcal{E})]. \quad (10)$$

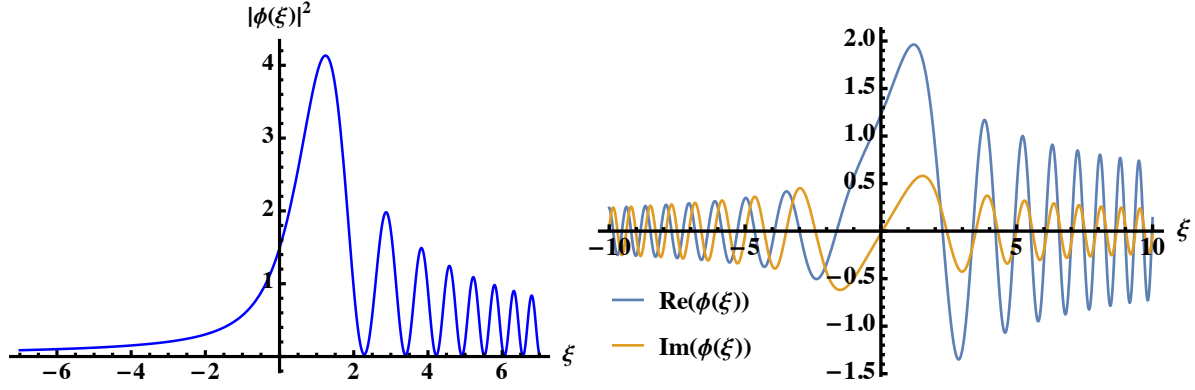


Figure 2: The figure on the top left shows the probability density $|\phi(\xi)|^2$ as a function of ξ , where $\phi(\xi)$ is the energy eigenfunction of the IHO given by $\phi(\xi) = D_{iE-1/2}(+e^{-i3\pi/4}\xi)$ whose real and imaginary parts are shown on the right. The numerical results are shown for the choice $E = 0.1$.

As argued in Appendix A, the naive tunnelling probability for the mode-functions computed as in Schrödinger scattering becomes the pair-production rate once applied to the fully second-quantized problem. Indeed, (10) agrees with the leading exponential part of the Schwinger pair-production expression [1], as given in (1).

The energy eigenfunctions of the IHO are parabolic cylinder functions [4, 82, 119] which can be expressed in terms of Whittaker's function $D_\nu(z)$. There are two linearly independent solutions (with non-vanishing Wronskian) for each energy E

$$\phi(\xi) = N(E) D_{iE-\frac{1}{2}}\left(\sqrt{2}e^{-3i\pi/4}\xi\right) \quad , \quad N(E) D_{-iE-1/2}\left(\sqrt{2}e^{-i\pi/4}\xi\right) \quad (11)$$

with coefficient $N(E) = \Gamma(1/2 + iE) e^{\pi E/4}$. These states exist for any E such that the spectrum forms a continuum (and can be arbitrarily negative). Even though the energy eigenfunctions are smooth for small values of ξ , the infinite fall-off of the scalar potential ensures that they oscillate increasingly quickly and suffer logarithmic singularities as $\xi \rightarrow \infty$, with asymptotic forms that for our purposes can be expressed as [see Fig. 2]

$$\phi(\xi) \sim \frac{C_1}{\sqrt{\xi}} e^{i\left(\frac{\xi^2}{2} - E \ln(\sqrt{2}\xi) + \frac{\theta}{2} + \frac{\pi}{4}\right)} + \frac{C_2}{\sqrt{\xi}} e^{-i\left(\frac{\xi^2}{2} - E \ln(\sqrt{2}\xi) + \frac{\theta}{2} + \frac{\pi}{4}\right)} \quad (12)$$

where C_1 and C_2 are constants, $\theta = \arg \Gamma(1/2 + iE)$, and we use the symbol ‘ \sim ’ to indicate ‘asymptotically equal’. Note that here we use C_1 and C_2 for the decomposition of a single parabolic cylinder function, whereas our total solution is in general a linear combination of two parabolic cylinder functions that can also be decomposed into a form similar to Eq. (12) but with coefficients α and β as indicated in Fig. 1.

As described in Appendix A, the reflection and transmission probabilities for scattering of Klein-Gordon particles from an electric field are examples of Klein’s ‘paradox’: they famously do not sum to unity in the usual way, leading to over-reflection (where more particles are reflected than were incident in the first place). This is ultimately a consequence of the fact that the mode function $u_n(x)$ is not a probability

amplitude and instead knows about the second-quantized effects of pair production and stimulated emission for the scattered particle [120, 121]. In this paper we show that we can incorporate particle production into our first-quantized treatment by imposing a non-hermitian boundary condition (to be described in Sec. 2.3) on the far right hand side which fixes the ratio of the amplitudes of the right (α) and left (β) travelling wave components that together form the asymptotics of the total solution.

2.2. Discrete symmetries: \mathcal{CPT} , \mathcal{CP} , and \mathcal{PT} symmetry

At first sight the IHO Hamiltonian $H = \frac{1}{2}(p_\xi^2 - \xi^2)$ seems formally hermitian, $H^\dagger = H$, but the fact that H is unbounded from below means that the eigenvalue problem is incompletely posed without providing additional information about whether probability can be gained or lost at very long distances. In practice this boils down to the need to impose appropriate boundary conditions in this region and the system can be self-adjoint or non self-adjoint depending on how these are chosen.

In the present instance it turns out that non self-adjoint boundary conditions are ultimately what allow particle production to be described by the IHO. In fact, this discussion has a close parallel with the physics of fall-to-the-centre in an inverse-square potential [58, 101], for which EFT techniques [7] provide insight into how these boundary conditions are related to the underlying physics they are meant to describe. We here adapt these techniques to the IHO (and so also to the Klein-Gordon pair-production problem).

Non-hermitian hamiltonians do not generally conserve probability and so are often used to model non-conservative or open quantum systems with probability sources and drains. They provide a shortcut to describing an open quantum system by using wave functions rather than density matrices and without the need to go through the more complete but laborious process of explicitly treating the environment. In 1998 Bender and collaborators pointed out that non-hermiticity is not in itself sufficient for describing such systems because non-hermitian quantum systems displaying \mathcal{PT} symmetry have real energies and so display quasi-hermitian behaviour [99]. Here \mathcal{P} denotes parity transformation and \mathcal{T} is time reversal.

Conversely, when \mathcal{PT} symmetry is broken the eigenvalues of the hamiltonian become complex allowing for probability non-conservation. Generally speaking, \mathcal{PT} symmetry is preserved as long as the probability gain and loss is perfectly balanced [100]. Since we wish to describe *net* particle production (with more gain than loss) we expect the IHO problem describing Schwinger pair production to break \mathcal{PT} symmetry.

With this in mind it is important to understand the discrete symmetries of our system (and we see below that continuous scaling symmetry also plays an important role). The full time-dependent Klein Gordon equation of Eq. (2) is invariant under the discrete symmetry of \mathcal{CPT} , where \mathcal{C} denotes charge conjugation ($q \rightarrow -q$) while \mathcal{P} (as usual) is $x \rightarrow -x$ and \mathcal{T} is the *anti-unitary* transformation that implements both $t \rightarrow -t$ with $i \rightarrow -i$ [122, 123].

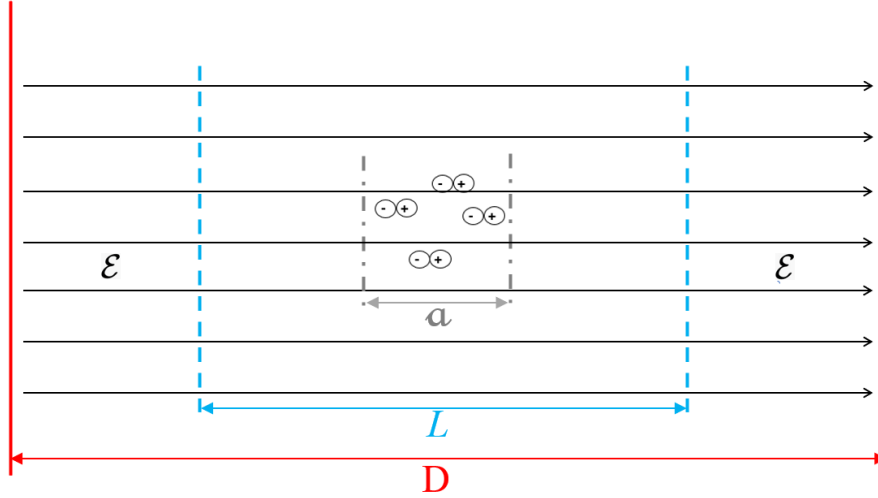


Figure 3: The figure illustrates the hierarchy of scales present in the physics of Schwinger pair production. The smallest scale is $a = 2m/q\mathcal{E}$ which is the minimum length needed extract the rest mass of a particle-antiparticle pair from the electric field. Schwinger’s celebrated result assumes the electric field extends to $\pm\infty$, but in a laboratory fields can extend only over a maximum length D and this scale D complicates calculations. Our interest for the effective description is to replace the physics associated with D with a boundary condition at an arbitrary position L chosen in the regime $a \ll L \ll D$ since this is where universal behaviour described by RG evolution can arise.

It is harder to see \mathcal{PT} symmetry in the IHO hamiltonian, largely because the anti-unitary property of \mathcal{T} implies $e^{-i\omega t} \rightarrow e^{-i\omega t}$ and so $\omega \rightarrow \omega$. Sending $q \rightarrow -q$ is also less useful because of our choice $q\mathcal{E} \geq 0$ needed to keep ξ real. However, \mathcal{T} is usually only chosen to be antiunitary because this prevents having $H \rightarrow -H$ (which is important when H is bounded from below). Nothing requires \mathcal{T} be antiunitary for systems (like the IHO) where H is *not* bounded from below. Following Wigner [124], for such cases we can use the alternative definition where time reversal is a unitary transformation ($t \rightarrow -t$). If so, then energies and frequencies also change sign [84, 125]. Defining time reversal as unitary in this way then gives $\xi \rightarrow -\xi$ under a \mathcal{PT} transformation, because $\omega \rightarrow -\omega$ for unitary \mathcal{T} together with $x \rightarrow -x$ under \mathcal{P} . This is the \mathcal{PT} symmetry of the IHO Schrödinger equation that allows us to make a direct connection to the results of non-hermitian quantum mechanics.

Given that the IHO eigen-equation (6) is \mathcal{PT} symmetric, one might therefore expect that our system is hermitian or quasi-hermitian. However, this ignores the boundary conditions and in our case we find that Schwinger pair production maps onto the IHO system with a boundary condition for large ξ that makes our problem non self-adjoint.

2.3. Finite-size effects

Why are boundary conditions at large x or large ξ necessary? The reason is that electric fields created in the laboratory do not actually extend over infinite distances and so the unlimited energy extraction suggested by the Schwinger calculation (or its unbounded-from-below IHO counterpart) is not really that physical. Furthermore, in actual experiments observational results often depend in detail on precisely how the fields turn off.

It is the physics of this turn-off that the boundary conditions encode; they play a role once we seek how finite-sized electric field regions differ from the Schwinger prediction in their pair-production rates. We argue here that the resulting boundary conditions suggest a renormalization-group framework that leads to a universality of description in the limit where the system becomes very large (and so deviations from the infinite-size Schwinger prediction become small).

In an actual experiment the system will have some finite size, call it D . Our interest is the regime where the length scale D is much greater than the length scale $a = 2m/q\mathcal{E}$ set by the pair-production process. The expectation that the physics at distances of order a is insensitive to the details of how the fields get turned off at large distances is what allows the pair-production rate to be universally described by the Schwinger rate. We here argue that there is also universality in the experimental signatures that are sensitive to the finite size D in the limit $D \gg a$, essentially due to the breaking of a hidden scale symmetry.

In what follows we identify the dependence of pair production on the distant physics that eventually cuts off electric fields by using tools developed in another context [7–9] to capture the how the effects of small objects (like nuclei) on much larger objects (like atoms) can be parameterized in what amounts to a systematic extension of the multipole expansion [10, 126, 127]. The same techniques have also been applied to the effects of different kinds of physics near the boundaries of a region (such as the event horizon of a black hole [81]). The idea is that any distant physics ultimately contributes to physics in the pair production region through reflection and transmission coefficients for the mode functions, and these can be captured by imposing boundary conditions at a hypothetical boundary surface at a distant position $x = L$, where

$$a \ll L \ll D . \tag{13}$$

This hierarchy of length scales is illustrated in Fig. 3.

To this end we imagine there being a fictitious boundary at some large distance L with the boundary condition chosen at L being related to a boundary action describing the physics at this boundary, with the normal derivative of the field $n \cdot \partial\phi$ at the boundary being related to the derivative of the boundary action with respect to the field, $\delta S_b/\delta\phi$ [7]. At low energies standard effective-field theory reasoning suggests the boundary action should be organized into terms involving the fewest possible powers of fields and their derivatives, and in the present instance charge conservation implies

that the smallest number of fields possible is quadratic: $\|\phi^*\phi$. This leads to a linear Robin-style (logarithmic derivative) boundary condition of the form ¶

$$\left(\frac{\partial\phi}{\partial\xi}\right)_{\xi=\xi_L} = (\lambda\phi)_{\xi=\xi_L} \quad \text{where} \quad \xi_L := \sqrt{q\mathcal{E}} \left(L + \frac{\omega}{q\mathcal{E}}\right). \quad (14)$$

Here λ is a constant that is in principle specified by the choice of boundary action, but in practice is actually fixed by the requirement that physical observables not depend in detail on the arbitrary position L of the fictitious boundary surface.

That is, we choose the constant λ to depend on (or ‘run’ with) L in precisely the way required in order to make physical observables not depend in detail on the precise value taken by L , which after all is an arbitrary parameter that is related only implicitly to the real physical scale D associated with cutting off pair production at large distances. In this language the running of λ is obtained by solving a Callan-Symanzik renormalization-group (RG) evolution equation that enforces that physical quantities are held fixed as L is varied and physical scales like D emerge as a renormalization-group (RG) invariants of this running. The real physics at D need not be so simple as being described by a boundary condition like (14), since it might really be a potential like the Sauter potential (where electric field switches on and off smoothly) or something else. It is only for $L \ll D$ that its effects can nonetheless be captured by such a simple boundary condition. We show in the next section how the Schwinger pair-production rate for an infinite electric field emerges as the result when λ is evaluated at the fixed point of this RG flow.

3. RG treatment of boundary condition

This section explores the implications of the boundary conditions at large L in the IHO problem in order to apply its RG understanding to the pair production problem. We then compare the result with several explicit specific models for how the electric field is cut off at large scales to see how different kinds of distant physics are captured by the effective RG description.

3.1. Boundary conditions and reflection coefficient

As described above, the basic proposal is that any effects due to distant physics can be parameterized by a boundary condition of the form of (14), reproduced here again for convenience of reference

$$\left(\frac{\partial\phi}{\partial\xi}\right)_{\xi=\xi_L} = (\lambda\phi)_{\xi=\xi_L}, \quad (15)$$

¶ Relating boundary conditions to boundary actions and using low-energy arguments ultimately leads to a theory of boundary conditions that allows one to understand why linear Robin-style boundary conditions are so commonly applicable throughout Nature (see *e.g.* [11] for a review).

¶ Strictly speaking gauge invariance implies the boundary condition has the form $(\partial_x - iqA_x)\phi = \lambda\phi$ at $x = L$ but the gauge potential A_x vanishes for the system of interest.

that is chosen in such a way as to capture the reflection and transmission of modes from large distances⁺. This boundary condition encodes a reflection coefficient because it modifies the mode functions in a way that introduces waves travelling in both directions. By doing so the constant λ acts as a proxy for whatever the distant physics really is that produces this reflection. Other examples of the use of Robin boundary conditions in non-hermitian systems can be found in references [128–132].

It is important to note that we do *not* assume λ is real since it may well be true that particles pass through the surface at $x = L$ and so make probability appear to be lost there. If so then the eigenvalue problem for $x < L$ should not conserve probability, but the resulting failure of unitarity should be localized at $x = L$. The connection between λ and probability loss through $x = L$ can be seen when the boundary condition is used in the formula for probability current,

$$J(\xi, t) = \frac{i}{2} \left(\phi \partial_\xi \phi^* - \phi^* \partial_\xi \phi \right) \quad (16)$$

which when evaluated at $x = L$ (or $\xi = \xi_L$) implies

$$J(\xi_L, t) = \frac{i}{2} (\lambda^* - \lambda) \left(\phi^* \phi \right)_{\xi=\xi_L} = \text{Im}(\lambda) \left(\phi^* \phi \right)_{\xi=\xi_L}. \quad (17)$$

The current is zero when λ is real but probability is not conserved in the region $\xi < \xi_L$ if λ is not real and $\phi^* \phi$ is nonzero at ξ_L . Probability is lost from the region $\xi < \xi_L$ when $\text{Im}(\lambda) > 0$ and gained when $\text{Im}(\lambda) < 0$.

To determine the relationship between λ and the reflection coefficient we use the boundary condition (15) to fix one of the integration constants in the solution of the Schrödinger equation. Since we assume L is large it suffices to work with the large- ξ asymptotic form of the IHO wave function. On the right hand side of the barrier this is given by [119, 133]:

$$\phi_+(\xi) \sim \frac{\alpha}{\sqrt{\xi}} e^{i\left(\frac{\xi^2}{2} - E \ln(\sqrt{2}\xi)\right)} + \frac{\beta}{\sqrt{\xi}} e^{-i\left(\frac{\xi^2}{2} - E \ln(\sqrt{2}\xi)\right)} \quad (18)$$

where α and β are the integration constants to be determined. Apart from different coefficients, we point out that in comparison to (12) we have also included any spatially constant phase factors in α and β .

At large values of ξ the first term in Eq. (18) can be interpreted as a right-moving wave while the second term corresponds to left moving wave, as depicted in Fig. 1*. This can be seen from the phase velocity given by $v_{\text{ph}} = K(\xi) = \pm(\xi - E/\xi)$, where $K(\xi) = \partial\Phi/\partial\xi$ is the derivative of the wave function's phase $\Phi(\xi)$. Consequently, if we

⁺ We emphasize that, in contrast to other treatments of pair production such as in [5], we are *not* referring here to reflection and transmission from the central potential barrier which is already incorporated in the parabolic cylinder functions we use because they are eigenfunctions of the IHO. Rather, the reflection and transmission that we refer to here is due to the boundaries of the electric potential which by assumption lie far away at large distances.

* If instead we used the group velocity, $v_g = (\partial K/\partial E)^{-1}$ our assignment of left and right moving waves would be the opposite [82], but that interpretation conflicts with the value of the quantum mechanical probability current

consider the situation where an input wave approaches from $-\infty$, α premultiplies the wave transmitted by the central parabolic barrier and β premultiplies the wave reflected from any boundary on the far right. The ratio β/α then determines the reflection coefficient from the far boundary and is fixed in terms of λ by the boundary condition (15).

Using the asymptotic expression (18) in (15) gives

$$\lambda = \frac{1}{\bar{L}\sqrt{q\mathcal{E}}} \left[-\frac{1}{2} + i(q\mathcal{E}\bar{L}^2 - E) \frac{(\alpha/\beta) e^{+2i\Theta(\bar{L})} - 1}{(\alpha/\beta) e^{+2i\Theta(\bar{L})} + 1} \right] \quad (19)$$

where as usual $E = m^2/(2q\mathcal{E})$ [eq. (7)] and we define $\bar{L} := L + \frac{\omega}{q\mathcal{E}}$ [so that $\xi_L = \bar{L}\sqrt{q\mathcal{E}}$, *c.f.* (5)] and

$$\Theta(\bar{L}) := \frac{q\mathcal{E}\bar{L}^2}{2} - E \ln \left(\sqrt{2q\mathcal{E}\bar{L}} \right). \quad (20)$$

These expressions can be simplified by redefining the coupling constant as

$$\Lambda := \frac{\lambda\sqrt{q\mathcal{E}\bar{L}} + \frac{1}{2}}{(q\mathcal{E}\bar{L}^2 - E)} \quad (21)$$

since this allows (19) to be rewritten as

$$\Lambda = i \frac{(\alpha/\beta) e^{+2i\Theta(\bar{L})} - 1}{(\alpha/\beta) e^{+2i\Theta(\bar{L})} + 1}, \quad (22)$$

or, equivalently,

$$\frac{\alpha}{\beta} = \frac{i + \Lambda}{i - \Lambda} e^{-2i\Theta}. \quad (23)$$

If λ is complex then (21) implies so will be Λ . In this case the real and imaginary parts of Λ are related to the modulus and phase of α/β by

$$\Lambda = \frac{i \left(\left| \frac{\alpha}{\beta} \right|^2 - 1 \right) - 2 \left| \frac{\alpha}{\beta} \right| \sin(2\Theta + \zeta)}{1 + \left| \frac{\alpha}{\beta} \right|^2 + 2 \left| \frac{\alpha}{\beta} \right| \cos(2\Theta + \zeta)} \quad (24)$$

where $\zeta = \arg(\alpha/\beta)$. Notice that if $\text{Im}(\Lambda) < 0$ then (24) implies $|\beta/\alpha|^2 > 1$. Regarded as the reflection coefficient for scattering in the non-hermitian IHO this corresponds to over-reflection of particles—a signature of Klein’s paradox. As might have been expected, it is the non-self adjoint part of the boundary condition of the IHO problem that ultimately describes particle production once mapped over to the Klein-Gordon equation.

3.2. Renormalization group interpretation

There are two equivalent ways to think about eqs. (22) and (23). The simplest way reads (23) as the solution for the ratio of the integration constants as a function of the boundary condition parameters Λ and L . Since observables like scattering rates

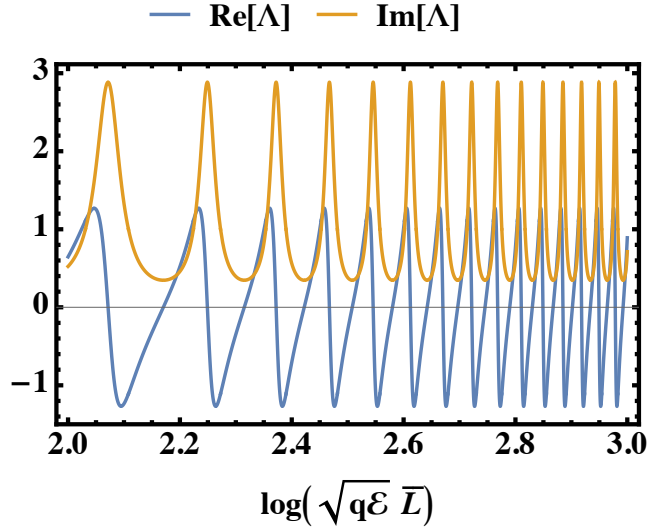


Figure 4: A plot of the solutions $\text{Re}(\Lambda)$ and $\text{Im}(\Lambda)$ to the RG evolution equation given in Eq. (25) as a function of $\ln(\sqrt{q\mathcal{E}}\bar{L})$ for given initial condition $\Lambda_0 = 0.5 + 2i$ at initial length scale \bar{L}_0 specified by $\ln(\sqrt{q\mathcal{E}}\bar{L}_0) = 2.0$. We have avoided small values of L for the plot because the boundary condition is implemented at long distances. The key thing to note is that the RG evolution is oscillatory and this is the case for any choice of complex initial condition, except $\Lambda = \pm i$ which correspond to the fixed points. Similar behaviour occurs in the RG flow for the ISP [58, 88–90], but there it is log periodic [for which the period is constant as a function of $\ln(\sqrt{q\mathcal{E}}\bar{L})$] whereas here it is faster than log periodic.

and pair-production rates depend on α/β this implicitly tells us how observables would depend on L if L were really a physical boundary in the problem.

For the present purposes it is instead (22) that is more useful, and we read it as telling us how Λ must depend on L if α/β is to remain unchanged as we change L . In this point of view we regard the surface at L to be a fictitious thing meant as a proxy for describing some real physics located even further away at $x = D \gg L$. In this case we should be free to change L so long as we do not change physical observables (*i.e.* the value of α/β), and this can be arranged if Λ is also changed as we change L . Eq. (22) tells us precisely how it must change in order to do so.

This evolution of Λ can also be expressed by differentiating (22) with respect to \bar{L} while holding α/β fixed. This leads to the RG evolution equation

$$\bar{L} \frac{d\Lambda}{d\bar{L}} = (E - q\mathcal{E}\bar{L}^2) (\Lambda^2 + 1), \quad (25)$$

where (as before) $E = m^2/(2q\mathcal{E})$. A characteristic feature of this beta function [right hand side of (25)] is the $(\Lambda^2 + 1)$ dependence on the coupling Λ . This means that the fixed points of the RG flow are at imaginary points $\Lambda = \pm i$, a feature shared with the ISP and seems to be a universal property of RG flow in scale invariance breaking systems, including the Efimov problem and the Berezinski-Kosterlitz-Thouless phase transition [110]. However, the IHO beta function is not identical to that of the ISP in all respects because (25) is also quadratic in the length scale \bar{L} whereas the ISP beta

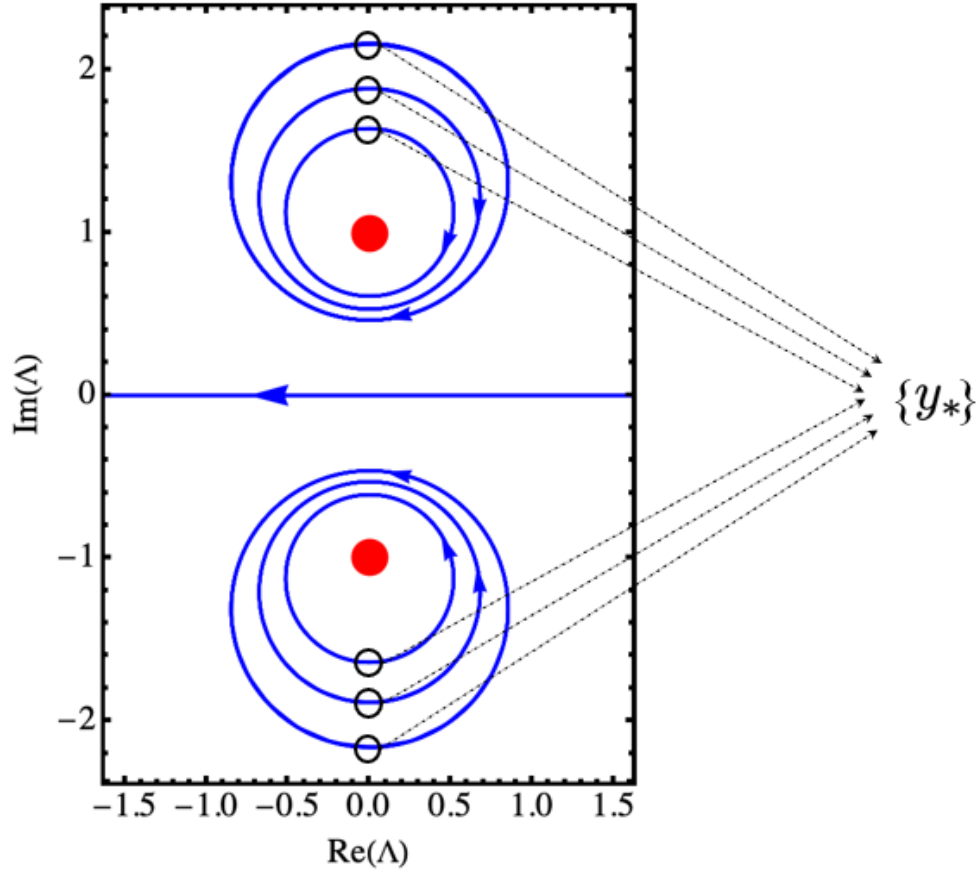


Figure 5: The phase portrait of the RG flow in the complex Λ plane. When Λ is not real the flow exhibits a limit cycle behaviour. Each flow trajectory corresponds to a single physical situation, with a fixed value of α/β . The fixed points of the flow are purely imaginary and are shown as red dots. A convenient RG-invariant label of the flow lines is $y_* = \text{Im}(\Lambda(\bar{L}_*))$ (where \bar{L}_* is the scale when $\text{Re}(\Lambda)$ crosses from negative to positive values) to label each RG trajectory.

function is independent of \bar{L} [58].

The solutions to (25) are trajectories in the complex Λ plane,

$$\Lambda(L) = i \frac{C e^{+2i\Theta(\bar{L})} - 1}{C e^{+2i\Theta(\bar{L})} + 1}. \quad (26)$$

where C is an integration constant. This (unsurprisingly) agrees with (22) if the integration constant is given by $C = \alpha/\beta$. The key idea of the RG is that physical things—or their proxies like α/β —only depend on the RG *trajectory* $\Lambda(\bar{L})$ obtained by solving (25), given a particular initial condition Λ_0 at initial length scale L_0 . In other words, physical observables are fixed along any one trajectory, and different trajectories correspond to different values of the physical observables. Fig. 4 shows the real and imaginary parts of this solution as a function of \bar{L} , for a fixed value of electric field and a given initial condition.

Notice that (25) or (26) implies an initially real coupling stays real as L changes;

this corresponds to the special case of a self-adjoint extension to the IHO. However, the generic case has complex solutions to the RG evolution equation which describe limit cycles in the complex Λ plane [see Fig. 5] and this corresponds to non-self-adjoint extensions that physically describe absorption or emission of particles.

For any solution to the RG evolution, the ratio α/β can then be written in terms of $\Lambda(\bar{L})$ using (23), and the result depends only on the integration constant ratio labelling the curve, rather than on L and $\lambda(L)$ —or on \bar{L} and $\Lambda(\bar{L})$ —separately. Since physical quantities depend only on RG-invariant characterizations of the curve $[L, \Lambda(L)]$, it is useful to identify invariant labels for the RG trajectories obtained from the evolution equation (25). Two convenient choices [64] that specify any solution are (L_*, y_*) where y_* is the value of $\text{Im } \Lambda$ at the point where the trajectory crosses the imaginary axis (with increasing $\text{Re } \Lambda$)—see Fig. 5—and (for trajectories not at the fixed point) L_* is the value of L where this happens. For a fixed value of y_* there can be infinitely many values for L_* because the orbits are closed [see Fig. 5] and thus one gets a discretely broken scale invariance that can lead to fractal structure [134]. One can think of L_* as a length scale that naturally emerges from the RG flow and y_* as specifying the boundary condition at that scale.

In terms of these parameters the ratio α/β of the integration constants is given by

$$\frac{\alpha}{\beta} = \frac{1 + y_*}{1 - y_*} e^{-2i\Theta(\bar{L}_*)}, \quad (27)$$

This form of the boundary condition equation suggests an intriguing possibility: thus far we have insisted that α/β be fixed along a trajectory because the scale L at which we applied the boundary condition was arbitrary, but imagine now that we have a physical system where the previously fictitious boundary is actually a real boundary (such as occurs in a finite system). Then we can interpret L_* as the position of this real boundary. Since the scale L_* always appears in the dimensionless product of the form $\sqrt{q\mathcal{E}}\bar{L}_*$ —see *e.g.* the RG evolution equation (25) or the definition of $\Theta(\bar{L})$ given in Eq. (20)—one can use (27) to see how physical observables derived from the ratio α/β vary as physical parameters such as the electric field strength \mathcal{E} or the size of the system L_* are varied. Indeed, we expect that the limit cycles give rise to oscillatory behaviour even as the physical parameters are varied monotonically. This would be, in our opinion, quite counter-intuitive and surprising and will be taken up in Sec. 5.

4. Fixed points and Schwinger pair production

Of particular interest are the fixed points of the RG flow, defined by

$$\bar{L} \frac{d\Lambda}{d\bar{L}} = 0 \quad \text{which occur for (25) when} \quad \Lambda = \pm i. \quad (28)$$

The effective boundary condition coupling Λ for systems prepared at these fixed points does not depend on L at all. From (23) we see that the fixed point $\Lambda = -i$ corresponds to the case $\alpha/\beta \rightarrow 0$ (or zero reflection for waves incoming from the far right from any boundary on the far left) while $\Lambda = +i$ implies $\alpha/\beta \rightarrow \infty$ (or zero reflection for

waves coming in from the far left from any boundary on the far right). Physically, the fixed points correspond to the case where the electric field extends forever (in which case there can be no reflection from a boundary). If we consider the situation where there is an input wave on the far left then the $\Lambda = -i$ fixed point (and nearby limit cycles) describes particle emission as it gives rise to over-reflection. The other fixed point, $\Lambda = +i$, describes particle absorption and is relevant, e.g., to black hole-type physics.

At a fixed point the L -dependence of λ can be found relatively simply due to the absence of reflection. The wave function in the asymptotic regime then reduces to a single term because either α or β vanishes. In terms of the WKB approximation we have

$$\phi(\xi) \propto \frac{1}{\sqrt{p_\xi(\xi)}} \exp \left[\pm i \int d\xi p_\xi(\xi) \right] \quad (29)$$

which satisfies $\# d\phi/d\xi \simeq \pm i p_\xi \phi$. Once evaluated at $\xi = \xi_L$ this implies $\lambda(L) \simeq \pm i p_\xi(\xi_L)$. In classically allowed regions (for which p_ξ is real) this means that

$$\text{Im}(\lambda) \simeq \pm p_\xi \quad (30)$$

If we specialize to the $\Lambda = -i$ fixed point, which implies $\beta/\alpha = \infty$ and $\text{Im}(\lambda) \simeq -p_\xi$, the current J in Eq. (17) will point in the negative ξ direction. Taking an input wave of unit amplitude at $+\infty$, then the output wave at $-\infty$ has amplitude T , where T is the transmission amplitude through the barrier given by (9). Thus, evaluating (29) at $-\xi_L$ gives

$$(\phi^* \phi)_{-\xi_L} \simeq \frac{|T|^2}{p_\xi} . \quad (31)$$

Inserting this and equation (30) in (17) gives the following result for the probability current at $x = -L$

$$J_{\text{fixedpoint}} \simeq \text{Im}(\lambda) \left(\phi^* \phi \right)_{\xi=-\xi_L} = -|T|^2 . \quad (32)$$

Using the IHO tunneling amplitude given in (10) then shows that the probability current evaluated at the fixed point agrees with the Schwinger result. As is clear from the dependence on $\text{Im} \lambda$, it is the boundary condition breaking \mathcal{PT} symmetry that lies at the root of the loss of probability once cast in terms of the quantum mechanics of the IHO.

5. Finite size effects (work in progress)

We emphasize that this part of the thesis is very much a work in progress and the results presented here are incomplete and speculative.

$\#$ As usual for the WKB approximation we neglect derivatives of p_ξ compared with powers of p_ξ . This semiclassical approximation is nonperturbative and is valid when $\int p dx \gg \hbar$. In the present case this translates to $E \gg 1$, see Eq. (7). Restoring units this implies $mc^2 \gg q\mathcal{E}l_c$ where $l_c = \hbar/mc$ is the Compton wavelength.

Having only a finite region containing nonzero electric field introduces deviations from the idealized Schwinger pair-production rate given by J in equation (32) above. These can potentially be captured by the boundary condition at $x = L$ to the extent that the main finite-size effects are the introduction of reflection from the region where the electric fields go to zero. These are described by trajectories $\lambda(L)$ that are *not* at the fixed points because only at the fixed points do these reflections vanish. Given that away from fixed points $\lambda(L)$ undergoes periodic limit cycles as the scale is changed, it is interesting to ask whether measurable observables can undergo periodic behaviour.

5.1. Schwinger current away from the fixed point

Upon applying the defining expression for the probability current J [Eq. (16)] to the general wave function ϕ_+ given in Eq. (18) when away from fixed point, i.e. including a non-zero α , one finds

$$J = \frac{q\mathcal{E}L^2 - E}{q\mathcal{E}L^2} (|\alpha|^2 - |\beta|^2) = \frac{q\mathcal{E}L^2 - E}{q\mathcal{E}L^2} |\beta|^2 \left(\left| \frac{\alpha}{\beta} \right|^2 - 1 \right) \quad (33)$$

$$\approx |\beta|^2 \left(\left| \frac{\alpha}{\beta} \right|^2 - 1 \right) \quad (34)$$

where the second line holds when $L \gg \sqrt{E/q\mathcal{E}}$. The term $-|\beta|^2$ corresponds to the pure emitter fixed point ($\Lambda = -i$) contribution to the probability current. The other term involves the ratio α/β , which has a small magnitude when in the vicinity of the fixed point and if we think in terms of a finite physical system with a boundary at scale L_* then we can express α/β in terms of (L_*, y_*) using Eq. (27). We see from (27) that as we change L_* the ratio α/β oscillates but all this oscillation is contained in the pure phase factor $\exp[-2i\Theta(\bar{L}_*)]$ that determines the position around the limit cycle. However, the current in (33) depends on $|\alpha/\beta|^2$ and this does not oscillate assuming we stay on the same cycle such that y_* is fixed. Therefore, according to our model we do not expect the Schwinger current to oscillate as a function of system size.

It should be said that this conclusion does not take into account any L_* dependence of $|\beta|^2$, which appears by itself in (33). Our simple model does not make a prediction for $|\beta|^2$ and additional physical details about the system would be needed to understand how it behaves. Consider, for example, a system consisting of an electric field confined inside a condenser made of two parallel conducting plates separated by distance $2L_*$. The amplitude β describes the left travelling Klein-Gordon wave just inside the right hand plate. We would like to know how β depends on L_* . Then, there is a strong analogy with how laser light behaves when incident on a Fabry-Pérot resonator or etalon (made of two partial mirrors), and we can immediately predict that β will be an oscillatory function of L_* due to a ladder of resonances $n\lambda/2 = 2L_*$, labelled by the integer n , and determined by the ratio of the laser light wavelength λ to the cavity length [135]. At each resonance a large fraction of the incident light enters the cavity and between resonances much less light enters due to destructive interference. Thus, it seems likely

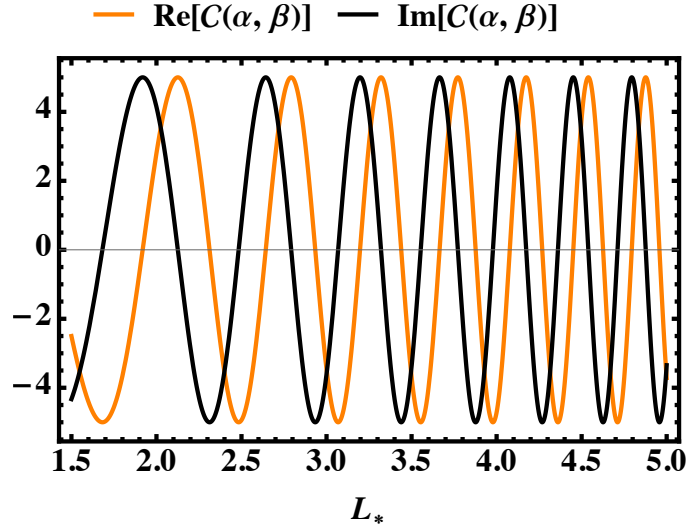


Figure 6: The figure shows the real and imaginary parts of the observable $\mathcal{C}(\alpha, \beta)$ given in Eq. (37) as a function of L_* which can in principle be chosen to be the physical scale D . For the plot we choose a numerical value of $L'_* = 1$ and a particular value of $y_* = 0.5, y'_* = 0.25$ that sets the amplitude A . It exhibits a periodic behaviour (faster than log periodic) as a consequence of limit cycles shown in the previous figure.

that a realistic model of β will lead to an oscillatory current J in (33) although that may have little to do with limit cycles.

It is therefore more relevant to consider an observable that directly depends on α/β (rather than $|\alpha/\beta|^2$) and one possibility is a correlation function that depends on fields evaluated at different points, i.e. the off-diagonal parts of a current operator rather than a diagonal quantity like the current. We consider this case in the next section.

5.2. Current correlation function away from the fixed point

Using the ratio α/β expressed in an RG invariant way, we now calculate an observable that oscillates periodically as a function of L_* .

Using Eq. (27) that relates the ratio α/β to RG invariants (L_*, y_*) we find

$$\left(\frac{\alpha}{\beta}\right)_{(L_*, y_*)} = \frac{1 + y_*}{1 - y_*} e^{-2i \left[\frac{q\mathcal{E}}{2} L_*^2 - E \ln(\sqrt{2q\mathcal{E}} L_*) \right]} \quad (35)$$

and we can construct a correlation function by multiplying α/β by the complex conjugate $(\alpha/\beta)^*$ but evaluated using a different set of RG labels L'_* and y'_*

$$\left(\frac{\alpha}{\beta}\right)^*_{(L'_*, y'_*)} = \frac{1 + y'_*}{1 - y'_*} e^{2i \left[\frac{q\mathcal{E}}{2} L'^2_* - E \ln(\sqrt{2q\mathcal{E}} L'_*) \right]}. \quad (36)$$

Then a simple correlation function is formed by taking the product

$$\mathcal{C}(\alpha, \beta) = \frac{\alpha}{\beta}_{(L_*, y_*)} \left(\frac{\alpha}{\beta}\right)^*_{(L'_*, y'_*)} = A e^{-2i \left[q\mathcal{E}(L_*^2 - L'^2_*) - E \ln(L_*/L'_*) \right]} \quad (37)$$

where we define amplitude $A = \frac{1+y_*}{1-y_*} \frac{1+y'_*}{1-y'_*}$, which is real. As long as the two physical scales L_* and L'_* are different we would see oscillations originating from limit cycles. A physical implementation would require two different systems and mixing their currents at a beam splitter in order to measure a correlation function. An example of the signal is shown in Fig. 6. Due to the fact that L_* appears together with \mathcal{E} one could see these effects by varying the electric field rather than the physical length of the system.

6. Future work

In the future we would like to check if our RG approach to finite system effects really is universal by applying it to two concrete examples where the electric field switches off in two very different manners at scales $D \gg L$. These calculations are incomplete and should be treated as discussions of these systems. So far we have not made a detailed comparison to our simple model.

6.1. Parallel plate case

The first model that would be instructive to compare is the case of a pair of parallel capacitors separated by a distance D . The probability current for this system evaluated midway between the two plates is computed in [12]. Their result approaches the Schwinger result in the limit $D \rightarrow \infty$ but for finite D the produced current shows an oscillatory behaviour as a function of D . The leading deviation from the Schwinger result in this case, evaluated in the limit of large D as found in [12] but converted to our notation is

$$\begin{aligned} \delta J_{\text{parallel plate}}(D) &= 2e^{-2\pi E} \sqrt{1 + e^{-2\pi E}} \frac{\sqrt{-E + \frac{1}{8}q\mathcal{E}D^2}}{\sqrt{q\mathcal{E}D}} \cos[2\Theta(D) + \theta] \\ &\approx \frac{1}{\sqrt{2}} e^{-2\pi E} \sqrt{1 + e^{-2\pi E}} \cos[2\Theta(D) + \theta] \end{aligned} \quad (38)$$

where the second equality hold when $q\mathcal{E}D^2 > E$ which implies $D > m/q\mathcal{E}$ (which is the limit we are interested in) and $\Theta(D) = \frac{q\mathcal{E}}{8}D^2 - E \ln \left(\sqrt{\frac{q\mathcal{E}}{2}} D \right)$, (as usual) $E = m^2/(2q\mathcal{E})$ as given in Eq. (7), $\theta = \arg(\Gamma(1/2 + iE))$. To obtain the above formula for the transmitted probability current, we have used Eqns. (2.19) and (4.17) in [12] and also we have taken due consideration of appropriate normalization constants defined for the transmission amplitude, so as to conform with our model $\dagger\dagger$.

Testing whether this result can be compared against a near fixed point expansion of the probability current as a function of L_* and y_* is currently a work in progress. However, from our discussion above in Sec. 5.1, the oscillatory behaviour predicted by

$\dagger\dagger$ Wang and Wong in [12] use plane waves on the far left and far right and they match them with parabolic cylinder states in the middle. They also include appropriate relativistic normalization constants for plane waves on the far left and far right. We take this into account when writing the expression for the probability current given in Eq. (38).

(38) may be due to the resonance structure of the cavity. Does this have anything to do with limit cycles? Perhaps one can argue that the transmission resonances are a feature of broken scale invariance.

6.2. Sauter regularization

The second model that we might use to check if universal finite size effects are present is the Sauter potential. This regulates the electric field by replacing the linear potential in the Klein-Gordon equation by the Sauter potential $A_0 = q\mathcal{E}D \left[1 + \tanh\left(\frac{x}{D}\right)\right]$ (the shift up in the potential by the first term in the brackets does not affect the electric field, it varies as $\text{sech}^2(x/D)$). This is distinctly different from the parallel plate setup, because the electric field turns on/off smoothly. The resulting effective Schrödinger equation is modified from that of the IHO to:

$$\left(\frac{\partial^2}{\partial x^2} + \left[\omega_n + q\mathcal{E}D \left(1 + \tanh\left(\frac{x}{D}\right)\right)\right]^2\right) \chi = m^2 \chi \quad (39)$$

We will consider the current near the centre of the system where $x \ll D$, such that the boundary is far away and we can use EFT. Expanding \tanh for small x/D gives

$$\left(\frac{\partial^2}{\partial x^2} + \left[\omega_n + q\mathcal{E} \left(D + x - \frac{x^3}{3D^2} + \mathcal{O}(x^5)\right)\right]^2\right) \chi = m^2 \chi \quad (40)$$

To construct the WKB solution, we extract from Eq. (40) the momentum function

$$p(x) = \sqrt{(q\mathcal{E})^2 \left(\frac{\omega}{q\mathcal{E}} + D + x\right)^2 - \frac{2(q\mathcal{E})^2 x^3}{3D^2} \left(\frac{\omega}{q\mathcal{E}} + D + x\right) - m^2} \quad (41)$$

which upon expanding the square root gives

$$p \sim q\mathcal{E}(x + D + \omega/q\mathcal{E}) - \frac{m^2}{2q\mathcal{E}(x + D + \omega/q\mathcal{E})} - \frac{q\mathcal{E}}{3D^2} x^3. \quad (42)$$

The WKB wave function is then given by [6]

$$\begin{aligned} \chi(x) \sim \frac{1}{\sqrt{p(x)}} & \left(C_1 e^{-i\left(\frac{q\mathcal{E}}{2}\left(x+D+\frac{\omega}{q\mathcal{E}}\right)^2 - E \ln\left(\sqrt{2q\mathcal{E}}\left(x+D+\frac{\omega}{q\mathcal{E}}\right)\right) - \frac{q\mathcal{E}}{12D^2}x^4\right)} \right. \\ & \left. + C_2 e^{i\left(\frac{q\mathcal{E}}{2}\left(x+D+\frac{\omega}{q\mathcal{E}}\right)^2 - E \ln\left(\sqrt{2q\mathcal{E}}\left(x+D+\frac{\omega}{q\mathcal{E}}\right)\right) - \frac{q\mathcal{E}}{12D^2}x^4\right)} \right) \end{aligned} \quad (43)$$

where C_1 and C_2 are the incident and reflected wave amplitudes. Consider now the probability current $J = p\chi^*\chi$. The factor of p will precisely cancel with the factor of $1/p$ in $|\chi|^2$. Our expansion holds in the regime of small x/D . In principle we should evaluate J only at small fractions of D , say at $x = fD$, where $f \ll 1$. This gives

$$J = \left(|C_1|^2 + |C_2|^2 + 2|C_1||C_2| \cos \left[2 \left(\eta + \frac{1}{2} \arg(C_2/C_1) \right) \right] \right) \quad (44)$$

where

$$\eta = \frac{q\mathcal{E}}{2} \left(fD + D + \frac{\omega}{q\mathcal{E}} \right)^2 - E \ln \left(\sqrt{2q\mathcal{E}} \left(fD + D + \frac{\omega}{q\mathcal{E}} \right) \right) - \frac{q\mathcal{E}f^4D^2}{12} \quad (45)$$

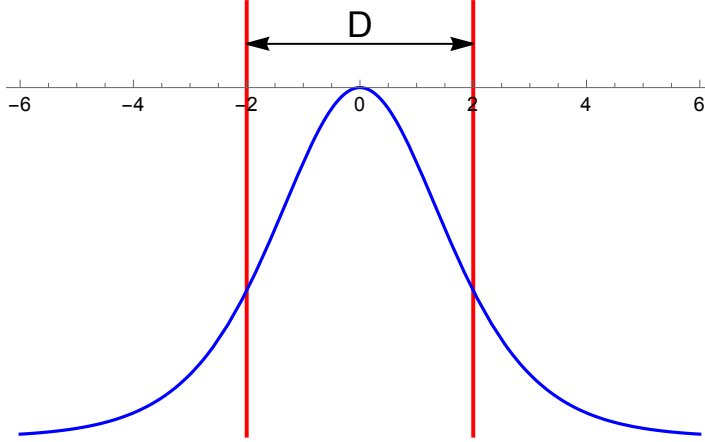


Figure 7: The figure shows the smoothly regulated IHO potential using a Sauter regulator given in Eq. (39). Here we have chosen $\omega = 0$ for simplicity and $D = 2$ for the plot. One can see that in the large D limit the Sauter regularization approaches the constant electric field case, where the potential is an IHO barrier as shown in Fig. 1.

The first two terms in Eq. (44) correspond to the probability current at the two possible fixed points, so we do not consider these terms. The third interference-like cross term is given by

$$\delta J_{\text{Sauter}} = 2\sqrt{\frac{1}{1+e^{-2\pi E}}} \cos \left[2 \left(\eta + \frac{1}{2} \arg(C_2/C_1) \right) \right] \quad (46)$$

To obtain the above formula we read off $|C_1| = 1$, $|C_2| \sim \sqrt{\frac{1}{1+e^{-2\pi E}}}$ which is the reflection amplitude in the limit $D \rightarrow \infty$ [5, 6].

Evaluating the current at $\xi_{\text{mid}} = (\xi_{\text{left}} + \xi_{\text{right}})/2 = \sqrt{q\mathcal{E}}(D + \omega/q\mathcal{E})$, where $\xi_{\text{left}} = \sqrt{q\mathcal{E}}(D + \omega/q\mathcal{E} - fD)$, $\xi_{\text{right}} = \sqrt{q\mathcal{E}}(D + \omega/q\mathcal{E} + fD)$, i.e. we evaluate the current at $x = 0$, we have

$$\delta J_{\text{Sauter}} = 2\sqrt{\frac{1}{1+e^{-2\pi E}}} \cos \left[2 \left(\frac{q\mathcal{E}}{2} \bar{D}^2 - E \ln \left(\sqrt{2q\mathcal{E}} \bar{D} \right) \right) \right] \quad (47)$$

where $\bar{D} = D + \frac{\omega}{q\mathcal{E}}$ (we do not take into account D independent phase factors). This result appears to be oscillatory as a function of \mathcal{E} or \bar{D} , which is rather remarkable because it concerns the ‘diagonal’ part of the current. Testing whether this result can also be compared against a near fixed point expansion of the probability current as a function of L_* and y_* would lead us to another data point to test the universality of the EFT approach, irrespective of the nature of the regulator imposed.

7. Discussion and Conclusion

In this paper we have mapped the Klein-Gordon equation describing spinless relativistic charged particles in the presence of an electric field onto an effective time-independent Schrödinger equation for the IHO (4) *plus* a non-hermitian Robin boundary condition as given in equation (14). This type of boundary condition can be justified using

EFT reasoning and has previously been applied to problems that give rise to power-law potentials which are singular at the origin in a way reminiscent of the multipole expansion in electrostatics [7–9, 11, 64]. In those cases the boundary condition is imposed at small scales in order to encode the effects of the high energy physics at the origin in a way that is agnostic about the precise form of the regularization, e.g. in order to understand the effect of nuclear physics on the low energy degrees of freedom of the electrons in an atom [10, 126, 127]. In the present case we have the opposite situation since the IHO diverges at $\pm\infty$ and so our boundary condition is imposed at large distances. The Robin boundary condition can impose hermitian or non-hermitian physics depending on whether λ in equation (14) is real or complex, respectively.

The boundary coupling fixes the reflection coefficient and thereby determines the necessary boundary condition that describes pair creation. The fixed points are the scale invariant points of the RG flow and occur in a complex conjugate pair corresponding to pure emission and pure absorption. The extra flux of particles at the emitter fixed point is due to particle creation and it is captured by the imaginary part of the boundary condition. Using the imaginary part of the boundary coupling, corresponding to the pure emitter fixed point, we have derived the standard leading term for Schwinger pair production probability in the form $e^{-\frac{\pi m^2 c^3}{q\mathcal{E}\hbar}}$ using a semiclassical WKB formula for transmission through the boundary. The scale invariant pure emitter fixed point boundary condition that yields Schwinger’s pair production probability breaks \mathcal{PT} symmetry.

Furthermore, we also showed that, when the initial condition is away from the fixed point of the RG flow, then as a consequence of the limit cycle type RG evolution of the IHO, then certain correlations can exhibit a periodic behaviour (periodic but faster than log periodic) as a function of system size D or electric field \mathcal{E} .

Acknowledgements

CB and DO acknowledge funding from the Natural Sciences and Engineering Research Council (NSERC) of Canada. Research at the Perimeter Institute is supported in part by the Government of Canada through NSERC and by the Province of Ontario through MRI. SS dedicates this paper to the memory of his beloved mother Chithra Narayanan.

Appendix A. QFT interpretation of 1st-quantized scattering

This appendix provides the interpretation for first quantized scattering for a Klein Gordon field in the presence of a background electric field that turns off after a large but finite distance that is implied by a more complete second-quantized treatment [120].

The essence of the pair-production problem is the interpolation between mode functions in the two asymptotic field free regions. We zoom out so that the region with nonzero field can be regarded as being a negligibly short interval $-\ell < x < \ell$,

outside of which A_0 is constant. A basis of solutions to the Klein Gordon equation have the form $\varphi(x, t) \propto u(x) e^{-i\omega t}$, where $u(x)$ satisfies

$$-u'' + \left[-\omega^2 + m^2 - q^2 A_0^2 - 2qA_0\omega \right] u = 0 \quad (\text{A.1})$$

where $A_0 = A_0^L = +v$ to the left and $A_0 = A_0^R = -v$ to the right of the region of nonzero field respectively. The solutions for $u(x)$ in the regions of constant A_0 can be written $u_p(x) = C_R e^{ipx} + C_L e^{-ipx}$ where $p \geq 0$ satisfies

$$p^2 = (\omega + qA_0)^2 - m^2 = (\omega - m + qA_0)(\omega + m + qA_0). \quad (\text{A.2})$$

The classically allowed regions correspond to those for which p is real, which requires the right-hand-side to be positive. This is impossible to satisfy when ω lies within a forbidden range

$$qA_0 - m < \omega < qA_0 + m, \quad (\text{A.3})$$

corresponding to a forbidden band of width $2m$ centered on qA_0 that separates the positive- and negative-frequency solutions from one another.

For a given p the mode frequencies are $\omega_{p\pm} = -qA_0 \pm \sqrt{m^2 + p^2}$ and so the mode's contribution to the energy density is

$$\begin{aligned} \mathcal{H}(u) &= \partial_t u_p^* \partial_t u_p + \nabla u_p^* \nabla u_p + (m^2 - q^2 A_0^2) u_p^* u_p \\ &= 2\omega_{p\pm} \left[\omega_{p\pm} + qA_0 \right] |C|^2 = \pm \frac{\omega_{p\pm}}{\mathcal{V}}, \end{aligned} \quad (\text{A.4})$$

where \mathcal{V} denotes the volume of space. The last equality uses that normalization for Klein-Gordon modes implies $|C|^2 = (2|\omega_{p\pm} + qA_0|\mathcal{V})^{-1}$. The energy of the mode therefore is

$$\varepsilon_{p\pm} := \mathcal{H}(u)\mathcal{V} = \pm\omega_{p\pm} = \mp qA_0 + \sqrt{p^2 + m^2}, \quad (\text{A.5})$$

and so is bounded from below and depends on A_0 as appropriate for particle and antiparticle having opposite charge.

To confirm the charge explicitly, evaluate the current density carried by a mode using

$$J^\mu(u) = iq \left(u_p D^\mu u_p^* - u_p^* D^\mu u_p \right) \quad (\text{A.6})$$

giving the charge density

$$\begin{aligned} J^0(u) &= -iq \left(u_p \partial_t u_p^* - u_p^* \partial_t u_p \right) + 2q^2 A_0 u_p^* u_p \\ &= 2q \left[\omega_{p\pm} + qA_0 \right] |C|^2 = \pm \frac{q}{\mathcal{V}}. \end{aligned} \quad (\text{A.7})$$

The contribution of a mode to the vector current J is similarly

$$J(u) = iq \left(u_p \nabla u_p^* - u_p^* \nabla u_p \right) = 2q|C|^2 p = \pm \frac{q v_g}{\mathcal{V}}, \quad (\text{A.8})$$

which uses the usual definition of group velocity

$$v_g := \frac{d\omega_{p\pm}}{dp} = \frac{p}{\omega_{p\pm} + qA_0} = \pm \frac{p}{\sqrt{p^2 + m^2}}. \quad (\text{A.9})$$

Notice that (A.7) and (A.8) show how positive and negative frequency states carry opposite charge and carry charge in opposite directions, as appropriate for antiparticles, but *only* because (A.9) shows that the direction of particle motion, v_g , is parallel to (antiparallel to) the direction of p for positive (negative) frequency states. This plays an important role when interpreting first-quantized scattering involving negative-frequency modes.

Scattering occurs because the change of A_0 near $x = 0$ breaks momentum conservation and to compute it we must match solutions from the left and the right of the region of nonzero electric field. We've seen that the frequency of these solutions is

$$\begin{aligned}\omega_{p\pm}^R &= -qv \pm \sqrt{m^2 + p^2} \quad (\text{right of step}) \\ \omega_{p\pm}^L &= qv \pm \sqrt{m^2 + p^2} \quad (\text{left of step}),\end{aligned}\tag{A.10}$$

and so particle production occurs once the step is large enough (*i.e.* when $qv > m$) that the energy of a positive-frequency state on one side of the step can correspond to a negative-frequency state on the other side. Inspection of (A.3) shows that the frequency window where positive-frequency states on one side and negative-frequency states on the other side share the same energy corresponds to the interval

$$-qv + m < \omega < qv - m.\tag{A.11}$$

In the small- ℓ limit the region with nonzero electric field can be regarded as a step in the electrostatic potential and so solutions to the left and right of the step can be simply matched to one another at $x = 0$ by demanding continuity of both the mode functions and their first derivatives there. In particular, the value of p must differ on either side, with eq. (A.2) implying

$$p_L^2 = (\omega - qv)^2 - m^2 \quad \text{and} \quad p_R^2 = (\omega + qv)^2 - m^2.\tag{A.12}$$

Writing $u_A = C_{A-}e^{-i(px+\omega t)} + C_{A+}e^{i(px-\omega t)}$ for $A = L, R$ one finds continuity of $u_p(x)$ and $u'_p(x)$ at $x = 0$ implies

$$C_{L+} + C_{L-} = C_{R+} + C_{R-} \quad \text{and} \quad ip_R(C_{R+} - C_{R-}) = ip_L(C_{L+} - C_{L-}).\tag{A.13}$$

These conditions fix two of the four integration constants $C_{A\pm}$ and state normalization fixes one more, leaving a single free parameter that can be fixed by a scattering boundary condition in the standard way.

Specializing to energies corresponding to positive frequency on the right of the step (so $\omega > m - qv$) and negative frequency to its left (so $\omega < qv - m$) implies the momentum on each side of the step is given by

$$p_R^2 = (\omega - m + qv)(\omega + m + qv) \geq 0 \quad \text{and} \quad p_L^2 = (m + qv - \omega)(qv - \omega - m) \geq 0.\tag{A.14}$$

A key observation at this juncture – made above in (A.9) – is that for negative frequency modes the group velocity v_g points in the *opposite* direction to the quantum number p . This means a negative-frequency mode to the left of the step with $p < 0$ is *approaching* the step whilst a mode with $p > 0$ actually moves away from it.

Consider then a state for which the negative-frequency state moves from the left towards $x = 0$, which from the above discussion corresponds to choosing $p < 0$ and so $C_{L+} = 0$. Continuity of the wave function and its derivative then imply

$$C_{L-} = C_{R-} + C_{R+} \quad \text{and} \quad ip_R(C_{R+} - C_{R-}) + ip_L C_{L-} = 0, \quad (\text{A.15})$$

and so

$$\frac{C_{R-}}{C_{R+}} = \frac{p_R + p_L}{p_R - p_L} \quad \text{and} \quad \frac{C_{L-}}{C_{R+}} = 1 + \frac{C_{R-}}{C_{R+}} = \frac{2p_R}{p_R - p_L}. \quad (\text{A.16})$$

It is convenient to include a factor of $p^{-1/2}$ as part of the mode function when defining the transmission and reflection amplitudes, leading to the definitions

$$\tau := \frac{C_{L-}}{C_{R-}} \sqrt{\frac{p_L}{p_R}} \quad \text{and} \quad \rho := \frac{C_{R+}}{C_{R-}}, \quad (\text{A.17})$$

for which (A.16) implies

$$\rho = \frac{p_R - p_L}{p_R + p_L} \quad \text{and} \quad \tau = \frac{2\sqrt{p_R p_L}}{p_R + p_L}, \quad (\text{A.18})$$

and so $|\tau|^2 + |\rho|^2 = 1$.

A second-quantized calculation [120] shows that the transmission probability $|\tau|^2$ corresponds to the rate for the incoming antiparticle on the left to annihilate with the incoming particle on the right, with any excess particles being reflected back in the direction from which they came. By time-reversal invariance this means that $|\tau|^2$ can also be interpreted as the pair-creation rate for this specific mode (marginalized over what all other modes are doing).

If we denote by Λ_v the vacuum survival probability (*i.e.* the probability of producing zero pairs in a particular mode), then unitarity says that the sum of probabilities for producing any number of particle pairs should be unity, and so

$$1 = \Lambda_v + \Lambda_v |\tau|^2 + \Lambda_v |\tau|^4 + \cdots = \frac{\Lambda_v}{1 - |\tau|^2}, \quad (\text{A.19})$$

which implies $\Lambda_v = 1 - |\tau|^2 = |\rho|^2$. The mean number of particle pairs produced in this particular mode is similarly given by

$$\begin{aligned} \bar{n} &= \Lambda_v |\tau|^2 + 2\Lambda_v |\tau|^4 + 3\Lambda_v |\tau|^6 + \cdots = \frac{\Lambda_v |\tau|^2}{(1 - |\tau|^2)^2} \\ &= \frac{|\tau|^2}{1 - |\tau|^2} = \frac{|\tau|^2}{|\rho|^2} = \frac{4p_R p_L}{(p_R - p_L)^2}. \end{aligned} \quad (\text{A.20})$$

Notice that the component of the electric current density in the x direction is

$$J(u) = iq(u \partial_x u^* - u^* \partial_x u) = 2qp(|C_+|^2 - |C_-|^2), \quad (\text{A.21})$$

with $p = p_L$ or p_R depending on which side of $x = 0$ is of interest. Evaluating this using the solution for the C 's found above shows that the antiparticle contribution left of the electric field carries the current

$$J_L(u) = -2qp_L |C_{L-}|^2 = -2qp_R |\tau|^2 |C_{R-}|^2, \quad (\text{A.22})$$

which agrees with the sum of incident and reflected particles to the right of $x = 0$,

$$J_R(u) = 2qp_R(|C_{R+}|^2 - |C_{R-}|^2) = -2qp_R(1 - |\rho|^2)|C_{R-}|^2, \quad (\text{A.23})$$

as required by current conservation.

Consider next the case where the state at the left of $x = 0$ is chosen to be an outgoing negative-frequency state, corresponding to the choice $C_{L-} = 0$. In this case continuity of u_p and u'_p at $x = 0$ instead leads to the conditions

$$C_{L+} = C_{R-} + C_{R+} \quad \text{and} \quad ip_R(C_{R+} - C_{R-}) - ip_L C_{L+} = 0, \quad (\text{A.24})$$

which have as solutions

$$\frac{C_{R-}}{C_{R+}} = \frac{p_R - p_L}{p_R + p_L} \quad \text{and} \quad \frac{C_{L+}}{C_{R+}} = 1 + \frac{C_{R-}}{C_{R+}} = \frac{2p_R}{p_R + p_L}. \quad (\text{A.25})$$

The transition and reflection amplitudes in this case then are

$$\hat{\rho} = \frac{C_{R+}}{C_{R-}} = \frac{p_R + p_L}{p_R - p_L} \quad \text{and} \quad \hat{\tau} = \frac{C_{L+}}{C_{R-}} \sqrt{\frac{p_L}{p_R}} = \frac{2\sqrt{p_R p_L}}{p_R - p_L}, \quad (\text{A.26})$$

and so satisfy $|\hat{\rho}|^2 - |\hat{\tau}|^2 = 1$.

The result that $|\hat{\rho}|^2 + |\hat{\tau}|^2 \neq 1$ is known as the Klein ‘paradox’. It was initially regarded as paradoxical because the transmission probability for the outgoing negative-frequency antiparticle emerging on the left for each particle incident on the right

$$|\hat{\tau}|^2 = \frac{4p_R p_L}{(p_R - p_L)^2}, \quad (\text{A.27})$$

is positive, and this makes the likelihood of having a reflected particle emerge on the right

$$|\hat{\rho}|^2 = \frac{(p_R + p_L)^2}{(p_R - p_L)^2} = 1 + |\hat{\tau}|^2 \quad (\text{A.28})$$

larger than unity.

A second-quantized treatment shows this is to be interpreted as 100% reflection of the incoming particle on the right of the step, accompanied by the emission of a particle-antiparticle pair. Having the probability of producing this pair be $|\hat{\tau}|^2$ rather than $|\tau|^2$ can also be understood from the second-quantized point of view. To this end notice that comparing (A.20) to (A.27) shows that the mean number of pairs produced is $\bar{n} = |\hat{\tau}|^2$, and so for each incoming particle on the right the probability of finding an antiparticle coming out at the left can be written

$$|\hat{\tau}|^2 = \frac{|\tau|^2}{1 - |\tau|^2} = |\tau|^2(1 + \bar{n}). \quad (\text{A.29})$$

This shows that this probability is larger than the probability $|\tau|^2$ for producing the pair in the vacuum by precisely the stimulated-emission factor of $1 + \bar{n}$ expected for bosons.

References

- [1] Schwinger J 1951 *Phys. Rev.* **82** 664
- [2] Schwinger J 1962 *Phys. Rev.* **128**(5) 2425–2429 URL <https://link.aps.org/doi/10.1103/PhysRev.128.2425>
- [3] Parentani R and Brout R 1992 *Nuclear Physics B* **388** 474–508
- [4] Brout R, Massar S, Parentani R and Spindel P 1995 *Physics Reports* **260** 329–446
- [5] Srinivasan K and Padmanabhan T 1999 *Phys. Rev. D* **60** 024007
- [6] Kim S P and Page D N 2002 *Phys. Rev. D* **65** 105002
- [7] Burgess C P, Hayman P, Williams M and Zalavári L 2017 *Journal of High Energy Physics* **2017** 106
- [8] Burgess C P, Hayman P, Rummel M, Williams M and Zalavari L 2017 *JHEP* **07** 072 (*Preprint* 1612.07334)
- [9] Burgess C P, Hayman P, Rummel M and Zalavari L 2017 *JHEP* **09** 007 (*Preprint* 1706.01063)
- [10] Burgess C P, Hayman P, Rummel M and Zalavári L 2021 *Phys. Lett. A* **390** 127105 (*Preprint* 2008.09719)
- [11] Burgess C P 2020 *Introduction to Effective Field Theory* (Cambridge University Press) ISBN 978-1-139-04804-0, 978-0-521-19547-8
- [12] Wang R C and Wong C Y 1988 *Phys. Rev. D* **38** 348
- [13] Martin C and Vautherin D 1988 *Phys. Rev. D* **38**(11) 3593–3595 URL <https://link.aps.org/doi/10.1103/PhysRevD.38.3593>
- [14] Martin C and Vautherin D 1989 *Phys. Rev. D* **40**(5) 1667–1673 URL <https://link.aps.org/doi/10.1103/PhysRevD.40.1667>
- [15] Sauter F 1931 *Zeit. f. Phys.* **69** 742
- [16] Sauter F 1931 *Zeit. f. Phys.* **69** 45
- [17] Gies H and Torgrimsson G 2016 *Phys. Rev. Lett.* **116** 090406
- [18] Gies H and Torgrimsson G 2017 *Phys. Rev. D* **95** 016001
- [19] Dunne G V 2009 *Eur. Phys. J. D* **55** 327–340
- [20] Dunne G V 2010 *Int. J. Mod. Phys. A* **25** 2373–2381
- [21] Narozhny N B and Fedotov A M 2014 *The European Physical Journal Special Topics* **223** 1083–1092
- [22] Martinez E A, Muschik C A, Schindler P, Nigg D, Erhard A, Heyl M, Hauke P, Dalmonte M, Monz T, Zoller P and Blatt R 2016 *Nature* **534** 516–519
- [23] Piñeiro A M, Genkina D, Lu M and Spielman I B 2019 *New J. Phys.* **21** 083035
- [24] Yang B, Sun H, Ott R, Wang H Y, Zache T V, Halimeh J C, Yuan Z S, Hauke P and Pan J W 2020 *Nature* **587** 392–396
- [25] Berdyugin A I, Xin N, Gao H, Slizovskiy S, Dong Z, Bhattacharjee S, Kumaravadivel P, Xu S, Ponomarenko L A, Holwill M, Bandurin D A, Kim M, Cao Y, Greenaway M T, Novoselov K S, Grigorieva I V, Watanabe K, Taniguchi T, Fal’ko V I, Levitov L S, Kumar R K and Geim A K 2022 *Science* **375** 430–433
- [26] Schmitt A, Vallet P, Mele D, Rosticher M, Taniguchi T, Watanabe K, Bocquillon E, Fève G, Berroir J M, Voisin C, Cayssol J, Goerbig M O, Troost J, Baudin E and Plaças B 2023 *Nat. Phys.* **19** 830–835
- [27] Szpak N and Schützhold R 2011 *Phys. Rev. A* **84** 050101
- [28] Szpak N and Schützhold R 2012 *New J. Phys.* **14** 035001
- [29] Zohar E, Cirac J I and Reznik B 2012 *Phys. Rev. Lett.* **109**(12) 125302 URL <https://link.aps.org/doi/10.1103/PhysRevLett.109.125302>
- [30] Banerjee D, Dalmonte M, Müller M, Rico E, Stebler P, Wiese U J and Zoller P 2012 *Phys. Rev. Lett.* **109**(17) 175302 URL <https://link.aps.org/doi/10.1103/PhysRevLett.109.175302>
- [31] Wiese U J 2013 *Ann. Phys. (Berlin)* **525** 777–796
- [32] Tagliacozzo L, Celi A, Zamora A and Lewenstein M 2013 *Ann. Phys.* **330** 160–191

- [33] Zohar E, Cirac J I and Reznik B 2016 *Rep. Prog. Phys.* **79** 014401
- [34] Kasper V, Hebenstreit F, Oberthaler M and Berges J 2016 *Phys. Lett. B* **760** 742–746
- [35] Kasper V, Hebenstreit F, Jendrzejewski F, Oberthaler M K and Berges J 2017 *New J. Phys.* **19** 023030 URL <https://dx.doi.org/10.1088/1367-2630/aa54e0>
- [36] Aidelsburger M 2018 *J. Phys. B: At. Mol. Opt. Phys.* **51** 193001
- [37] Surace F M, Mazza P P, Giudici G, Leroise A, Gambassi A and Dalmonte M 2020 *Phys. Rev. X* **10**(2) 021041 URL <https://link.aps.org/doi/10.1103/PhysRevX.10.021041>
- [38] Halimeh J C, McCulloch I P, Yang B and Hauke P 2022 *PRX Quantum* **3**(4) 040316 URL <https://link.aps.org/doi/10.1103/PRXQuantum.3.040316>
- [39] Cheng Y, Liu S, Zheng W, Zhang P and Zhai H 2022 *PRX Quantum* **3**(4) 040317 URL <https://link.aps.org/doi/10.1103/PRXQuantum.3.040317>
- [40] Wang H Y, Zhang W Y, Yao Z, Liu Y, Zhu Z H, Zheng Y G, Wang X K, Zhai H, Yuan Z S and Pan J W 2023 *Phys. Rev. Lett.* **131** 050401
- [41] Hauke P, Marcos D, Dalmonte M and Zoller P 2013 *Phys. Rev. X* **3**(4) 041018 URL <https://link.aps.org/doi/10.1103/PhysRevX.3.041018>
- [42] Andrade B, Davoudi Z, Graß T, Hafezi M, Pagano G and Seif A 2022 *Quantum Sci. Technol.* **7** 034001 URL <https://dx.doi.org/10.1088/2058-9565/ac5f5b>
- [43] Katz O, Cetina M and Monroe C 2023 *PRX Quantum* **4**(3) 030311 URL <https://link.aps.org/doi/10.1103/PRXQuantum.4.030311>
- [44] García-Álvarez L, Casanova J, Mezzacapo A, Egusquiza I L, Lamata L, Romero G and Solano E 2015 *Phys. Rev. Lett.* **114**(7) 070502 URL <https://link.aps.org/doi/10.1103/PhysRevLett.114.070502>
- [45] Farrell R C, Illa M, Ciavarella A N and Savage M J 2024 *PRX Quantum* **5**(2) 020315 URL <https://link.aps.org/doi/10.1103/PRXQuantum.5.020315>
- [46] Schützhold R, Gies H and Dunne G 2008 *Phys. Rev. Lett.* **101** 130404
- [47] Kleinert H, Ruffini R and Xue S S 2008 *Phys. Rev. D* **78** 025011
- [48] Dumlu C K and Dunne G V 2010 *Phys. Rev. Lett.* **104** 250402
- [49] Dumlu C K and Dunne G V 2011 *Phys. Rev. D* **83** 065028
- [50] Hebenstreit F 2016 *Phys. Lett. B* **753** 336–340
- [51] Zener C 1934 *Proc. R. Soc. Lond. A* **145** 523–529
- [52] Taguchi Y, Matsumoto T and Tokura Y 2000 *Phys. Rev. B* **62**(11) 7015–7018 URL <https://link.aps.org/doi/10.1103/PhysRevB.62.7015>
- [53] Dunne G V 2012 The Heisenberg-Euler effective action: 75 years on *Int. J. Mod. Phys.: Conf. Ser.* vol 14 (World Scientific) pp 42–56
- [54] Rau J and Müller B 1996 *Phys. Rep.* **272** 1–59
- [55] Oka T and Aoki H 2005 *Phys. Rev. Lett.* **95**(13) 137601 URL <https://link.aps.org/doi/10.1103/PhysRevLett.95.137601>
- [56] Green A G and Sondhi S L 2005 *Phys. Rev. Lett.* **95**(26) 267001 URL <https://link.aps.org/doi/10.1103/PhysRevLett.95.267001>
- [57] Oka T and Aoki H 2009 *Nonequilibrium Quantum Breakdown in a Strongly Correlated Electron System* (Berlin, Heidelberg: Springer Berlin Heidelberg) pp 1–35 ISBN 978-3-540-85428-9 URL https://doi.org/10.1007/978-3-540-85428-9_9
- [58] Sundaram S, Burgess C P and O’Dell D H J 2024 *New J. Phys.* **26** 053023
- [59] Lifshitz E, LD and (JB) S L 1965 *Quantum Mechanics; Non-relativistic Theory* (Pergamon Press)
- [60] Perelomov A M and Popov V S 1970 *Theoretical and Mathematical Physics* **4** 664–677
- [61] Lévy-Leblond J M 1967 *Phys. Rev.* **153**(1) 1–4
- [62] Camblong H E, Epele L N, Fanchiotti H and García Canal C A 2001 *Phys. Rev. Lett.* **87**(22) 220402
- [63] Denschlag J, Umshaus G and Schmiedmayer J 1998 *Phys. Rev. Lett.* **81** 737
- [64] Plestid R, Burgess C P and O’Dell D H J 2018 *J. High Energy Phys.* **2018** 59
- [65] Efimov V 1970 *Phys. Lett. B* **33** 563–564

- [66] Efimov V 1973 *Nucl. Phys. A* **210** 157–188
- [67] Braaten E and Hammer H W 2006 *Phys. Rep.* **428** 259–390
- [68] Kraemer T, Mark M, Waldburger P, Danzl J G, Chin C, Engeser B, Lange A D, Pilch K, Jaakkola A, Nägerl H C and Grimm R 2006 *Nature* **440** 315–318
- [69] Williams J R, Hazlett E L, Huckans J H, Stites R W, Zhang Y and O’Hara K M 2009 *Phys. Rev. Lett.* **103**(13) 130404
- [70] Pollack S E, Dries D and Hulet R G 2009 *Science* **326** 1683
- [71] Tung S K, Jiménez-García K, Johansen J, Parker C V and Chin C 2014 *Phys. Rev. Lett.* **113**(24) 240402
- [72] Huang B, Sidorenkov L A, Grimm R and Hutson J M 2014 *Phys. Rev. Lett.* **112**(19) 190401
- [73] Nisoli C and Bishop A R 2014 *Phys. Rev. Lett.* **112**(7) 070401
- [74] Calogero F 1969 *J. Math. Phys.* **10**(12) 2191–2196
- [75] Sutherland B 1971 *Phys. Rev. A* **4**(5) 2019–2021
- [76] Gurappa N and Panigrahi P K 1999 *Physical Review B* **59** R2490
- [77] Gurappa N and Panigrahi P K 2000 *Physical Review B* **62** 1943
- [78] Moroz S 2010 *Phys. Rev. D* **81** 066002
- [79] Birmingham D, Gupta K S and Sen S 2001 *Physics Letters B* **505** 191–196
- [80] Camblong H E and Ordonez C R 2003 *Phys. Rev. D* **68** 125013
- [81] Burgess C, Plestid R and Rummel M 2018 *J. High Energy Phys.* **2018** 1–31
- [82] Barton G 1986 *Annals of Physics* **166** 322–363
- [83] Yuce C, Kilic A and Coruh A 2006 *Physica Scripta* **74** 114
- [84] Subramanyan V, Hegde S S, Vishveshwara S and Bradlyn B 2021 *Annals of Physics* **435** 168470
- [85] Bhattacharyya A, Chemissany W, Haque S S, Murugan J and Yan B 2021 *SciPost Phys. Core* **4** 002 URL <https://scipost.org/10.21468/SciPostPhysCore.4.1.002>
- [86] Landau L 1932 *Phys. Z. Soviet Union* **2** 46–51
- [87] Zener C 1932 *Proc. R. Soc. Lond. A* **137** 696–702
- [88] Gupta K S and Rajeev S G 1993 *Phys. Rev. D* **48** 5940
- [89] Bawin M and Coon S 2003 *Phys. Rev. A* **67** 042712
- [90] Mueller E J and Ho T L 2004 *arXiv preprint cond-mat/0403283*
- [91] Wilson K G 1971 *Phys. Rev. D* **3** 1818
- [92] Glazek S D and Wilson K G 2002 *Phys. Rev. Lett.* **89** 230401
- [93] Callan Jr C G, Coleman S and Jackiw R 1970 *Ann. Phys.* **59** 42
- [94] Coon S A and Holstein B R 2002 *American Journal of Physics* **70** 513–519
- [95] Essin A M and Griffiths D J 2006 *Am. J. Phys.* **74** 109–117
- [96] Olshanii M, Perrin H and Lorent V 2010 *Phys. Rev. Lett.* **105** 095302
- [97] da Silva U C 2018 *Ann. Phys.* **398** 38–54
- [98] da Silva U C, Pereira C F and Lima A A 2024 *Ann. Phys.* **460** 169549
- [99] Bender C M and Boettcher S 1998 *Phys. Rev. Lett.* **80** 5243
- [100] Bender C M, Dorey P E, Dunning C, Fring A, Hook D W, Jones H F, Kuzhel S, Lévai G and Tateo R 2019 *PT Symmetry* (WORLD SCIENTIFIC (EUROPE)) (Preprint <https://www.worldscientific.com/doi/pdf/10.1142/q0178>) URL <https://www.worldscientific.com/doi/abs/10.1142/q0178>
- [101] Sundaram S, Burgess C P and O’Dell D H J 2021 Fall-to-the-centre as a symmetry breaking transition *J. Phys.: Conf. Ser.* vol 2038 (IOP Publishing) p 012024
- [102] Stålhammar M, Larana-Aragon J, Rødland L and Kunst F K 2023 *New J. Phys.* **25** 043012
- [103] Lee T D 1954 *Phys. Rev.* **95** 1329
- [104] Lee T D and Wick G C 1969 *Nuclear Physics B* **9** 209–243
- [105] Sudarshan E C G 1961 *Phys. Rev.* **123** 2183
- [106] Bender C M, Brandt S F, Chen J H and Wang Q 2005 *Phys. Rev. D* **71** 025014
- [107] Bender C M and Mannheim P D 2008 *Journal of Physics A: Mathematical and Theoretical* **41** 304018

- [108] Bender C M, Felski A, Klevansky S P and Sarkar S 2021 Symmetry and renormalisation in quantum field theory *J. Phys.: Conf. Ser.* vol 2038 (IOP Publishing) p 012004
- [109] LeClair A, Román J M and Sierra G 2004 *Nuclear Physics B* **700** 407–435
- [110] Kaplan D B, Lee J W, Son D T and Stephanov M A 2009 *Phys. Rev. D* **80** 125005
- [111] Moroz S and Schmidt R 2010 *Annals of Physics* **325** 491–513
- [112] Sierra G 2005 *Journal of Statistical Mechanics: Theory and Experiment* **2005** P12006
- [113] Nahum A, Chalker J T, Serna P, Ortuño M and Somoza A M 2015 *Phys. Rev. X* **5**(4) 041048 URL <https://link.aps.org/doi/10.1103/PhysRevX.5.041048>
- [114] Gorbenko V, Rychkov S and Zan B 2018 *SciPost Phys.* **5** 050 URL <https://scipost.org/10.21468/SciPostPhys.5.5.050>
- [115] Gorbenko V, Rychkov S and Zan B 2018 *J. High Energy Phys.* **2018** 108
- [116] Ma H and He Y C 2019 *Phys. Rev. B* **99** 195130
- [117] Halder A, Tavakol O, Ma H and Scaffidi T 2023 *Phys. Rev. Lett.* **131**(13) 131601 URL <https://link.aps.org/doi/10.1103/PhysRevLett.131.131601>
- [118] Tang Y, Ma H, Tang Q, He Y C and Zhu W 2024 *arXiv preprint cond-mat/2403.00852*
- [119] Ullinger F, Zimmermann M and Schleich W P 2022 *AVS Quantum Science* **4**
- [120] Hansen A and Ravndal F 1981 *Phys. Scripta* **23** 1036
- [121] Hasan F and O’Dell D H J 2016 *Phys. Rev. A* **94** 043823
- [122] Sakurai J J 1994 *Modern quantum mechanics; rev. ed.* (Reading, MA: Addison-Wesley) URL <https://cds.cern.ch/record/1167961>
- [123] Das A 2020 *Lectures on quantum field theory* (World Scientific)
- [124] Wigner E 1993 Unitary representations of the inhomogeneous lorentz group including reflections *The Collected Works of Eugene Paul Wigner: Part A: The Scientific Papers* (Springer) pp 564–607
- [125] Chruściński D 2003 *Journal of Mathematical Physics* **44** 3718–3733
- [126] Burgess C P, Hayman P, Rummel M and Zalavari L 2018 *Phys. Rev. A* **98** 052510 (*Preprint* 1708.09768)
- [127] Zalavari L, Burgess C P, Hayman P and Rummel M 2021 *Annals Phys.* **429** 168463 (*Preprint* 2008.09718)
- [128] Berry M V and Ishio H 2002 *J. Phys. A: Math. Gen.* **35** 5961–5972
- [129] Berry M V and Ishio H 2005 *J. Phys. A: Math. Gen.* **38** L513 URL <https://dx.doi.org/10.1088/0305-4470/38/29/L01>
- [130] Berry M V and Dennis M R 2008 *J. Phys. A: Math. Theor.* **41** 135203 URL <https://dx.doi.org/10.1088/1751-8113/41/13/135203>
- [131] Marlettta M and Rozenblum G 2009 *J. Phys. A: Math. Theor.* **42** 125204 URL <https://dx.doi.org/10.1088/1751-8113/42/12/125204>
- [132] Berry M V 2009 *J. Phys. A: Math. and Theor.* **42** 165208 URL <https://dx.doi.org/10.1088/1751-8113/42/16/165208>
- [133] Olver F W, Lozier D W, Boisvert R F and Clark C W 2010 *NIST handbook of mathematical functions hardback and CD-ROM* (Cambridge university press)
- [134] Berry M V and Lewis Z V 1980 *Proc. R. Soc. Lond. A* **370** 459–484
- [135] Born M and Wolf E 1999 *Principles of Optics* (Cambridge, United Kingdom: Cambridge University Press) ISBN 0-521-64222-1

SUMMARY, CONCLUSIONS, AND FUTURE WORK

In summary, this thesis involves the study of two unstable quantum mechanical systems, the attractive inverse square potential (ISP) and the inverted harmonic oscillator (IHO) and we address the question of implementing appropriate boundary conditions for both the systems, near the origin for the ISP and at long distances for the IHO, using the methods of EFT in a renormalization group invariant way.

In chapter 2 (paper 1) we study the ISP and its connection to \mathcal{PT} symmetry breaking transitions. Using the methods of PPEFT we implement a linear (Robin) boundary condition, which dominates at low energies, at a short distance scale ϵ . The fact that physical predictions should be independent of the arbitrary position where we evaluate the boundary condition means that we need to renormalize the boundary coupling within the PPEFT action. In this chapter we study the fixed point merger of the RG flow of the boundary coupling as we tune the strength of the ISP from sub-critical ($\alpha < 1/4$) to super-critical regime ($\alpha > 1/4$). We point out that the fixed point merger exhibits a \mathcal{PT} phase transition, where two real fixed points in the sub-critical case which is \mathcal{PT} symmetric, merge at the critical coupling $\alpha_c = 1/4$ and become complex in the super-critical case breaking \mathcal{PT} symmetry.

In chapter 3 (paper 2), the main result of the study is that the quantum mechanics of the IHO system can be mapped to the super-critical ISP system. Apart from mapping the Hamiltonians, we also map the linearly independent states of the ISP to the IHO states using the technique of quantum canonical transformation. Furthermore, with the knowledge of how the states map we also address the question of how the boundary conditions map from the ISP (near the origin) to the IHO (at

long distances) using EFT and RG methods. At low energies it is the linear (Robin) boundary condition that dominates, and it is evaluated at a finite short distance ϵ for the ISP and at long distances L for the IHO system. The fact that the boundary condition is evaluated at an arbitrary position which is not physical, requires the boundary coupling to be renormalized. We show that the RG evolution for the IHO system exhibits limit cycle behaviour in the complex plane like the ISP potential. For the super-critical ISP, the log periodic behaviour of physical quantities as a function of tunable physical parameters is due to the emergence of a scale anomaly, where the classical continuous scale invariance is broken and leads to discrete scaling symmetry. However, the RG flow for the IHO exhibits faster than log periodic behaviour as a function of the cut-off scale. This is because scaling symmetry is not explicit for the IHO system. However, we show that the IHO is part of a larger $\text{su}(1,1)$ spectrum generating algebra in which the generator of scale transformations $(xp + px)/2$ is also a part.

Finally, in chapter 4 (paper 3) we apply the RG methods developed for the IHO in chapter 3 to study Schwinger pair creation. It is known that the classical Klein-Gordon equation in the presence of a constant electric field \mathcal{E} can be mapped to a time independent Schrödinger equation with an IHO potential. In chapter 4 we address the question of implementing an appropriate non-selfadjoint extension for the IHO that describes pair creation. The linear (Robin) boundary condition is evaluated at a large finite distance $L \gg a$, where $a = \frac{2mc^2}{q\mathcal{E}}$ is the microscopic pair production length scale, and $L \ll D$, where D is the physical scale where electric field is switched on/off. The fact that the scale L at which we evaluate the boundary condition is arbitrary up to the fact that it should satisfy $a \ll L \ll D$, calls for renormalizing the boundary coupling. At the RG fixed point, we show that the constant field result emerges, physically the fixed point is the region of zero reflection from the boundary, i.e. where the electric field extends forever. When one is away from the fixed point the fact the RG flow of the boundary coupling exhibits a limit cycle behaviour is suggestive that observables such as the current correlation function exhibits faster than log periodic behaviour as a function of electric field or system size.

Outlook

Universal finite size effects using the RG framework in Schwinger pair production

In chapter 4 we show that Schwinger's pair production probability for uniform fields emerges at the RG fixed point corresponding to pure emission, which is physically

the region of zero reflection from the boundary. Future work will look at the case where one is away from the fixed point but also not too far from it, expanding the probability current in the limit of small reflection probability, to see if it leads to a universal description of finite size effects by comparing it against specific regulator models in the literature such as (i) a setup of parallel plate capacitors which introduces a sharp (sudden) cut-off to the electric field at the boundary (ii) a Sauter potential that allows for a spatially adiabatic turning off of the electric field. We believe this is an interesting and experimentally relevant question to ask and is currently a work in progress.

Implications of the duality between the inverted harmonic oscillator and inverse square potentials in the theory of Hawking radiation

One interesting application of the duality between the quantum inverted harmonic oscillator and inverse square potentials would be to see its implications in the theory of Hawking radiation. It is well known that in the Schwarzschild metric the physics near the event horizon of a black hole is described by an effective Schrödinger equation with an attractive ISP, that describes fall to the centre. The implications of the RG evolution of the inverse square boundary coupling has been studied before in the context of black hole echoes [26], where the pure absorber fixed point describes the standard in-falling black hole boundary condition. Now that we know the IHO problem is related to ISP via a canonical transformation, it would be interesting to see what the implications of the IHO physics would be in the context of Hawking radiation. Would any of the RG fixed points of the IHO boundary coupling reproduce the Hawking formula?

Application of RG methods in optics

The resolution of optical devices are limited by the wavelength of light and the numerical aperture which is known as Abbe's diffraction limit. However, there are several interesting proposals to beat this limit including by super resolved fluorescence microscopy which led to the 2014 Nobel prize in Chemistry. It has important practical applications in biological systems such as, imaging molecules within a cell etc. Another proposed pathway to super resolution is by using superlenses such as Maxwell's fisheye lens, Luneburg lens and the Eaton lens. Maxwell's fisheye lens is a spherically symmetric lens with a refractive index of the form $n_{\text{MFEL}}(r) \propto \frac{1}{1+r^2}$. According to Maxwell, the lens is special because "all the rays proceeding from any point in the medium will meet accurately at another point". The refractive index of a Luneburg lens is of the form $n_{\text{Luneburg}}(r) \propto \sqrt{1 - \left(\frac{r}{R}\right)^2}$. The Helmholtz wave equation can be written in the form of a Schrödinger equation with the $U - E = -n^2/2$, where U is

the potential energy term and E is the energy eigenvalue. Thus, the Luneburg lens is described by a simple harmonic oscillator potential and Maxwell's fisheye lens is described by a potential of the form $U - E \propto -1/[1 + (r/R)^2]^2$. The theory of superlenses remains as a controversial and a challenging subject till now with researchers doubting it can really do perfect imaging.

Inspired by the duality mapping of the IHO to ISP, we conjecture that one can map the smoothly regularized IHO potential (a Poschl-Teller potential) to the above form of a Maxwell's fisheye potential using a coordinate transformation. This remains a work in progress. It would be interesting to apply the RG methods in implementing appropriate boundary conditions and see if they could have consequences in perfect imaging, including the case of a non-hermitian lens where light is absorbed or pumped into the system.

BIBLIOGRAPHY

- [1] Burgess, C. P., Hayman, P., Williams, M. & Zalavari, L. Point-particle effective field theory I: classical renormalization and the inverse-square potential. *J. High Energ. Phys.* **2017**, 106 (2017)
- [2] Subramanyan, V., Hegde, S., Vishveshwara, S. & Bradlyn, B. Physics of the Inverted Harmonic Oscillator: From the lowest Landau level to event horizons. *Ann. Phys.* **435** pp. 168470 (2021)
- [3] Bhattacharyya, A., Chemissany, W., Haque, S., Murugan, J. & Yan, B. The multi-faceted inverted harmonic oscillator: Chaos and complexity. *SciPost Phys. Core.* **4**, 002 (2021)
- [4] Barton, G. Quantum mechanics of the inverted oscillator potential. *Ann. Phys.* **166**, 322-363 (1986)
- [5] Parentani, R. & Brout, R. Vacuum instability and black hole evaporation. *Nucl. Phys. B.* **388**, 474-508 (1992)
- [6] Brout, R., Massar, S., Parentani, R. & Spindel, P. A primer for black hole quantum physics. *Phys. Rep.* **260**, 329-446 (1995)
- [7] Chruscinski, D. Quantum mechanics of damped systems. *J. Math. Phys.* **44**, 3718-3733 (2003)
- [8] Rajeev, K., Chakraborty, S. & Padmanabhan, T. Inverting a normal harmonic oscillator: physical interpretation and applications. *General Relativity And Gravitation.* **50** pp. 1-38 (2018)
- [9] Prakash, G. & Agarwal, G. Mixed excitation-and deexcitation-operator coherent states for the SU (1, 1) group. *Phys. Rev. A.* **50**, 4258 (1994)
- [10] Glauber, R. Amplifiers, Attenuators, and Schrodinger's Cat. *Ann. N. Y. Acad. Sci.* **480**, 336-372 (1986)

- [11] Gietka, K. & Busch, T. Inverted harmonic oscillator dynamics of the nonequilibrium phase transition in the Dicke model. *Phys. Rev. E*. **104**, 034132 (2021)
- [12] Gentilini, S., Braidotti, M., Marcucci, G., DelRe, E. & Conti, C. Physical realization of the Glauber quantum oscillator. *Sci. Rep.* **5**, 15816 (2015)
- [13] Srinivasan, K. & Padmanabhan, T. Particle production and complex path analysis. *Phys. Rev. D*. **60**, 024007 (1999)
- [14] Schutzhold, R. & Unruh, W. Hawking radiation with dispersion versus breakdown of the WKB approximation. *Phys. Rev. D*. **88**, 124009 (2013)
- [15] Das, A., Panda, S. & Roy, S. Origin of the geometric tachyon. *Phys. Rev. D*. **78**, 061901 (2008)
- [16] Dhar, A., Mandal, G. & Wadia, S. Discrete-state moduli of string theory from the $c=1$ matrix model. *Nucl. Phys. B*. **454**, 541-560 (1995)
- [17] Sen, A. Infrared finite semi-inclusive cross section in two dimensional type 0B string theory. *J. High Energ. Phys.* **2023**, 1-21 (2023)
- [18] Berry, M. & Keating, J. $H=xp$ and the Riemann Zeros. *Supersymmetry And Trace Formulae: Chaos And Disorder*. pp. 355-367 (1999)
- [19] Landau, L. & Lifshitz, E. Quantum mechanics: non-relativistic theory. (Elsevier, 2013)
- [20] Camblong, H. & Ordonez, C. Anomaly in conformal quantum mechanics: From molecular physics to black holes. *Phys. Rev. D*. **68**, 125013 (2003,12), <https://link.aps.org/doi/10.1103/PhysRevD.68.125013>
- [21] Birmingham, D., Gupta, K. & Sen, S. Near-horizon conformal structure of black holes. *Phys. Lett. B*. **505**, 191-196 (2001)
- [22] Burgess, C.P. Quantum Gravity in Everyday Life: General Relativity as an Effective Field Theory. *Living Rev. Relativ.* **7**, 5 (2004).
- [23] Burgess, C. P. Introduction to effective field theory. (Cambridge University Press, 2020)
- [24] Burgess, C. P. An introduction to effective field theory. *Annu. Rev. Nucl. Part. Sci.* **57** pp. 329-362 (2007)

- [25] Plestid, R., Burgess, C. P. & O'Dell, D. H. J. Fall to the centre in atom traps and point-particle EFT for absorptive systems. *J. High Energ. Phys.* **2018**, 59 (2018)
- [26] Burgess, C. P., Plestid, R. & Rummel, M. Effective field theory of black hole echoes. *J. High Energ. Phys.* **2018**, 1-31 (2018)
- [27] Zalavari, L., Burgess, C. P., Hayman, P. & Rummel, M. Precision nuclear-spin effects in atoms: EFT methods for reducing theory errors. *Ann. Phys.* **429** pp. 168463 (2021)
- [28] Ruiz, D. Investigation of Point-Particle Effective Field Theory for the Inverse-Square Model. (2020)
- [29] Moroz, S. Below the Breitenlohner-Freedman bound in the nonrelativistic AdS/CFT correspondence. *Phys. Rev. D.* **81**, 066002 (2010)
- [30] Braaten, E. & Hammer, H. Universality in few-body systems with large scattering length. *Phys. Rep.* **428**, 259-390 (2006)
- [31] Leonhardt, U. Perfect imaging without negative refraction. *New J. Phys.* **11**, 093040 (2009)
- [32] Sundaram, S. & Panigrahi, P. On the origin of the coherence of sunlight on the earth. *Opt. Lett.* **41**, 4222-4224 (2016)
- [33] Gurappa, N. & Panigrahi, P. Free harmonic oscillators, Jack polynomials, and Calogero-Sutherland systems. *Phys. Rev. B.* **62**, 1943 (2000)
- [34] Frank, W., Land, D. & Spector, R. Singular potentials. *Rev. Mod. Phys.* **43**, 36 (1971)
- [35] Case, K. Singular potentials. *Phys. Rev.* **80**, 797 (1950)
- [36] Gupta, K. & Rajeev, S. Renormalization in quantum mechanics. *Phys. Rev. D.* **48**, 5940 (1993)
- [37] Bouaziz, D. & Bawin, M. Singular inverse-square potential: renormalization and self-adjoint extensions for medium to weak coupling. *Phys. Rev. A.* **89**, 022113 (2014)
- [38] Bawin, M. & Coon, S. Singular inverse square potential, limit cycles, and self-adjoint extensions. *Phys. Rev. A.* **67**, 042712 (2003)

- [39] Bethe, H. & Peierls, R. Quantum theory of the dipion. *Proc. R. Soc. Lond. A.* **148**, 146-156 (1935)
- [40] GOLDSTEIN, H. Classical Mechanics. *Addison-Wesley*. pp. 11-16 (1980)
- [41] Dirac, P. On the analogy between classical and quantum mechanics. *Rev. Mod. Phys.* **17**, 195 (1945)
- [42] Gell-Mann, M. & Low, F. Quantum electrodynamics at small distances. *Phys. Rev. Lett.* **95**, 1300 (1954)
- [43] Ward, B. Solving Equations of the Gell-Mann-Low and Callan-Symanzik Type. *Phys. Rev. Lett.* **33**, 37 (1974)
- [44] Wilson, K. Renormalization group and critical phenomena. I. Renormalization group and the Kadanoff scaling picture. *Phys. Rev. B.* **4**, 3174 (1971)
- [45] Wilson, K. Renormalization group and critical phenomena. II. Phase-space cell analysis of critical behavior. *Phys. Rev. B.* **4**, 3184 (1971)
- [46] Wilson, K. The renormalization group and critical phenomena. *Rev. Mod. Phys.* **55**, 583 (1983)
- [47] Wilson, K. Renormalization group and strong interactions. *Phys. Rev. D.* **3**, 1818 (1971)
- [48] Huang, K. A critical history of renormalization. *Int. J. Mod. Phys. A.* **28**, 1330050 (2013)
- [49] Jackiw, R. Delta-function potentials in two-and three-dimensional quantum mechanics. MAB Beg Memorial Volume. pp. 25-42 (1991)
- [50] Thorn, C. Quark confinement in the infinite-momentum frame. *Phys. Rev. D.* **19**, 639 (1979)
- [51] Bender, C. & Boettcher, S. Real spectra in non-Hermitian Hamiltonians having P T symmetry. *Phys. Rev. Lett.* **80**, 5243 (1998)
- [52] Bender, C. PT symmetry: In quantum and classical physics. (World Scientific,2019)
- [53] Sakurai, J. & Napolitano, J. Modern quantum mechanics. (Cambridge University Press,2020)

- [54] Wigner, E. Unitary representations of the inhomogeneous Lorentz group including reflections. *The Collected Works Of Eugene Paul Wigner: Part A: The Scientific Papers*. pp. 564-607 (1993)
- [55] Sun, Y., Tan, W., Li, H., Li, J. & Chen, H. Experimental demonstration of a coherent perfect absorber with PT phase transition. *Phys. Rev. Lett.* **112**, 143903 (2014)
- [56] Bender, C., Berntson, B., Parker, D. & Samuel, E. Observation of PT phase transition in a simple mechanical system. *Am. J. Phys.* **81**, 173-179 (2013)
- [57] Bender, C., Dunne, G., Meisinger, P. & Simsek, M. Quantum complex henon heiles potentials. *Phys. Lett. A*. **281**, 311-316 (2001)
- [58] Bender, C., Berry, M. & Mandilara, A. Generalized PT symmetry and real spectra. *J. Phys. A: Math. Gen.* **35**, L467 (2002)
- [59] Karthiga, S., Chandrasekar, V., Senthilvelan, M. & Lakshmanan, M. Systems that become PT symmetric through interaction. *Phys. Rev. A*. **94**, 023829 (2016)
- [60] Raja, S., Govindarajan, A., Mahalingam, A. & Lakshmanan, M. Multifaceted dynamics and gap solitons in PT-symmetric periodic structures. *Phys. Rev. A*. **100**, 033838 (2019)
- [61] Znojil, M. PT symmetric models in more dimensions and solvable square-well versions of their angular Schrodinger equations. *J. Phys. A: Math. Gen.* **36**, 7825 (2003)
- [62] Bender, C. & Weir, D. PT phase transition in multidimensional quantum systems. *J. Phys. A: Math. Theor.* **45** (2012)
- [63] Mandal, B., Mourya, B. & Yadav, R. PT phase transition in higher-dimensional quantum systems. *Phys. Lett. A*. **377**, 1043-1046 (2013)
- [64] Raval, H. & Prasad Mandal, B. Deconfinement to confinement as PT phase transition. *XXIII DAE High Energy Physics Symposium: Select Proceedings*. pp. 617-630 (2021)
- [65] Mandal, B. Examples of PT Phase Transition: QM to QFT. *J. Phys.: Conf. Ser.* **2038**, 012017 (2021)

- [66] Pal, T., Modak, R. & Mandal, B. DNA Unzipping as PT-Symmetry Breaking Transition. *ArXiv Preprint ArXiv:2212.14394*. (2022)
- [67] Hatano, N. & Nelson, D. Localization transitions in non-Hermitian quantum mechanics. *Phys. Rev. Lett.* **77**, 570 (1996)
- [68] Staalhammar, M., Larana-Aragon, J., Rodland, L. & Kunst, F. PT symmetry-protected exceptional cones and analogue Hawking radiation. *New J. Phys.* **25**, 043012 (2023)
- [69] Ruter, C., Makris, K., El-Ganainy, R., Christodoulides, D., Segev, M. & Kip, D. Observation of parity time symmetry in optics. *Nat. Phys.* **6**, 192-195 (2010)
- [70] Choi, Y., Hahn, C., Yoon, J. & Song, S. Observation of an anti-PT-symmetric exceptional point and energy-difference conserving dynamics in electrical circuit resonators. *Nat. Commun.* **9**, 2182 (2018)
- [71] Sauter, F. On the behavior of an electron in a homogeneous electric field in Dirac's relativistic theory. *Zeit. F. Phys.* **69**, 45 (1931)
- [72] Heisenberg, W. & Euler, H. Consequences of Dirac theory of the positron. *ArXiv Preprint Physics/0605038*. (2006)
- [73] Dunne, G. The Heisenberg-Euler effective action: 75 years on. *Int. J. Mod. Phys.: Conf. Ser.* **14** pp. 42-56 (2012)
- [74] Schwinger, J. On gauge invariance and vacuum polarization. *Phys. Rev.* **82**, 664 (1951)
- [75] Dunne, G. New strong-field QED effects at extreme light infrastructure: Non-perturbative vacuum pair production. *Eur. Phys. J. D.* **55** pp. 327-340 (2009)
- [76] Narozhny, N. & Fedotov, A. Creation of electron-positron plasma with super-strong laser field. *Eur. Phys. J. Spec. Top.* **223** pp. 1083-1092 (2014)
- [77] Allor, D., Cohen, T. & McGady, D. Schwinger mechanism and graphene. *Phys. Rev. D.* **78**, 096009 (2008)
- [78] Fillion-Gourdeau, F. & MacLean, S. Time-dependent pair creation and the Schwinger mechanism in graphene. *Phys. Rev. B.* **92**, 035401 (2015)
- [79] Schmitt, A., Vallet, P., Mele, D., Rosticher, M., Taniguchi, T., Watanabe, K., Bocquillon, E., Fève, G., Berroir, J., Voisin, C. & Others Mesoscopic Klein-Schwinger effect in graphene. *Nat. Phys.* **19**, 830-835 (2023)

- [80] Pineiro, A., Genkina, D., Lu, M. & Spielman, I. Sauter,ÄSchwinger effect with a quantum gas. *New J. Phys.* **21**, 083035 (2019)
- [81] Vajna, S., Dora, B. & Moessner, R. Nonequilibrium transport and statistics of Schwinger pair production in Weyl semimetals. *Phys. Rev. B.* **92**, 085122 (2015)
- [82] Fillion-Gourdeau, F., Lorin, E. & Bandrauk, A. Landau-Zener-Stuckelberg interferometry in pair production from counterpropagating lasers. *Phys. Rev. A.* **86**, 032118 (2012)